Improved Prediction of MH370 Crash Location
Based on Drift Modeling of Floating Debris

Bobby Ulich, Ph.D. and Victor Iannello, Sc.D.

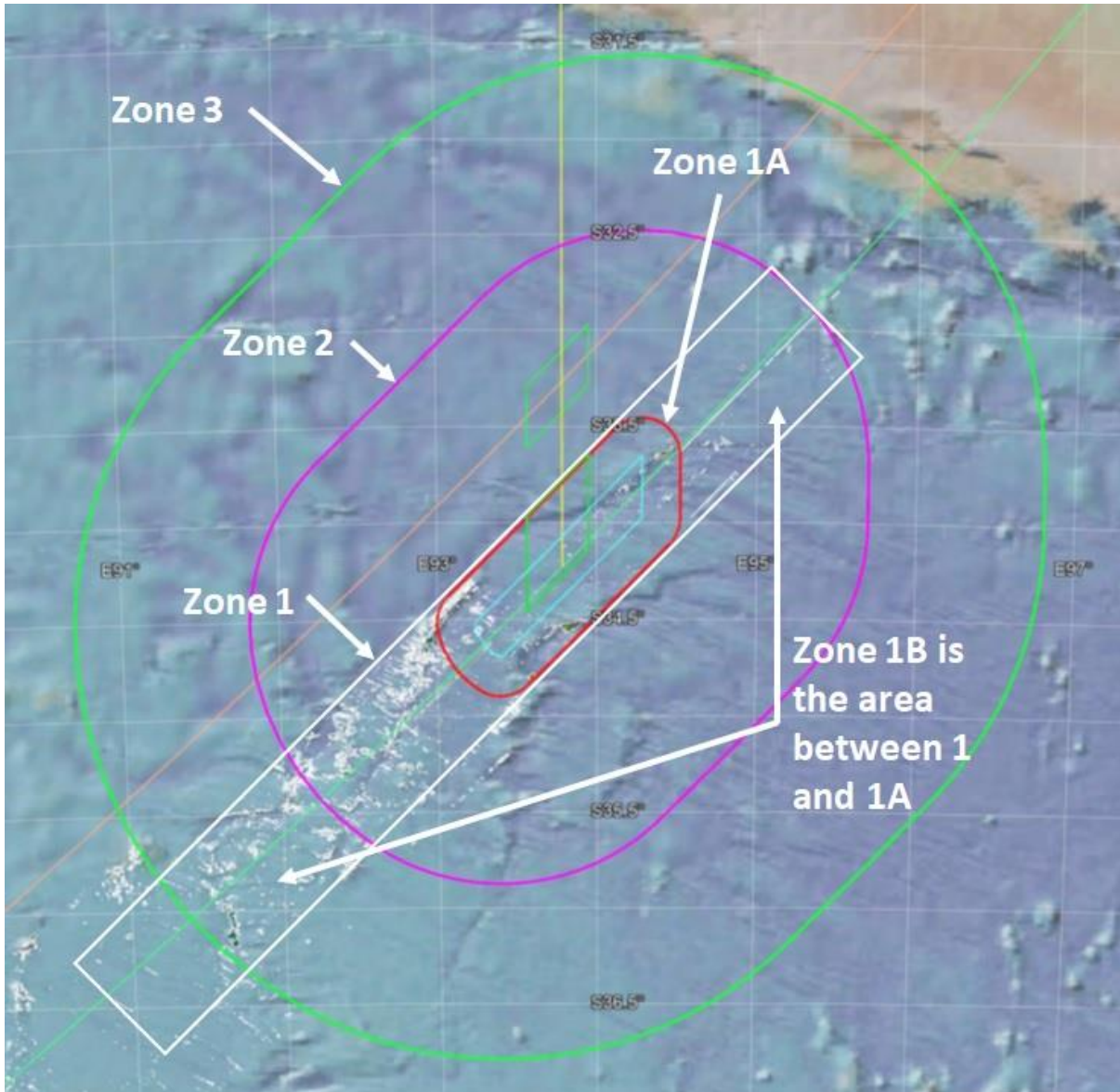**August 30, 2023**

Table of Contents

1. Introduction

Malaysian Airlines Flight MH370 crashed into the Southern Indian Ocean on 8 March 2014 [Malaysia Ministry of Transport (2018)]. Five clues provide reliable information regarding the location of the Point of Impact (POI):

1. Radio frequency communications occurred semi-periodically during the flight between the Airborne Earth Station (AES) onboard the aircraft 9M-MRO and the Inmarsat Ground Earth Station (GES) at Perth via the Inmarsat geostationary satellite 3F-1 serving the Indian Ocean Region (IOR). Inmarsat recorded communication link parameters at the GES in Australia, including the Coordinated Universal Time (UTC), the Burst Time Offset (BTO), and the Burst Frequency Offset (BFO). These parameters imply, with a high degree of certainty, the crash occurred in the Southern Indian Ocean (SIO) near the "7th Arc" [see pp. 16-33 in ATSB (2014a)]. Arc 7 is a line of constant distance from the satellite to the aircraft circa 00:19:30 UTC on 8 March 2014, shortly after fuel exhaustion occurred and not long before the crash. Subsequent analysis, using maximum likelihood estimation theory, of the statistical properties and degrees of correlations of these recorded BTO and BFO parameters indicates a most-likely Last Estimated Position (LEP) near Arc 7 at latitude -34.2 ± 0.5° [Ulich et al., or "UGIB" (2020)]. The final BFO measurement at 00:19:37 UTC indicates a very high rate of descent [Davey et al. (2016) and Holland (2018)].

2. Post-crash aerial searches from 18 March 2014 to 28 April 2014 were coordinated by AMSA (2014) and JACC (2014). These failed to detect a drifted floating-debris field [see Section 4 in Griffin et al. (2016)]. Portions of Arc 7 from -33° to - 42° latitude were incompletely searched [see Figure 4.1 in Griffin et al. (2016)].

3. Shortly after the crash, during the period 21-23 March 2014, space-based synthetic aperture radar [Iannello (2021a)] and visual-band imaging [Minchin et al. (2017)] detected several large floating objects predicted to be near -35.4°N, 92.8°E on the crash date [Iannello (2021a) and Griffin and Oke (2017a)]. However, it is not clear if these objects were floating debris from MH370, or if the number of items seen in the imagery is typical of the region or not. The sizes of the detected objects are larger than the fragments of floating crash debris from MH370 which were later recovered at distant shorelines, and which indicated a violent, high-speed crash had occurred. It is possible that a few large pieces of floating aircraft debris existed for weeks after the crash but failed to reach distant shores.

4. Beginning 18 months after the crash, floating aircraft fragments began washing up on shores to the west of Arc 7. About three dozen fragments were found and reported [see the eighteen debris reports by the Malaysia Ministry of Transport (2017a-2017r)]. Twenty debris were confirmed (or deemed to be from "likely" to "almost certain") to be parts of the B777-200ER aircraft with serial number 9M-MRO, which was flown on 7-8 March 2014 as Flight MH370.

5. Rydberg (2015) used the drift model by van Sebille et al. (2012) to predict a POI latitude of -34 ± 1° for the origin of the Flaperon found at La Réunion. The CSIRO in Australia developed a detailed model of the drift patterns of floating debris in the Southern Indian Ocean, based on the large historical data base of instrumented undrogued drifters and the ocean model BRAN2015 [Griffin et al. (2016, 2017) and Griffin and Oke (2017a and 2017b)]. CSIRO used 86,400 trials of this model and the MH370 debris reports to predict the POI was near the 7th Arc in a zone at latitudes -32° to -36° (and more likely near -35°). Wijeratne and Pattiaratchi (2017) used their ocean drift model to predict a POI latitude of -32.5 ± 0.4° [see also Thomas (2017)]. Godfrey (2020) predicted -34.13 ± 1.06° using the CSIRO drift tracks. Our analyses indicate prior estimates of crash location based on analyses of MH370 debris reports have deficiencies which cause systematic probability errors and underestimated uncertainties.

In this paper, which represents three years' work, we present a new method with multiple refinements for processing the CSIRO ocean drift model tracks to provide more accurate estimates of the most-likely POI latitude and especially the relative values and uncertainties of the probabilities at different locations along Arc 7. We

combine this new drift-based prediction, applying maximum likelihood probability theory and Bayesian statistics, with an improved estimate for the fuel/route/glide range probability (matching the SATCOM and GDAS data) and with the aerial search probability, to produce an improved prediction of the Point of Impact (POI) of 9M-MRO near Arc 7.

2. Summary of Results

2.1. MH370 debris drift probability

Figure 2.1-1 presents our prediction, based on MH370 debris reports and CSIRO drift tracks, of the latitude dependence of the probability of 9M-MRO crashing near Arc 7.
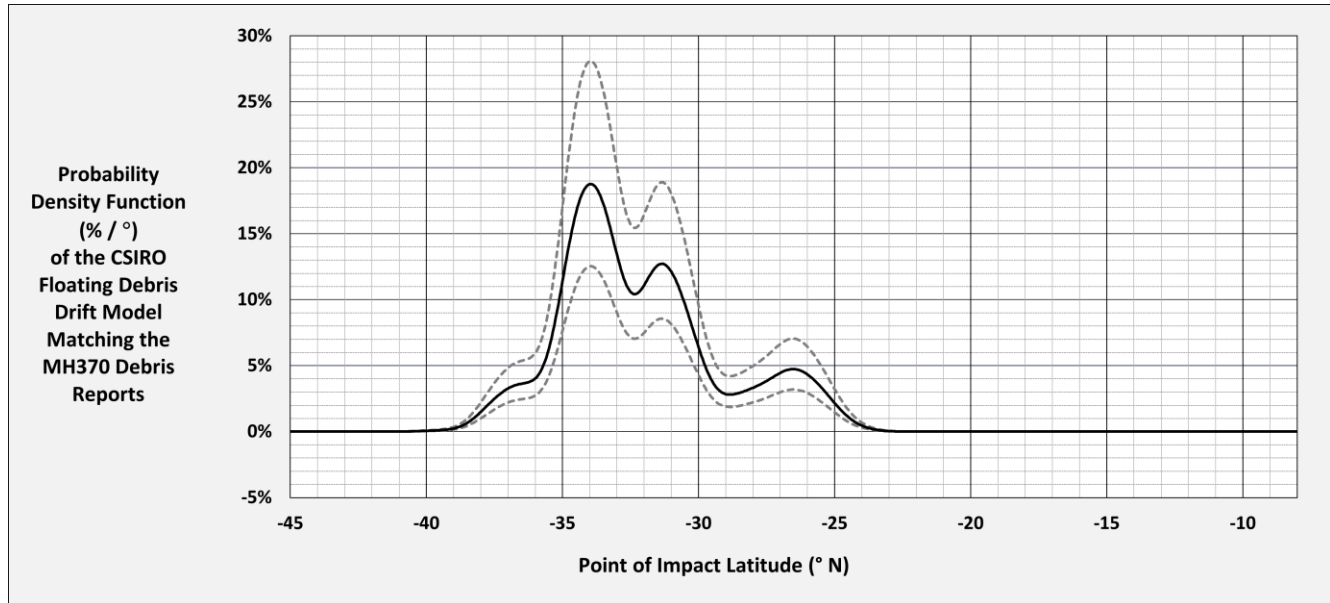
Figure 2.1-1 The PDF of the CSIRO floating debris drift model matching the MH370 debris reports

The solid black line is the value of the probability density function (PDF). It has an area under the PDF curve of unity, corresponding to the assumed 100% probability that the aircraft crashed near Arc 7 in the Southern Indian Ocean. The black dashed lines are the ± 1σ uncertainties in the PDF value, taking into consideration both the statistical errors and the localization error of the CSIRO ocean model.

The most-likely Point of Impact (POI) is at -34.0° latitude. This new impact latitude prediction is only 41 NM northeast along Arc 7 from the Last Estimated Position (-34.23 ± 0.5°N, 93.79°E) previously predicted by UGIB (2020) based on the satellite and weather data. The agreement between these two independent methods predicting crash location provides confidence that they are both substantially correct.

Figure 2.1-1 also indicates that, while the peak in drift probability is at -34.0°, the probability at nearby latitudes is significant over a considerable latitude range from -30° to -36°. This is not unexpected, because of the limited number of verified MH370 debris, their very long transit times (years), and especially because the debris windages and arriving dates are generally not well known. As discussed in Appendix D, having no reports of MH370 debris in Western Australia implies the possibility that the crash could have been slightly north of -34°, and possibly as far north as -31.4°. However, crash latitudes north of -33° appear to be ruled out by the aerial search.

Factors we used in making this drift probability prediction include the following:

1. seventeen reliable MH370 debris reports with unique locations and finding dates,

1. 86,400 drift trials predicted by CSIRO using the BRAN2015 ocean model with regional debiasing and with wind-induced drift parameters based on flaperon sea trials,

2. 86,400 drift trials predicted by CSIRO using the BRAN2015 ocean model with regional debiasing and CSIRO-estimated wind-induced drift parameters of generic (non-flaperon) debris,

3. the range of possible windages for generic MH370 debris, as estimated by CSIRO,

4. a Bayesian statistic for the localization error of BRAN2015 drift tracks, based on a CSIRO estimate,

5. errors in the BRAN2015 near-surface current speeds, and in the wind speeds at 10 m height, as estimated by us,

6. minimum and maximum reporting delays (i.e., the elapsed time between a debris arriving and being found) based on three classes of barnacle encrustation (many, few, or no attached barnacles), as estimated by us,

7. maximum likelihood estimation theory,

8. a processing method for computing a PDF and estimating its uncertainty, which is performed identically at each latitude "bin" of drift trial origins along Arc 7,

9. a Bayesian statistic for accommodating a large range of allowable windages (estimated by CSIRO) of generic MH370 debris, by means of adjusting the average transit drift speed of the CSIRO-generated trials, and

10. validation of the basic processing method, through non-blind, partially blind, and blind tests, which demonstrated the POI-latitude prediction accuracy given seventeen arriving dates at the MH370 debris sites.

2.2. Overall probability of MH370 crash latitude

Figure 2.1-1 below is our new prediction of the MH370 POI latitude based on the following factors:

1. the predicted probability of an autopiloted post-19:41 route matching the BTO, BFO, and GDAS data [i.e., the "route probability", which is unchanged from UGIB (2020)],

2. the predicted probability of such a route matching the fuel exhaustion time [i.e., the "fuel probability", which is updated from UGIB (2020)],

3. the probability of the post-fuel-exhaustion glide range (i.e., the "glide range probability", which is a new Bayesian statistic),

4. the probability of the post-crash aerial search not detecting the floating debris field (i.e., the "aerial search probability"), and

5. the probability of crash latitude based on our analysis of MH370 debris reports (i.e., the "drift probability" as given in Figure 2.1-1 above).

The solid black line in Figure 2.2-1 is the probability density function of MH370 impacting at different latitudes near Arc 7 based on the route, fuel, glide, aerial search, and drift probabilities. The red dashed vertical lines in Figure 2.2-1 are the boundaries of the latitude range of the Last Estimated Position (LEP) predicted by UGIB (2020) plus and minus the estimated probable glide distance of 47 NM (i.e., ± 1σ).

The close agreement of these two predictions, as indicated in Figure 2.2-1 below, implies the post-fuel-exhaustion glide range is probably less than 47 NM. A search from -32.9° to -36.4° along Arc 7, as indicated by

the two vertical green lines, and within 94 NM of Arc 7 would achieve about 90% cumulative detection probability (CDP).
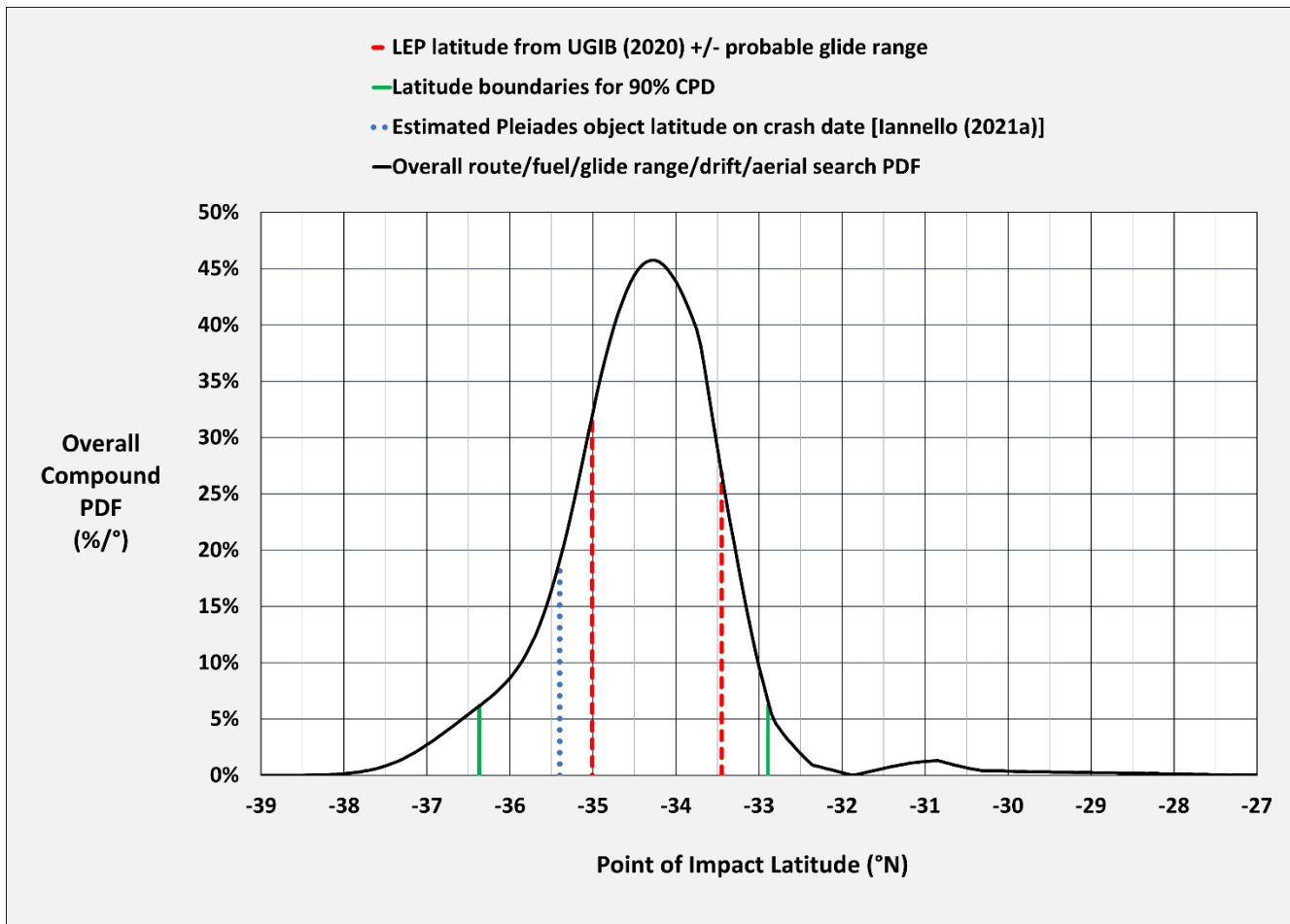
Figure 2.2-1 Probability of MH370 crash latitude

Appendix D presents a discussion of the possible range of effects on the MH370 search zone of (a) the non-reporting of MH370 debris in Western Australia and (b) the exclusion of the estimated aerial search probability.

2.3. Search area recommendations

Our prioritised recommendations for a future sea-floor search for the MH370 debris field are as follows:

1. Closely inspect those portions of the area from -32.9° to -36.4°, and within the previously searched width along Arc 7, which are:

   a. holidays (i.e., unsearched areas),
   b. areas with difficult terrain,
   c. areas with lower-quality sonar data, and
   d. previous contacts by GO Phoenix and Ocean Infinity which could be misclassified.

   This Zone 1 is the area enclosed by the white rectangle in Figure 2.3-1 below. When those portions listed above are completed, Zone 1 includes 22% of the cumulative detection probability (CDP). We recommend prioritising the portion of this Zone 1 which is also within the predicted 00:21:07 boundary,

which is shown by the red racetrack (i.e., Zone 1A). Zone 1B is that portion of Zone 1 which is outside the 00:21:07 boundary (i.e., outside the red racetrack), and this area is lower in priority than Zone 1A.

2. If #1 is unsuccessful, then widen the search to ± 70 NM from the UGIB Arc 7. This Zone 2 achieves a 90% CDP, and it is indicated by the purple racetrack in Figure 2.3-1.

3. If #2 is unsuccessful, then widen the search to ± 140 NM from the UGIB Arc 7. This Zone 3 achieves a 98% CDP, and it is indicated by the very large green racetrack in Figure 2.3-1.

These three recommended search zones (Zones 1-3) and the possible 00:21:07 boundary (which segregates Zone 1A from Zone 1B) are shown in Figure 2.3-1.
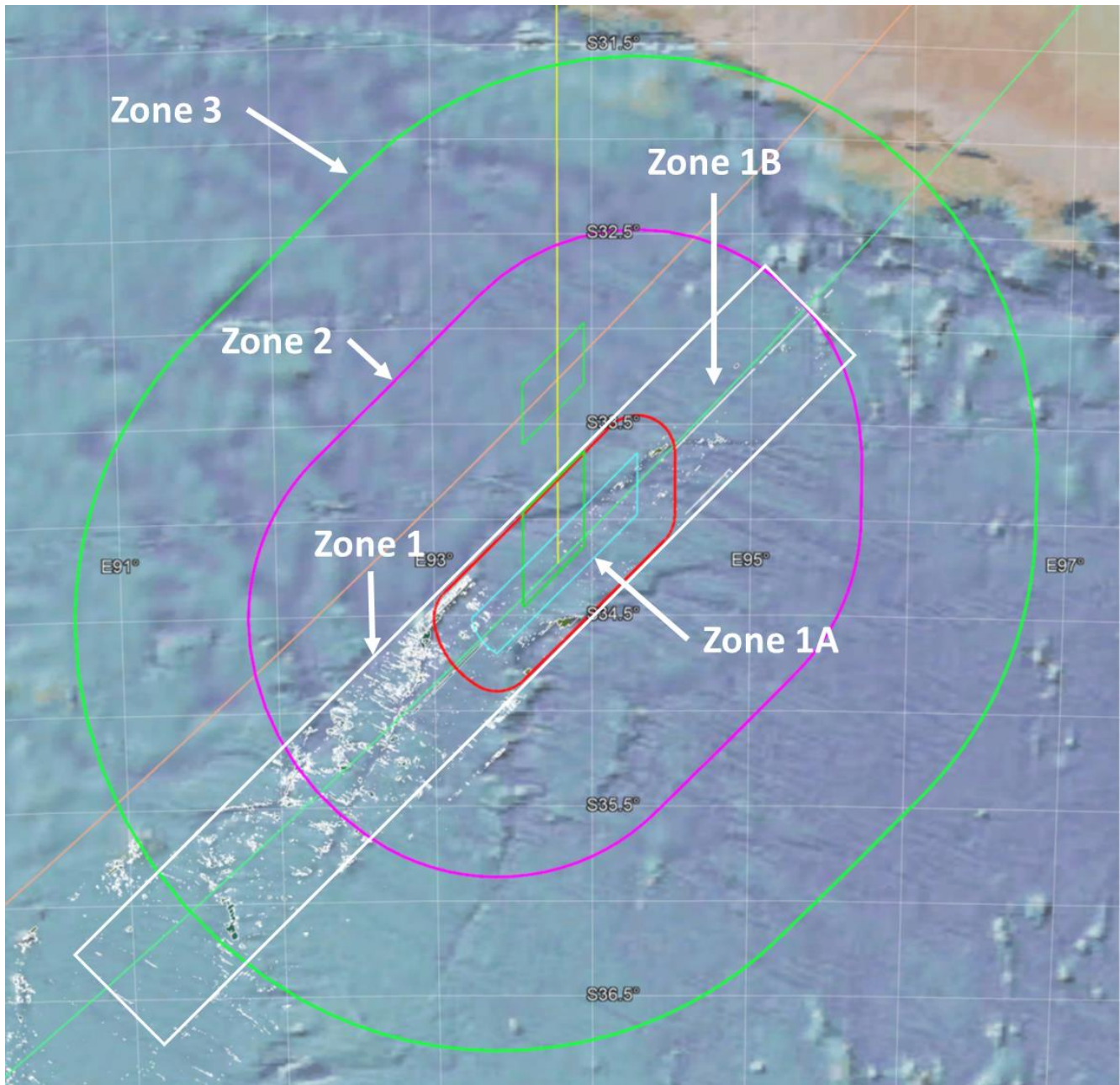
Figure 2.3-1 Map of recommended search zones

These recommendations are based on the inclusion of the aerial search probability and the assumption that it is reasonably accurate. If the aerial search probability were excluded, the northern ends of the recommended search zones would move 3.1° north, thereby doubling the search areas.

3. Drift Probability Method

The location of a floating debris cannot be uniquely predicted over long distances and time scales by simply stepping the time parameter in an ocean surface drift model in either the forward direction (by assuming an origin and a starting date) or in the reverse direction (by assuming a destination and an arriving date). This is because debris from multiple origins can arrive simultaneously at the same destination. Similarly, debris from the same origin can arrive at the same destination at different times, at different destinations at the same time, and at different destinations at different times. Despite these limitations, we can use conditional probability theory, the method of maximum likelihood estimation, Bayesian statistics, and a very large number of pseudo-random drift trial paths to determine which origin is statistically most likely to be true (i.e., which POI latitude has the highest probability of matching the debris finding locations and estimated arriving dates). A drift "trial" is one prediction of the path of a floating debris from an assumed origin (location and time).

For the MH370 drift problem, forward time modeling is preferred because we know the exact date on which the aircraft crashed, and, in most cases, we do not know the exact dates on which debris arrived at their finding locations. Thus, we increment time in the forward direction (a) from multiple assumed origins, finding the origin which produces the highest probability of arriving at a known destination or (b) from one assumed origin, finding the highest probability of arriving at one among many assumed destinations (i.e., a floating debris recovery site) at a time consistent with the arriving date. This forward-drift method works particularly well when matching historical data from undrogued drifters, which is used to verify and calibrate the ocean drift model. The forward-in-time drift model also works well for the MH370 debris drift problem because the debris origin is constrained by the satellite data to lie close to Arc 7 in the SIO. Thus, our origin search is effectively a one-dimensional probability-optimization problem. In this work, we used POI latitude as the origin search dimension. Having the POI area constrained to be near an arc simplifies the POI prediction problem, and predictions of POI latitude are possible using the method of maximum likelihood estimation.

We developed, refined, and validated a method of predicting the latitude of the MH370 POI near Arc 7, using as inputs various sets of known and predicted arriving dates at the same sites where MH370 debris were found and reported. Additional details of our drift probability method may be found in Appendix B.

3.1. CSIRO drift tracks

We obtained from CSIRO two sets of 86,400 predicted trial drifter tracks using the ocean model BRAN2015. Each trial was assumed to have originated at a unique location near Arc 7, in an array with a fairly uniform areal density and within 25 km of Arc 7 between -8° and -44° latitude. The location (latitude, longitude) of each trial drifter was predicted by CSIRO at 1 day intervals up to 1,027 days after crash (DAC). We call this time span from 0 to 1,027 DAC the "calculation window". We call the time and location data for each trial as 1,028 "trial-days". So, we have 86,400 trials, and each trial has 1,028 trial-days, with one trial-day comprising one location and one date for one trial. One set of 86,400 trials used the drift parameters CSIRO determined for the flaperon by sea trials with a cut-down flaperon. The other set was for non-flaperon debris and used a zero leeway angle and a 1.2% windage (with wind speed at 10 m height).

3.2. MH370 debris reports

There are twenty-one "positive" reports of debris classified by the Malaysia Ministry of Transport as being confirmed, almost certain, highly likely, or likely to be from MH370 [see the eighteen debris reports by the Malaysia Ministry of Transport (2017a-2017r)]. Three of these debris finds are redundant in location and time,

and two debris arrived too late to be analysed using the 1028-day calculation time window of the CSIRO drift tracks. Blaine Gibson found, collected, and reported numerous MH370 debris [Bowker and Galineau (2016), BBC News (2016), and Thomas (2021)]. The ATSB issued six reports of their analyses of MH370 debris [ATSB (2016a – 2016f)].

We did not include Debris Site # 4 (i.e., "D4", the debris called "Roy") in our predictions because it is a low-probability event for which the total number of CSIRO drift trials is inadequate to reliably predict probabilities using reasonable distance and time error limits. In two additional cases (our Debris Sites # 27 and #30), based on photographs of the found items, we included debris in our analysis that were not assessed by Malaysia Ministry of Transport. From these combined twenty-three (likely or better) MH370 reports, we analysed seventeen unique and reliable MH370 debris reports (each with a different location and reporting date) which had an adequate number of CSIRO trial predictions passing nearby to predict the latitude of the Point of Impact (POI) along Arc 7 using a basic processing method for probability estimation.

We did not process duplicate debris reports, having the same finding location and date, because they do not provide complete and independent information. When multiple MH370 debris were reported as a group, they were found previously at unknown dates but then collected and reported simultaneously. Thus, while there is some additional information in knowing that more than one debris arrived at certain locations, the lack of independent timing information for all reported debris is a drawback for all analysis methods.

Table 3.2-1 lists the MH370 positive debris reports. The seventeen items we analysed in detail are indicated by the cells shaded green. Appendix D provides additional details concerning our analyses of "negative" debris reports in Western Australia.

Table 3.2-1 MH370 debris reports

Debris Site # (D)	Malaysia Department of Civil Aviation Safety Investigation Report — Item #	Malaysia Department of Civil Aviation Safety Investigation Report — Classification of Being from 9M-MRO	Finding Date (dd-mm-yyyy)	Description	Location of Debris Site	Latitude (°N)	Longitude (°E)	Barnacle Encrustation	ρ = Distance Limit (km)	τ = Time Error Limit = Half Width of Time Window (days)	δ = Reporting Delay (days)	Transit Speed Correction Factor (TSCF) (%)	Reporting Date (days after crash)	Estimated Arriving Date (days after crash)
									Method III Window Optimization Results at -34°					
1	--	Not identifiable	2-Jul-2014	MAS towelette packet	Thirsty Point Beach, Cervantes, Australia	-30.51000	115.06000	None					116	
2	1	Confirmed	29-Jul-2015	Right flaperon	Saint-Andre de la Reunion	-20.91618	55.64915	Many	26	15	0	0.0%	508	508
3	--	--	15-Dec-2015	Panel	Sainte Luce, Madagascar	-24.75790	47.19251	None					647	
4	4	Almost certain	23-Dec-2015	Engine nose cowl name plate "Roy"	Klein Brak River, Mossel Bay, South Africa	-34.09377	22.14991	Many					655	
5	2	Almost certain	27-Dec-2015	No.7 flap fairing "676EB"	Daghatane Beach, Paindane Resort, Mozambique	-24.07806	35.49980	None	39	43	7	12.3%	659	652
6	24	Not identifiable	15-Feb-2016	Panel #1	Sainte Luce, Madagascar	-24.75790	47.19251	None					709	
7			15-Feb-2016	Panel #2				None					709	
8	3	Almost certain	27-Feb-2016	Right horizontal stabiliser panel "No Step"	Paluma Sandbank, Vilanculos, Mozambique	-22.08857	35.51902	None	39	81	7	15.5%	721	714
9	5	Almost certain	30-Mar-2016	Door R1 stowage closet	Var-Brûlé Beach, Rodrigues	-19.73871	63.47163	Few	18	80	30	0.0%	753	723
10	6	Almost certain	24-Apr-2016	Engine right fan cowl	South of Chidenguele, Mozambique	-24.95802	34.19637	None	--	--	--	--	778	#N/A
11	7	Likely	30-Apr-2016	Wing to body fairing	Anvil Bay, Chemucane, Mozambique	-26.45587	32.93243	None	--	--	--	--	784	#N/A
12	10	Confirmed	15-Mar-2016	Trailing edge of left outboard flap	Ilot Bernache, Mauritius	-20.02338	57.70139	None	54	57	7	4.5%	738	731
13	9	Highly likely	22-May-2016	Upper fixed panel forward of the left flaperon	Maçaneta Peninsular, Maputo Bay, Mozambique	-25.86302	32.74599	None	--	--	--	--	806	#N/A
14	8	Highly likely	24-May-2016	Flap support fairing tail cone	Gris-Gris Beach, Mauritius	-20.52245	57.53762	None	39	94	7	2.8%	808	801
15	11	Highly likely	6-Jun-2016	Seat back trim panel encasing the IFE monitor	Riake Beach, Nosy Boraha Island, Madagascar	-16.78694	49.98528	None	39	39	97	0.0%	821	724
16	12	Likely	6-Jun-2016	Bottom panel of wing or horizontal stabilizer				None					821	
17	13	Not identifiable	6-Jun-2016	Unknown	Riake Beach, Nosy Boraha Island, Madagascar	-16.78694	49.98528	None					821	
18	14	Not identifiable	6-Jun-2016	Interior panel				None					821	
19	15	Highly likely	6-Jun-2016	Upper fixed panel forward of the right flaperon				None					821	
20	16	Almost certain	12-Jun-2016	Cabin interior panel	Antsiraka Beach, Nosy Boraha Island, Madagascar	-16.81372	49.97755	None	38	37	103	0.0%	827	724
21	17	Not identifiable	12-Jun-2016	Unknown	Antsiraka Beach, Nosy Boraha Island, Madagascar	-16.81372	49.97755	None					827	
22	18	Highly likely	12-Jun-2016	Right forward nose landing gear door				None					827	
23	19	Confirmed	20-Jun-2016	Outboard flap	Kojani Island, Pemba, Tanzania	-5.05607	39.86809	Few	39	9	8	0.0%	835	827
24	20	Highly likely	21-Jun-2016	Right aft wing to body fairing	Kosi Bay Mouth, Kwa Zulu Natal, South Africa	-26.89381	32.88089	None	39	69	87	0.0%	836	749
25	25	Not identifiable	15-Jul-2016	Unidentified panel	St. Luce, Madagascar	-25.00000	47.00000	None					860	
26	21	Not identifiable	18-Jul-2016	Panel	Northern Kwa Zulu Natal, South Africa	-26.89381	32.88089	None					863	
27	--	--	19-Aug-2016	Panel	Praia de Rocha, Mozambique	-23.92967	35.52710	None	55	35	139	0.0%	895	756
28	22	Almost certain	26-Aug-2016	Right vertical stabiliser	Linga, Linga, Mozambique	-23.73931	35.40077	None	54	53	144	0.0%	902	758
29	--	Confirmed	1-Sep-2016	Right engine inner vortex generator	Maroantsetra Beach, Antongila Bay, Madagascar	-15.44690	49.71870	None	--	--	--	--	908	#N/A
30	--	--	1-Sep-2016	Panel	Antsiraka Beach, Nosy Boraha Island, Madagascar	-16.81372	49.97755	None	45	55	15	0.0%	908	893
31	23	Not identifiable	1-Oct-2016	Possible interior galley part	Riake Beach, Nosy Boraha Island, Madagascar	-16.78694	49.98528	None					938	
32	26	Highly likely	23-Dec-2016	Right aileron	Nautilus Bay, South Africa	-34.22081	21.97875	None					1,021	
33	27	Highly likely	27-Jan-2017	Right wing No. 7 flap support fairing	Mpame Beach, South Africa	-32.09748	29.06285	Few					1,056	
34	--	--	20-Aug-2018	Panel	Riake Beach, Nosy Boraha Island, Madagascar	-16.78694	49.98528	None					1,626	
35	--		15-Aug-2020	Spoiler panel	Ferreira Town, Jeffreys Bay, South Africa	-34.041	24.910						2,352	

Bobby Ulich and Victor Iannello   June 6, 2023   Improved Prediction of MH370 Crash Location Based on Drift Modeling of Floating Debris

3.3. Trial drifter origins

Figure 3.3-1 shows the locations near Arc 7 of the origins of the 86,400 trial drifters, the 23 MH370 debris sites, and those 17 debris sites we used in our analyses.
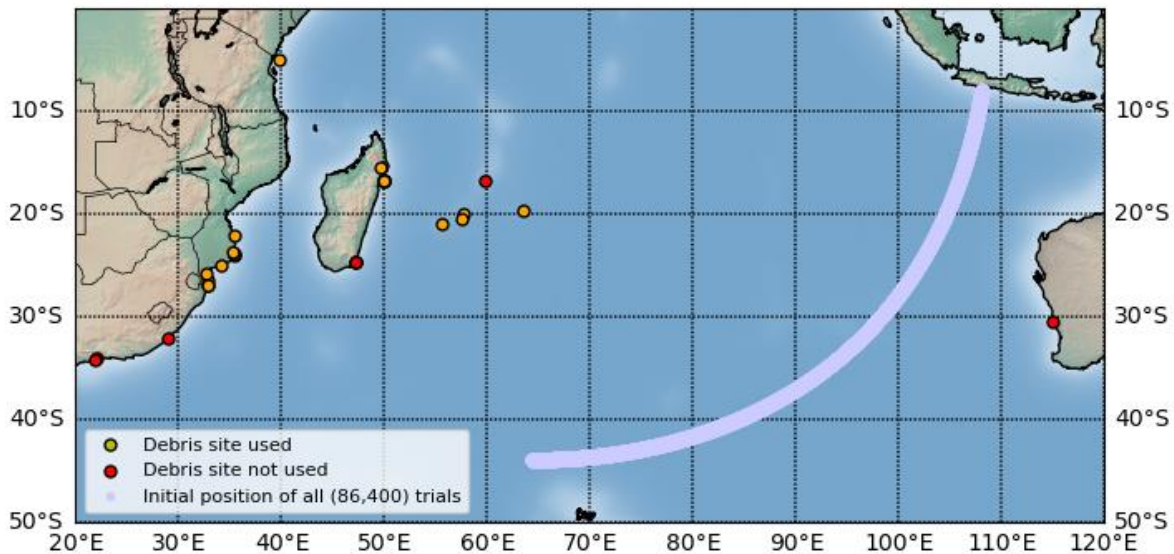

Figure 3.3-1 Trial drifter origins and MH370 debris sites

Each 1°-wide latitude bin along Arc 7 contains an average of about 2,300 trial origins.

3.4. Probability density function

For MH370, we calculated the POI-latitude probability density function (PDF, with units of % / °) as the (area-normalized) fraction of trials, originating in 1°-wide POI-latitude "bins" of trial origins near Arc 7, which fall within both distance and time "windows" at a given debris site for a given arriving date. A trial-day which is within both the time and distance windows is a plausible match to the debris report. The binned probabilities are then scaled so the sum of the probability densities over all POI-latitude bins is unity, matching the known probability (100%) that a MH370 debris was reported to have been found there and then.

Appendix A provides additional theoretical considerations and the probability equations we used in our drift probability predictions.

3.5. Time and distance windows

The widths of the time and distance windows, and the reporting delay (which sets the center of the time window), are variables which are adjusted to maximize the likelihood (i.e., the probability) that a trial drifter originating near Arc 7 in one bin of POI latitudes will be counted simultaneously within both time and distance windows at the debris reporting site, and thus be considered as an acceptable match in location and time to the MH370 debris report. We restricted the counting process so that a trial was never counted more than once for one debris even when there were multiple trial-days from the same trial in both windows. When that occurred, we counted only the trial-day nearest the debris site.

Because of the low average drift speed, a trial track can be within the distance limit of a debris site for several to dozens of days. In addition, the same trial may pass within the distance windows for multiple debris sites, and it is not excluded from being counted at more than one debris site. Each single-debris PDF uses all 86,400 trials.

4. Prediction Method I

The most basic probability prediction method (which we call Method I) applies the same time and distance window dimensions to all POI-latitude bins for a given debris. For debris found with no barnacles or with a few attached barnacles, the actual arriving date is unknown because the debris could have arrived months prior to being found. So, except for the flaperon, the center of the time window is a third fitted parameter, called the reporting delay, which is the elapsed time between the predicted arrival of the debris and the date it was found and reported. In our probability-maximizing fits, the reporting delay is simply the time between the center of the time window and the reporting date. Thus, the time window has two dimensions: the reporting delay sets its center date, and the half-width parameter sets its duration.

4.1. Distance limit

We allow the integer distance limit (ρ) to vary from 10 to 56 km. The upper limit of ρ corresponds to a maximum circle diameter of 112 km = 60 NM = 1.0° of arc within which trial drifters are counted as being within the distance limit. When a trial-day is in the "distance window" it is counted as being a plausible match to a landfall at the debris report location.

4.2. Time window width

We allow the integer half-width of the time window (τ) to vary from 7 to 100 days. The full width of the time window is $2 \cdot \tau + 1$ days. We found that the full width of the optimized time window is typically about the duration of an arriving wave. The upper limit on τ of 100 days limits the number of arriving waves of trial drifters which may be inside the time window to about two. Having a larger number of trials than 86,400 would improve the statistics and allow narrower time windows but adding a few marginal debris sites to the analysis might not significantly improve the accuracy of the POI-latitude prediction, especially if those additional debris reports were for barnacle-free debris and therefore had loose constraints on the arriving dates. When a trial-day is in the "time window" it is counted as being a plausible match to the debris report finding date.

4.3. Reporting delay

The reporting delay is bounded by a range of many months' duration for barnacle-free debris, but it is otherwise free to vary within its bounds because we don't know the actual arriving date, only that it was found after an unknown but possibly considerable length of time. Barnacle-free debris are typically less effective in discriminating crash latitude because the arriving date is loosely constrained. Barnacle-free debris depend primarily on their finding locations to discriminate crash latitude, rather than on their arriving date.

We allow the reporting delay (δ) to be from 10 to 150 days for debris with no barnacles attached, from 5 to 30 days for the two debris we analysed (D9 and D23) which were found with a few barnacles attached, or zero days for the flaperon (D2), which was found with many barnacles attached. Thus, the estimated arriving date has an allowed range of values which depend on the number of barnacles on the found debris. Those debris with no barnacles have a very wide range of allowed arriving dates (about 5 months plus the half-width of the time window). Therefore, the PDFs of those debris will suffer degraded temporal resolution, and they will discriminate mostly by spatial differences. On the other hand, those debris with many or a few barnacles will discriminate the POI latitude more strongly because they allow both spatial and temporal differences to be discriminated.

We also imposed a limit of 200 days prior to the reporting date for the earliest date in the time window for barnacle-free debris. This reduces the possibility that the time window will include arrivals from a previous arriving wave.

5. Validation Tests of Method I

Given the vast distance, long interval, and complexity of ocean currents, it might seem that seventeen is an inadequate number of debris items from which a POI can be inferred. We tested for that possibility by conducting multiple numerical experiments, in which we chose a hypothetical POI and used the CSIRO model to determine a synthetic set of seventeen arrival dates, from which we then attempted to infer the (known, but not to the inference algorithm) POI latitude. As we show below, these tests showed good agreement between the predicted POI and the hypothetical POI, demonstrating that seventeen is indeed a more-than-adequate number of debris reports, because of their geographically dispersed locations. These tests assume that the CSIRO model is "truth", which cannot be totally accurate, so while our experiments say something about the error due to the limited number of debris items, they do not provide an estimate of the total POI prediction error (which is included in our analysis as discussed later in this paper in Section 11).

We conducted two test exercises to develop, refine, assess, and validate a method for predicting the POI latitude, given a set of randomly selected arriving dates at the seventeen MH370 debris sites. The POI locations assumed in these exercises were located close to the UGIB (2020) Arc 7. We conducted both "non-blind" and "blind" validation tests of Method I with 1° latitude bins. In the "non-blind" tests, one of the authors (Iannello) provided sets of seventeen "synthetic" arriving dates and the associated hypothetical POI latitudes to the other author (Ulich). In the "blind" tests, Iannello provided only the arriving date sets to Ulich, without the associated assumed POI latitudes. The accuracy of the prediction Method I was evaluated by comparing the assumed (by Iannello) POI latitudes with the predicted (by Ulich) POI-latitude values for the non-blind and the blind tests. All comparisons matched closely, validating the accuracy of the method we used to determine the POI latitude.

Note that our validation tests do not assess the accuracy of the BRAN2015 drift model used by CSIRO to generate the drift trials, nor do they address the impact of loosely-constrained MH370 arriving dates. That is, the validation tests used dates with zero reporting delays, whereas in the MH370 case most of the debris were free of barnacles when found and therefore the arriving dates were poorly determined. This degrades the latitude resolution in the MH370 case compared to that of the validation tests.

We call each set of seventeen arriving dates a "test case". It comprises one randomly selected arriving date for each MH370 debris site. The process to select random arriving dates used the same CSIRO drift trials that we used to predict the POI latitude, assuring that the selected dates fall within the predicted distributions of arriving dates.

Additional details of the validation test method are given in Appendix C.

5.1. Non-blind and partially blind test results

We first conducted two non-blind tests and one partially blind test using the basic processing Method I. For the non-blind tests, the correct value of the assumed POI latitude was known to the person (Ulich) who developed, operated, and modified the computer program which predicted the POI latitude. This procedure allowed the prediction method to be assessed and refined as needed against known POI latitudes.

The general process was for Iannello to assume one specific latitude of trial origins and then select one trial-day from the CSIRO list which passed near each of the seventeen MH370 debris sites. The input data for Ulich to evaluate the latitude retrieval process was this list seventeen 17 arriving dates, one at each MH370 debris site.

We started with two non-blind "tests" of the POI-latitude retrieval process, with four "cases" for each test. That is, there are four sets of random dates (i.e., four cases), all originating near the same assumed POI for each test. Having four cases for each test latitude allows the determination of an approximate mean and standard deviation for the prediction error in POI latitude. Thus, we can avoid drawing a premature conclusion about performance, which might occur if the assessment were based on a single case. Having four cases provides a

useful degree of statistical analysis, using the estimated mean and the standard deviation of the latitude prediction errors.

For the two non-blind tests, Iannello assumed the POI latitudes were -28.0° and -34.2°. Iannello provided these values to Ulich, who processed the test cases, refining the method as needed, until the predictions were close to the known POI latitudes. We evaluated the precision and the accuracy of the prediction for each test case at these two latitudes.

Iannello also provided one test which was "partially blind". In this test, Iannello communicated the POI latitude to Ulich as -30.0 ± 0.5°. So, for this test only, Iannello indicated the true latitude was one of two values (-29.5° or -30.5°) which are 1° apart. This is a useful test, because a successful prediction method should have a latitude resolution and accuracy better than 1°, and this would indicate a useful prediction was possible. There were four cases for the partially blind test, the same as for each of the two non-blind tests.

Table 5.1-1 presents the results for the two non-blind tests and the one partially blind test.

Table 5.1-1 Non-blind and partially blind test results

Test Type	Test #	Mean Origin of Trials Used to Generate the Random Date List for One Test		Case	Test Case #	# Debris Sites Used in Joint PDF	Average % Rank of Arriving Dates of Sites Used in Joint PDF	Predicted POI Latitude Value ± 1σ (°S)	True Error in Sigmas (σ)	Mean Latitude Prediction Error (°)
		Latitude (°N)	Longitude (°E)							
Non-Blind	1	-28.00	99.9	A	25	15	65%	-28.12 ± 0.49	-0.24	-0.07
				B	26	16	39%	-28.02 ± 0.34	-0.05	
				C	27	17	45%	-28.21 ± 0.28	-0.78	
				D	28	14	52%	-27.95 ± 0.50	0.10	
	2	-34.20	93.8	A	17	17	44%	-34.14 ± 0.21	0.28	0.13
				B	18	15	58%	-34.04 ± 0.34	0.47	
				C	19	16	53%	-34.04 ± 0.16	1.01	
				D	20	14	49%	-34.05 ± 0.24	0.62	
Partially Blind	3	-30.50	97.7	A	21	16	58%	-30.75 ± 0.23	-1.07	-0.23
				B	22	17	44%	-30.80 ± 0.57	-0.52	
				C	23	16	48%	-30.85 ± 0.23	-1.49	
				D	24	15	59%	-30.52 ± 0.69	-0.03	

We analysed the four cases for each of these three tests. The twelve predicted POI latitudes are listed in the third column from the right in Table 5.1-1 . The 1-σ uncertainties in these predictions were 0.16-0.69°. The second column from the right lists the prediction errors as the number of sigmas of estimated error, which ranged from +1.01 σ to -1.49 σ. Therefore, no statistically significant prediction errors occurred in these twelve test cases. Thus, the prediction accuracy is confirmed to be within the estimated prediction error, for these non-blind and partially blind tests.

The method used by Ulich for the validation tests was to inspect the Method I PDFs for a large number of debris sites. Then a 3-bin wide Region of Interest in latitude was located so it included the largest common peak. The window dimensions were then optimized by maximizing the average probability in the ROI for each debris site. Occasionally, the ROI was iteratively shifted by one or two bins so that the two highest joint PDF values were inside the ROI. Then a gaussian was fit to the three joint PDF values in the ROI to interpolate the predicted latitude.

5.2. Blind test results

The purpose of the "blind" test exercise is to determine the accuracy of the retrieved POI latitude, using the same method developed during the non-blind test exercise. If the demonstrated accuracy is acceptable, then the POI retrieval method is validated.

For the four blind tests (with four cases each), Iannello selected the latitudes but did not communicate those to Ulich. So, there are a total of sixteen blind test cases. Iannello scored the sixteen predictions made by Ulich.

Table 5.1-1 presents the results for the four blind tests with four cases each.

Table 5.2-1 Blind test results

| Test Type | Test # | Mean Origin of Trials Used to Generate the Random Date List for One Test | | Case | Test Case # | # Debris Sites Used in Joint PDF | Average % Rank of Arriving Dates of Sites Used in Joint PDF | Predicted POI Latitude | True Error in Sigmas (σ) | Mean Latitude Prediction Error (°) |
		Latitude (°N)	Longitude (°E)					Value ± 1s (°S)		
Blind	4 (POI 1)	-26.95	100.6	A	7	14	57%	-27.00 ± 0.19	-0.27	-0.18
				B	10	14	57%	-26.96 ± 0.25	-0.03	
				C	13	17	39%	-26.95 ± 0.20	-0.02	
				D	5	15	54%	-27.60 ± 0.50	-1.30	
	5 (POI 2)	-28.30	99.6	A	9	17	42%	-27.97 ± 0.24	1.40	0.28
				B	2	15	56%	-27.76 ± 0.73	0.73	
				C	15	15	58%	-28.10 ± 0.44	0.46	
				D	12	16	60%	-28.24 ± 0.34	0.18	
	6 (POI 3)	-29.75	98.4	A	6	15	62%	-29.97 ± 0.49	-0.44	-0.21
				B	1	16	39%	-30.08 ± 0.39	-0.84	
				C	11	14	46%	-29.79 ± 0.41	-0.09	
				D	16	14	55%	-30.01 ± 0.27	-0.94	
	7 (POI 4)	-39.80	84.6	A	3	14	42%	-39.49 ± 1.08	0.29	-0.22
				B	14	14	48%	-39.96 ± 0.54	-0.30	
				C	8	14	43%	-40.56 ± 1.08	-0.70	
				D	4	17	48%	-40.05 ± 0.46	-0.54	

Again, we observed close agreement between the "blind" test latitudes and the predictions. These sixteen POI-latitude predictions had 1σ uncertainties ranging from 0.19° to 1.08°, and their prediction errors were in the range from -1.30 σ to +1.40 σ. Therefore, over the latitude range from -27° to -40°, the blind tests verified the prediction accuracy of Method I, with the caveat that a debris in fact drifted at the same average transit speed predicted by the CSIRO ocean model. Deviations in drift speed produce different arriving dates from the same POI, or the same arriving date from different POIs. The uncertainties in the actual drift speeds of MH370 debris are evaluated quantitatively later in this paper in Section 8, because this is a contributor to the uncertainty in the predicted MH370 POI latitude (and which is not addressed by the validation tests).

5.3. Accuracy of Method I

Figure 5.3-1 compares the validation test predictions with the true latitude values.

Each prediction of a validation test is shown by an "X" symbol in Figure 5.3-1. They all lie close to the line at 45°, which marks perfectly accurate latitude retrieval. Each retrieved (i.e., predicted) latitude has ± 1σ error bars indicating the estimated precision of the retrieved latitude. Note those error bars vary with latitude, being larger at the extreme values of latitude. This occurs because those latitudes in the vicinity of -40° or -28° have less-probable landfalls at the actual MH370 debris sites. This increases the statistical noise in the predicted

probabilities. The error bars in Figure 5.3-1 are smallest near the center of the latitude range, where more trials are predicted to arrive at MH370 debris sites.
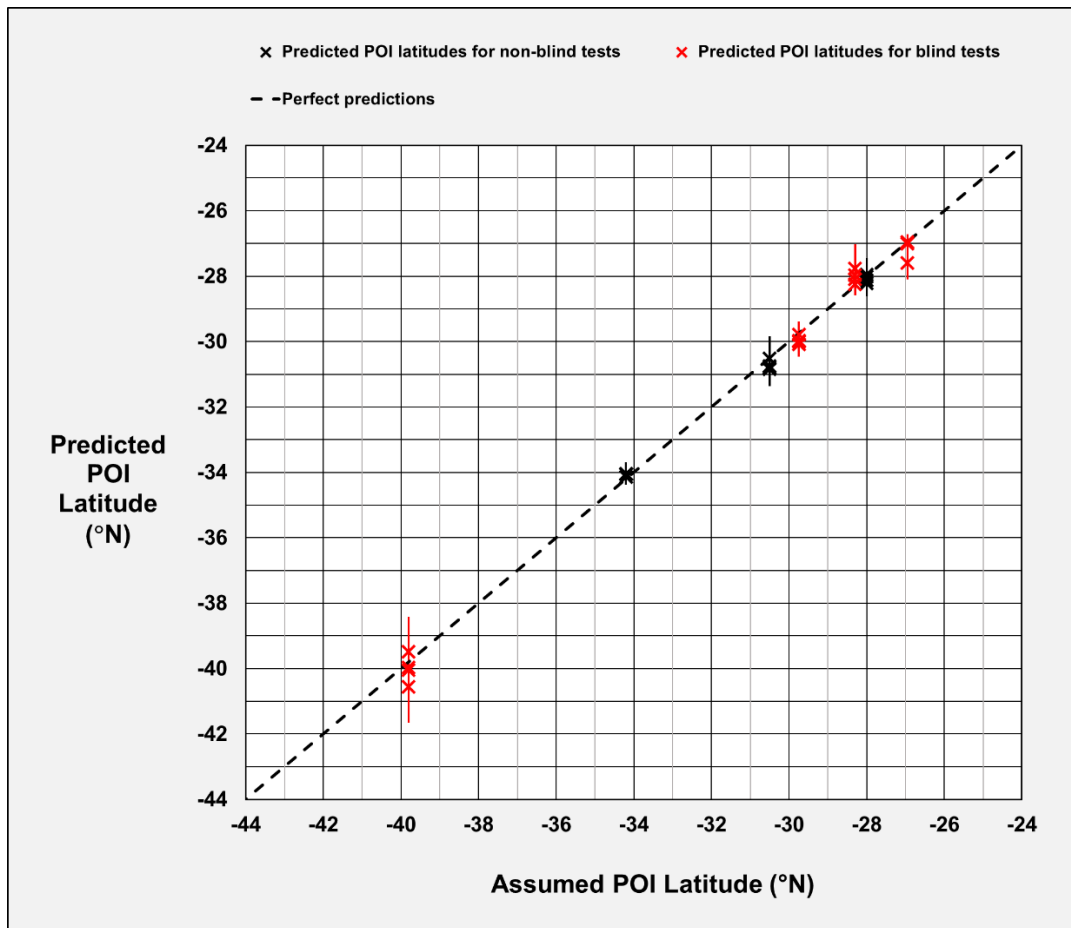

Figure 5.3-1 Results of validation tests

These results demonstrate the approximate precision with which the retrieval algorithm can predict the most likely MH370 POI latitude. The accuracy of the MH370 prediction is improved relative to the validation test cases because the debris sites we use are where MH370 debris were found, and we have no corresponding lists of likely destinations for debris originating from different latitudes. However, the MH370 prediction will also be somewhat degraded because we have reporting dates, not arriving dates, for all the debris except the flaperon. The net effect is the accuracy of the MH370 prediction should be comparable to the validation tests. Later in this paper, we show that a bias is introduced into predictions using this method due to the choice of time and distance windows for each debris.

6. Prediction Methods Used in Prior Drift Studies

Minor variations of the basic prediction Method I were used in all previous studies of MH370 debris drift. Probability predictions using Method I contain errors because the window dimensions are not optimal at all POI latitudes. That is, in Method I the likelihood is not maximized at all latitudes on Arc 7. Choosing one set of time/distance window dimensions enhances the predicted probabilities at certain crash latitudes but generally degrades the predicted probabilities at other crash latitudes. Our 28 validation tests demonstrated that it is possible to locate a single dominant latitude bin (or a pair of adjacent bins of comparable value) using multiple iterations of Method I, but the true probability at this "peak" latitude will be overestimated by a significant but

unknown factor. In addition, the probabilities of secondary peaks will be <u>underestimated</u> by significant and unknown factors. Therefore, in Method I the relative probabilities among peaks in the probability density function of POI latitude are highly uncertain. This deficiency lessens the utility of all prior published drift predictions for planning a search for 9M-MRO's debris field on the sea floor.

6.1. Limitations of prior drift studies

We illustrate this deficiency of Method I in Figure 6.1-1 and in Figure 6.1-2 below. Figure 6.1-1 is a plot of the PDF for the flaperon with window dimensions optimized for -34° POI latitude. In this case there is a huge peak at the optimized latitude bin. Note also in Figure 6.1-1 that we compute (and carry forward) the error bars on all latitude bins in drift PDFs. In this case the errors are statistical and result from the finite number of trials being processed and counted. This type of error analysis was not done in previous MH370 drift studies, and it is useful in assessing the reliability of conclusions regarding the crash location.
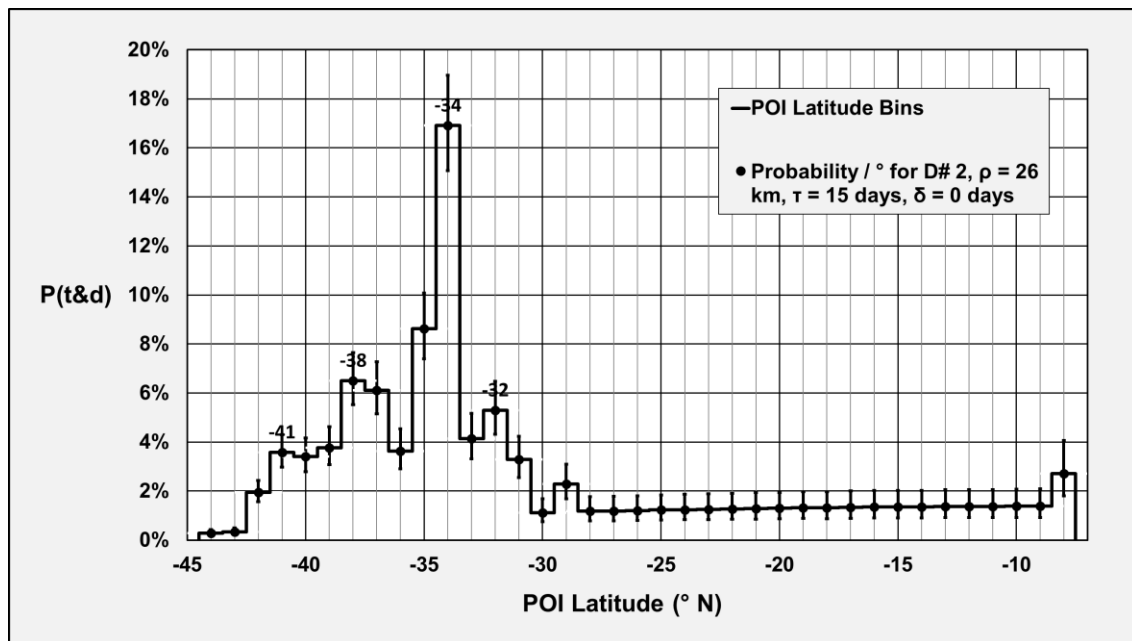

Figure 6.1-1 Method I probability for flaperon with windows optimized at -34°

Next, Figure 6.1-2 below is the same type of plot but with the window dimensions optimized at -38° POI latitude. Now the dominant peak is at the optimized bin at -38°, and a secondary peak is at -34°. Note the ratio of the two peaks at -34° and at -38° changed dramatically. Which one is correct: Figure 6.1-1 or Figure 6.1-2? The correct answer is that neither one is accurate.

We believe that the MH370 latitude prediction will always be <u>biased</u> using Method I, no matter how one chooses the single set of window dimensions. There is no "subjective" or "objective" way to do this which does not favor one bin or one latitude region and disfavor others. The deficiency arises from using one set of window parameters across the whole latitude range, no matter how the that one set of window parameters is determined.

As we have demonstrated above, prediction Method I (used in all prior drift studies) fails to produce an accurate probability curve. This deficiency impedes efficient searching for the aircraft debris field along Arc 7. Method I can, if used with care and in certain cases, be used to find the most probable latitude, but it can't be used to determine the relative probabilities of secondary peaks with a useful degree of accuracy.
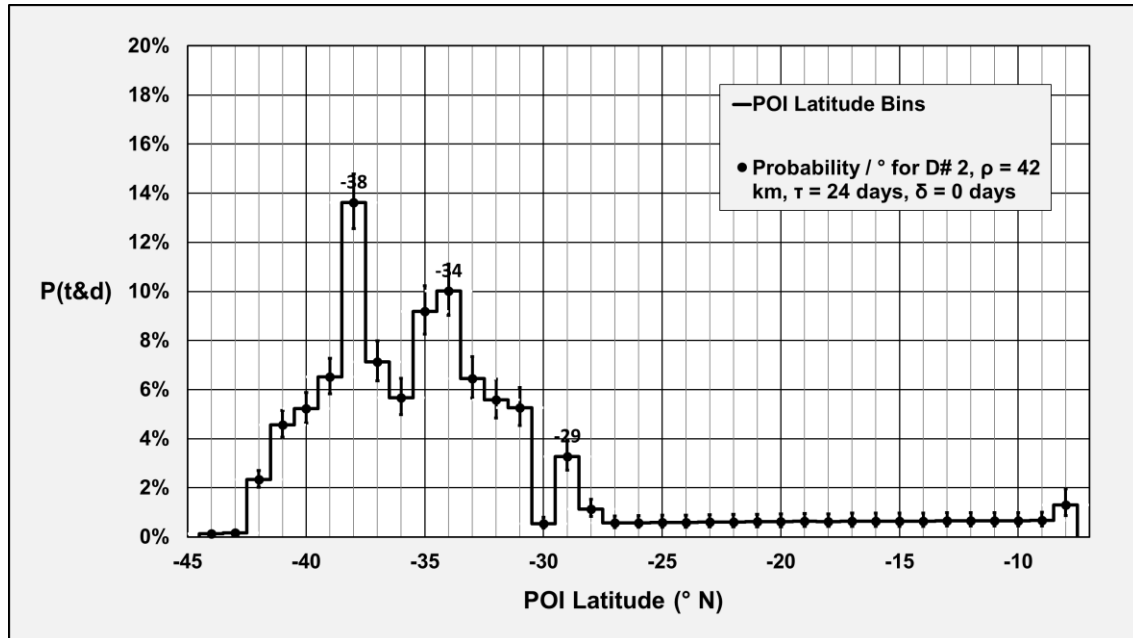
Figure 6.1-2 Method I probability for flaperon with windows optimized at -38°

7. Prediction Method II

The key to eliminating this bias is to perform identical calculations for each latitude bin. This is what we have done in prediction Method II, objectively performing the same maximum likelihood estimation process independently for each latitude bin. In Method II we fit the time and distance window widths and the reporting delay at each POI-latitude bin. Since there are dozens of POI-latitude bins (generally we used latitude bins 1° wide), the enhanced accuracy of Method II comes at a very large cost in computing time compared to Method I.

7.1. Flaperon Method II PDF

The PDF for the flaperon using prediction Method II is shown in below in Figure 7.1-1.

The two PDF peaks in Figure 7.1-1 are quite different in relative probability than was indicated by the two Method I examples shown above in Figure 6.1-1 and in Figure 6.1-2. We believe Method II provides much better accuracy than Method I. Now we can see there are actually two PDF peaks of comparable probability.
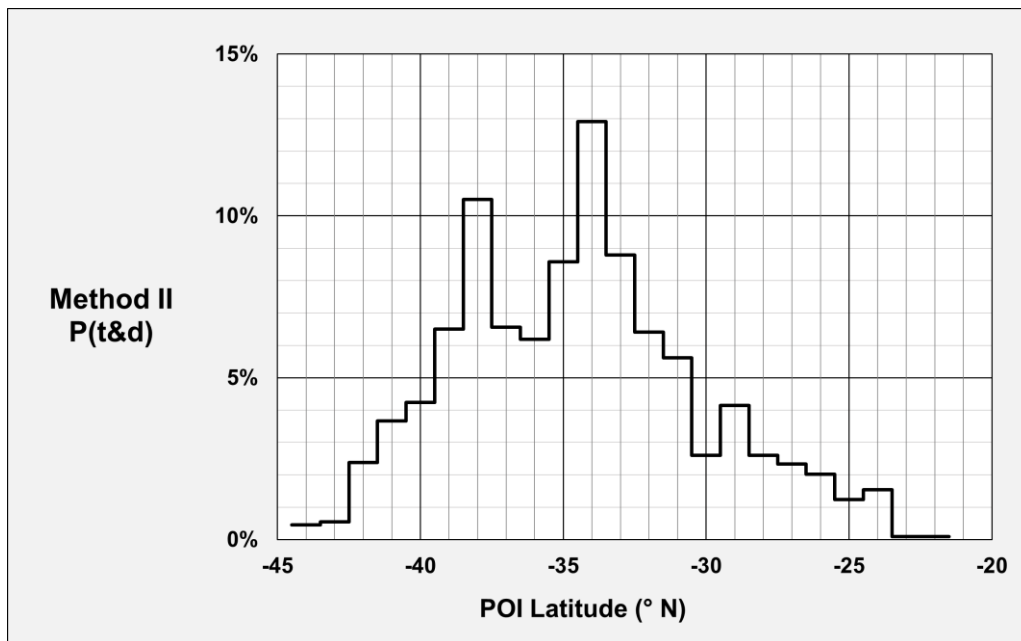
Figure 7.1-1 Method II probability for flaperon with windows optimized at each latitude bin

7.2. Trial-day information

Figure 7.2-1 below is an example of the CSIRO trial-day information, in this case for Debris #23 (the Pemba flap). Each black diamond represents the arrival of a trial which falls within the distance window. The arrivals in the distance window are segregated by their latitude bin of origin and by their arriving date. All the relevant dates are indicated by vertical lines. Histograms are plotted for the frequency of occurrence in both axes. The red diamonds are the trials which fall in both the distance and time windows.

The parameter values in this example are a debris number D = 23, a latitude bin φ = -36°, a distance limit ρ = 34 km, a finding date Δ = 835 days after crash, a reporting delay δ = 18 days, and a time window half-width τ = 52 days.

One can see the arriving waves in the plotted point density and in the histogram of the frequency of occurrence along the abscissa. The frequency of occurrence in latitude bins is shown by the green histogram along the ordinate. The PDF which is being optimized at the selected latitude bin is shown by the red solid line on the left side of this plot.

In some cases, the time window could include trial-days which appear to be from two arriving waves, because the time discrimination may be inadequate to discern whether the reported debris arrived near the beginning of an arriving wave or near the end of the previous arriving wave.
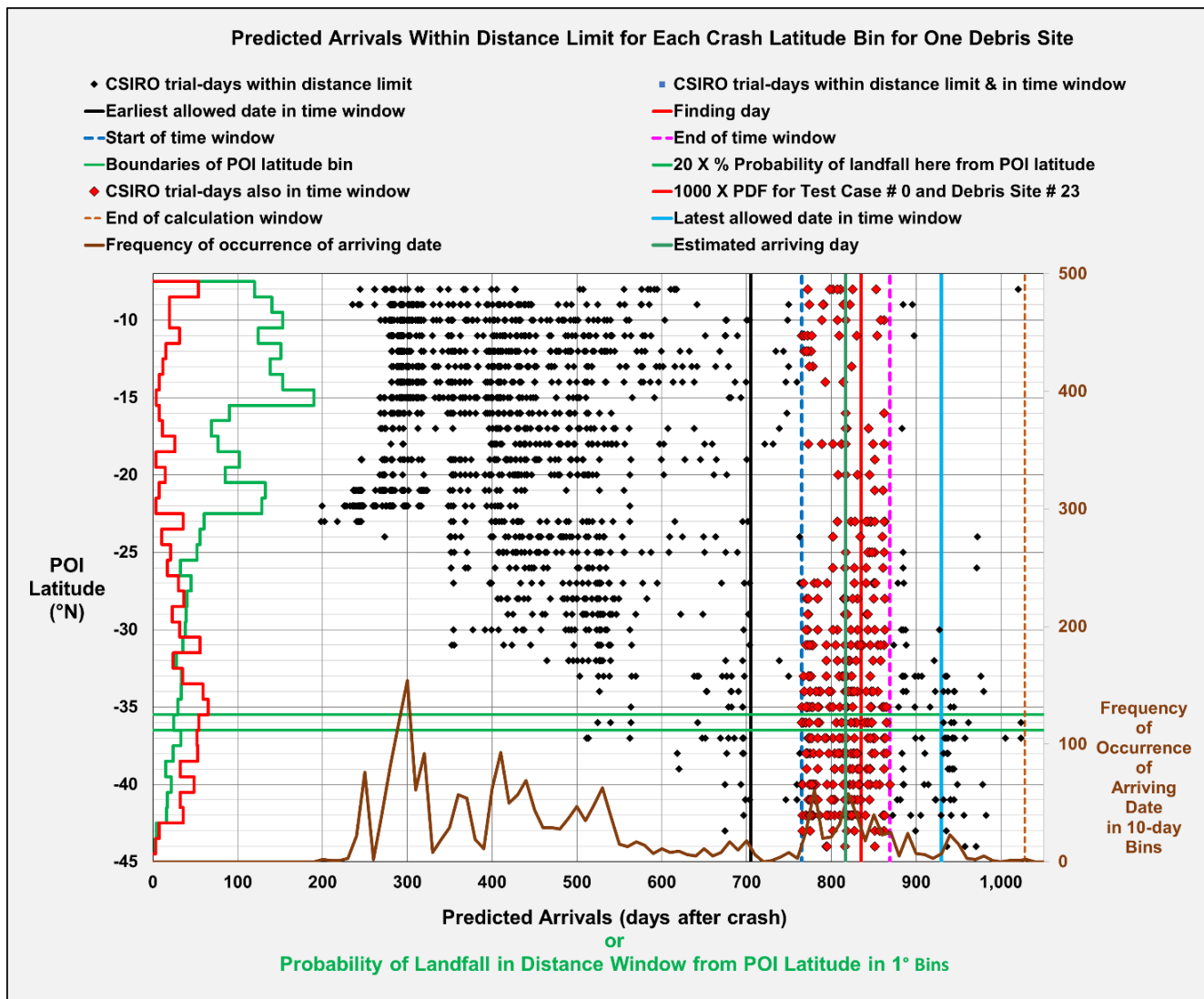
Figure 7.2-1 Plot of CSIRO arrivals in distance window for each POI-latitude bin

7.3. Trade-off between latitude bin width and SNR threshold

Wide distance and time windows are required in some cases to achieve adequate numbers of counts for acceptable statistical noise (i.e., to meet a SNR threshold) in the probability distribution for that debris. Having narrow windows, with improved spatio-temporal resolution, and thus improved POI-latitude discrimination, increases the statistical noise because the number of trial-days in both windows is reduced. Wider windows contain more trial-day counts (reducing the statistical noise and increasing the SNR) but have reduced latitude discrimination. Thus, there is always a trade-off in the optimization process, for both the distance and time windows, between spatio-temporal resolution and statistical noise, given that one has a finite number of predicted trials and given that a SNR threshold must be met to assure reliable predictions.

We found empirically that POI-latitude bins 1° wide with a single-bin SNR threshold of 6.5 is a good compromise between latitude resolution and SNR. This allowed most of the 17 MH370 debris we analysed to achieve a useful SNR in probability per latitude bin, even with the prediction enhancements we developed.

7.4. Example of trial origins map

Figure 7.4-1 shows, for this example case of D23 at -36°, a map of the origins of trials arriving in both the time and distance windows (the red squares).
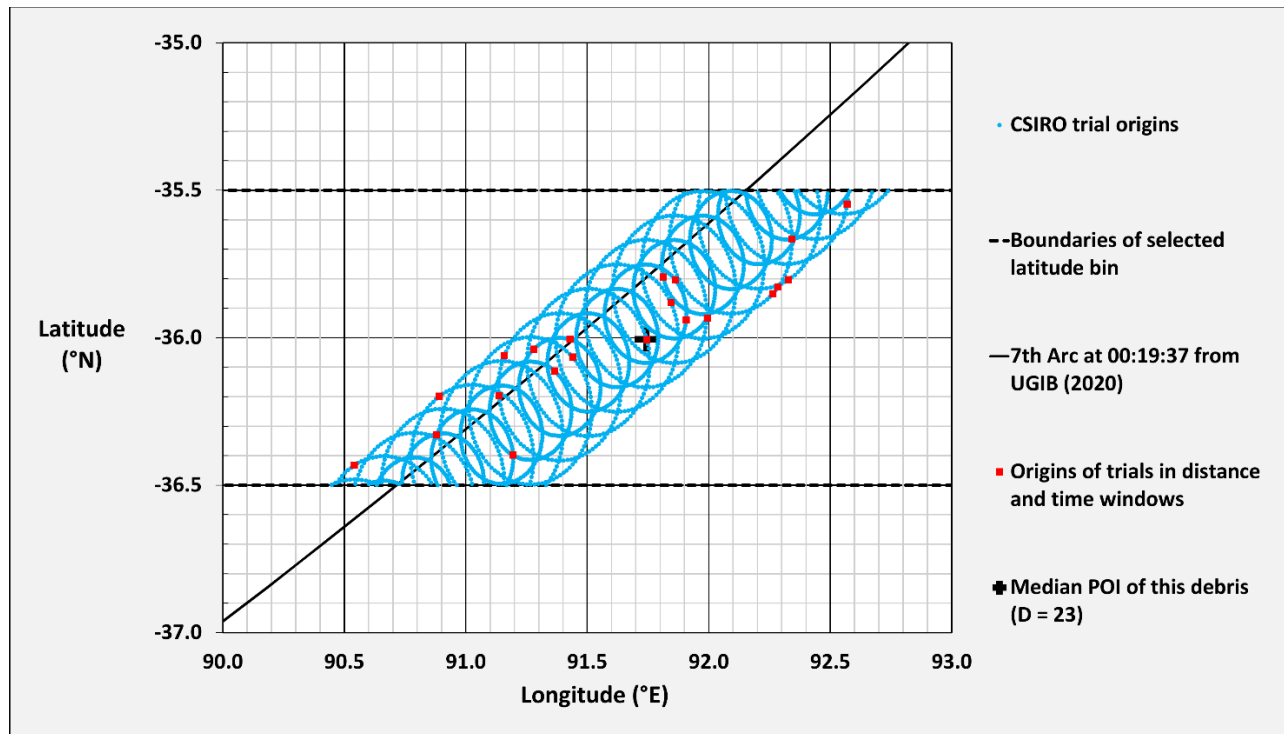

Figure 7.4-1 Map of origins of CSIRO trials in selected latitude bin arriving in time and distance windows

The blue dots show the portion of the 86,400 trial origins within the selected latitude bin. The black line is Arc 7 from UGIB (2020). It is about 5 NM "inside" the arc used by CSIRO to generate the set of trial origins.

7.5. Example of debris site map

Figure 7.5-1 is a map of the region around the D23 finding location (i.e., the Point of Recovery) with red squares indicating the trial-day locations for those trials from the selected latitude bin which are within both the distance and time windows at the debris site.

The selected trial-days are on the east (ocean) side of the Tanzania coast.
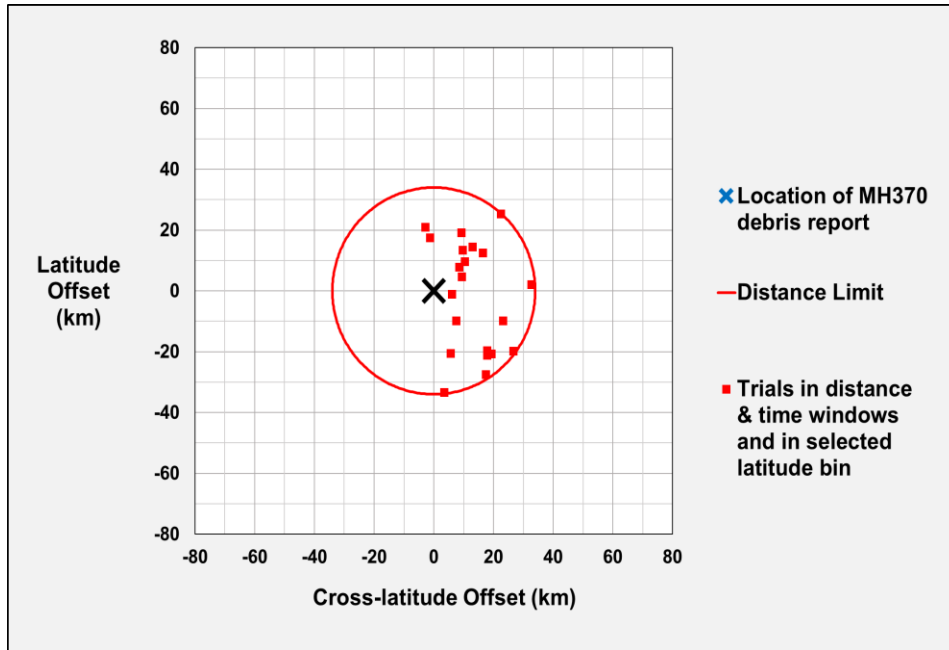
Figure 7.5-1 Map of trials from selected latitude bin arriving at debris site in distance and time windows

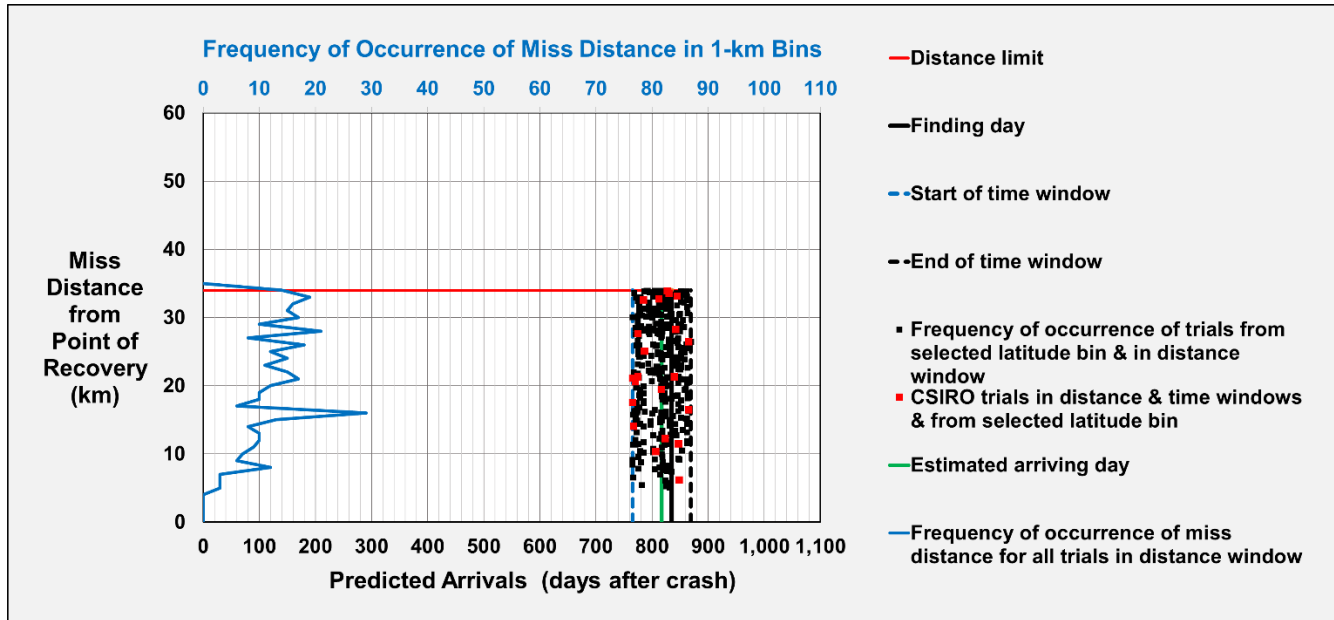Figure 7.5-2 plots the miss distance versus arriving date for the selected trial-days.

Figure 7.5-2 Miss distances of trials from selected latitude bin arriving at debris site

There is no obvious difference in the frequency of occurrence of miss distance of the trials in both windows compared to the trials only in the distance window.

8. Prediction Method III

8.1. Transit speed correction factor (TSCF)

Even the improved Method II fails to produce an accurate probability curve when the drift parameters of a given debris (such as windage and leeway angle) are not accurately known and used in the ocean drift model. Previous drift predictions did not allow for the fact that the drift parameters are only known for two of the debris [the right flaperon and "Roy", whose drift characteristics were empirically determined by CSIRO in sea trials; see Griffin et al. (2016)]. Therefore, if the windage, for example, of a particular debris is different from the value assumed in the ocean drift model, errors will certainly occur in the predicted arriving dates, thereby producing errors in the POI probability curve for that debris. Large windage errors can shift the probability peak by at least several degrees of POI latitude. Therefore, it is necessary to (a) use only debris whose drift speeds and directions have been characterized, or (b) use a prediction method which can compensate for this lack of knowledge, at least for debris with near-zero leeway angles. We followed option (a) for the flaperon and option (b) for the non-flaperon debris we analysed.

None of the previously published drift studies attempt to compensate for a transit speed error, or even include it as a specific contributor to a prediction error budget.

We minimized the impact of a windage error by allowing the average drift speed for each trial drifter transit to be adjusted by a fitted parameter, called the transit speed correction factor (TSCF) at each latitude bin. We then recalculated the times (in days after crash) for each trial-day as the CSIRO time value divided by 1+ TSCF. For example, with a +5% TSCF, the predicted locations are reached about 5% earlier in time, and for a -5% TSCF the predicted locations are reached about 5% later in time. In effect, the time interval between trial-days is thus 1/ (1+TSCF) days.

8.2. Method III

In a new Method III, we allow the TSCF to vary for each debris and for each assumed POI latitude, if needed. Making only transit speed adjustments assumes the leeway angle is close to zero, as CSIRO assumed for their generic drift track predictions. In addition, we assume the drift track is unchanged in location, and only the time axis is adjusted. Clearly this is a crude approximation, but it is a necessary one because we have only two sets of CSIRO tracks to process (for the assumed flaperon and non-flaperon drift parameters). So, for each debris and for each assumed POI-latitude bin, we fit three variables in Method III: (1) the distance radius, (2), the time error limit (i.e., the half-width of the time window), and (3) either the reporting delay (which moves the center of the time window) or the TSCF (which shifts the predicted arriving dates).

8.3. Comparison of prediction methods

Table 8.3-1 summarizes the features and differences of the three POI prediction methods we developed and assessed.

Table 8.3-1 POI-latitude prediction methods

Parameter	Symbol	Method		
		I	II	III
Distance Limit	τ	Chosen subjectively or fitted to one latitude or one region and used for all latitude bins	Fitted separately for each latitude bin to maximize P(t&d)	
Half-Width of Time Window	ρ			
Reporting Delay	δ			
Transit Speed Correction Factor (TSCF)	ε	--	--	Fitted when reporting delay is at an end of its allowed range

8.4. Transit speed errors

For the barnacle-free debris, there is already a partial accommodation of transit speed errors because of the wide range of acceptable reporting delays (we allowed from 7 to 150 days). One cannot fit both the reporting delay and the TSCF simultaneously because they have the same effect of moving the predicted arrivals relative to the time window. Therefore, they are not independent variables, but are highly correlated. Moving the time window earlier in time by increasing the reporting delay has approximately the same effect on probability as making the TSCF more negative, which shifts the predicted arrivals to later dates. So, in Method III, we first allow the center of the time window to move within the acceptable bounds of the reporting delay and with TSCF set to zero. If a greater time shift is needed (either earlier or later) to reach the probability peak during the optimization process, then the TSCF is varied while holding the reporting delay fixed at its boundary value. In this Method III, we still fit only 3 variables for each latitude bin, as in Method II, but we fit the reporting delay first with TSCF = 0, and then, if needed and in a second fit, we hold the reporting delay fixed at its boundary value and adjust the TSCF (as indicated in the last column in Table 8.3-1 above).

The TSCF values are affected by three drift speed errors in the CSIRO model:

1.   The effect of Stokes drift may vary from the 1.2% windage value assumed for generic MH370 debris.

2.   The windspeed at 10 m height used in the BRAN2015 model may be in error.

3.   The near-surface ocean current speeds in the BRAN2015 model may be in error.

Table 8.4-1 summarizes our analysis of these error sources contributing to transit drift speed errors in the CSIRO trials. The cells in Table 8.4-1 colored yellow contain parameter values estimated by Dr. David Griffin of CSIRO [private communication (2023)]. Note the near-surface water current contributes about 80% of the net trial drifter movement, and the wind induces the remaining 20% (at the nominal 1.2% windage used by CSIRO for generic MH370 debris). The windage of recovered MH370 debris was estimated by Dr. Griffin to range from 0.8% to 2.0%. Higher windages (3% to 5%) were certainly possible for items afloat in the early days of the aerial search, but none of the recovered debris appear obviously to require windages that high. Therefore, the wind contribution to net debris movement could be reduced by 33% (at 0.8% windage) or increased by 67% (at 2.0% windage), but the impact on the average transit speed will be 5X lower, or -6.7% to +13.3% (as shown in the eighth column in Table 8.4-1).

Table 8.4-1 Uncertainties in CSIRO model drift speed for floating MH370 debris

Drift Component	Estimated Fraction of Total Drift Speed	Quantity Contributing to Drift Speed Error			Estimated Fractional Error in Component Drift Speed		Fractional Error in Debris Drift Speed (Transit Speed Correction Factor)		
					%	Relative Probability at Estimated Value	%	Probability	Limit
Current drift	80%	BRAN 2015 near-surface current speed with regional debiasing			3.0%	± 1σ	2.4%	± 1σ	---
Wind drift	20%	Wind speed at 10 m height			5.0%	± 1σ	1.0%	± 1σ	---
		Debris windage	Minimum	0.8%	-33%	60.65%	-6.7%	- 1σ	-6.7%
			Nominal	1.2%	---	100%	13.3%	+ 1σ	13.3%
			Maximum	2.0%	67%	60.65%			
Total drift	100%						-7.16%	- 1σ	-14.31%
							13.58%	+ 1σ	27.17%

The cells colored green in Table 8.4-1 contain error estimates we made. We estimated the average near-surface current speed to have a 1-σ error of 3%, and the 10 m height windspeed data to have a 1-σ error of 5%.

8.5. Bayesian probability of transit speed correction factor

We combined the errors due to windage, near-surface currents, and 10 m windspeed in quadrature, assuming they are independent. That results in a combined error range of -7.2% to +13.6% in average transit drift speed (as shown in the last two rows colored blue in Table 8.4-1

Table 8.4-1 Uncertainties in CSIRO model drift speed for floating MH370 debris

Drift Component	Estimated Fraction of Total Drift Speed	Quantity Contributing to Drift Speed Error			Estimated Fractional Error in Component Drift Speed		Fractional Error in Debris Drift Speed (Transit Speed Correction Factor)		
					%	Relative Probability at Estimated Value	%	Probability	Limit
Current drift	80%	BRAN 2015 near-surface current speed with regional debiasing			3.0%	± 1σ	2.4%	± 1σ	---
Wind drift	20%	Wind speed at 10 m height			5.0%	± 1σ	1.0%	± 1σ	---
		Debris windage	Minimum	0.8%	-33%	60.65%	-6.7%	- 1σ	-6.7%
			Nominal	1.2%	---	100%	13.3%	+ 1σ	13.3%
			Maximum	2.0%	67%	60.65%			
Total drift	100%						-7.16%	- 1σ	-14.31%
							13.58%	+ 1σ	27.17%

). We next assumed that, within that range, all TSCF values were equally probable, since we have no windage estimates for the 16 generic debris we analysed – just for the flaperon. Therefore, from -7.2% to +13.6% the TSCF probability was assumed to be a constant (=1). However, TSCF values outside that range were less probable. We assumed that decay in probability was a gaussian out to twice the ± 1σ range, and zero beyond those limits.

Our assumed Bayesian probability statistic for TSCF is shown in Figure 8.5-1 below.
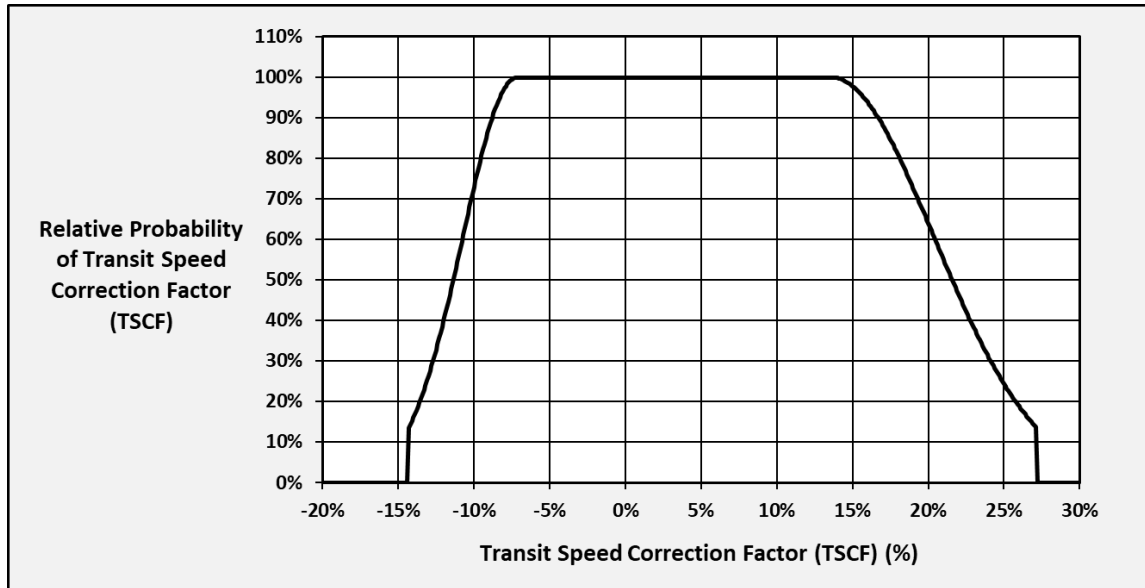
Figure 8.5-1 Assumed relative probability of TSCF for non-flaperon debris

In the Method III process, we maximized the PDF value for each latitude bin, and when one of those fitted parameters was TSCF (instead of the reporting delay), we maximized the product of the PDF value and the probability of the TSCF value as shown in Figure 8.5-1. So, from -7% to +14% there is no penalty for non-zero TSCF values. However, when TSCF was outside that range the penalty increased substantially and reduced the probability for that latitude bin by the factor indicated in Figure 8.5-1 above.

8.6. Example of Method III

Figure 8.6-1 below shows, as an example of Method III, the results for the PDF and the best-fit TSCF values for the flaperon. The purpose of this exercise was to check Method III by looking for significant drift speed "errors". CSIRO calibrated the drift speed of an instrumented cut-down flaperon and adjusted their model parameters to match their observed drift speeds. Therefore, one would expect the flaperon analysis to show a TSCF value close to zero from the true POI latitude. This notion was tested in Figure 8.6-1, and indeed that is what we found.

The reporting delay for the flaperon is always fixed at zero days because we know the date it arrived. Thus, the center of the flaperon time window is always fixed at the reporting date. Adjusting TSCF shifts the predicted arrivals with respect to this "stationary" time window.

The black line in Figure 8.6-1 below is the PDF using Method III with the TSCF optimized at each latitude bin. It is like the Method II PDF previously shown in Figure 7.1-1. We believe this Method III result shows the relative probability of the two peaks at -34° and -38° latitude most accurately among all methods.

The red line in Figure 8.6-1 below indicates the best-fit TSCF values are essentially zero at crash latitudes from -33° to -42°. From -33° to -38°, TSCF is a fraction of 1%, and this region also contains the two significant PDF peaks. That implies that the CSIRO trials arrive in La Réunion in precise alignment with the finding date, implying the flaperon drift parameters observed and used by CSIRO appear to be accurate (and despite there not being a discernible difference in average drift speed over a 6° latitude range). North of -31° all TSCF values are negative, as expected. South of -42° all TSCF values are positive, again as expected.
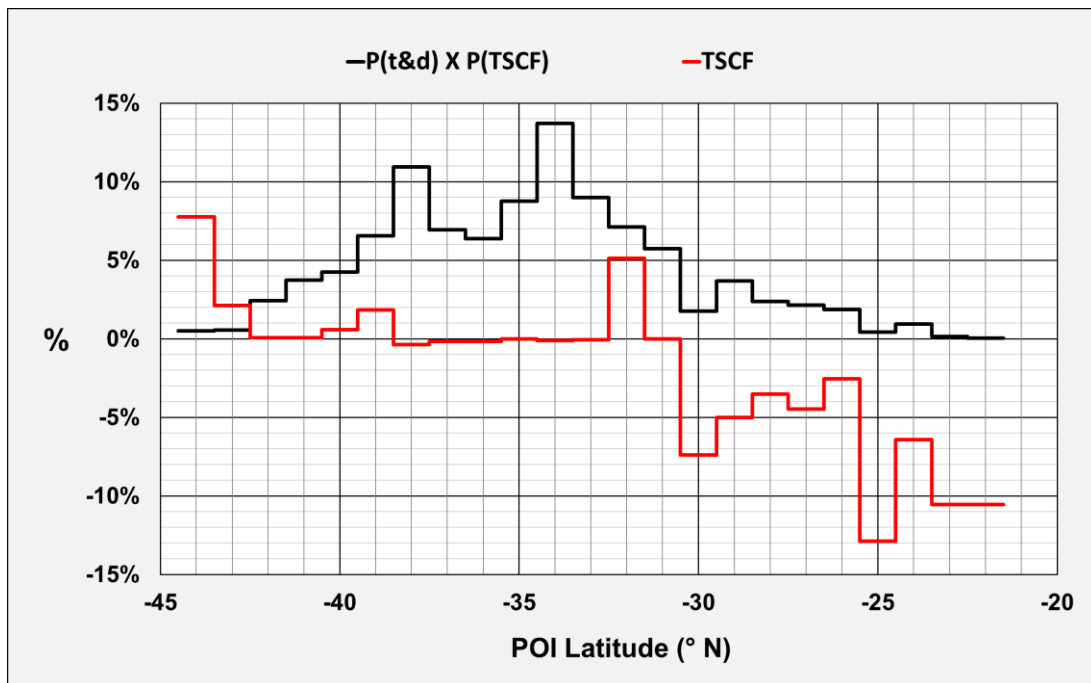
Figure 8.6-1 Method III PDF and best-fit transit speed for flaperon

Figure 8.6-1 demonstrates that the crash-latitude discrimination of the flaperon is not simply caused by a time difference in predicted arrivals. If that were true, we would see different TSCF values at the two peaks which are separated by 4° of latitude. The combination of the two plots in Figure 8.6-1 demonstrates that the predicted arrivals from -33° to -38° are highly overlapping temporally, but still can be discriminated spatially (by the distance window) and by the width of the time window. The time window width allows us to discriminate among arriving waves of trial drifters if they differ in the numbers of trials. Temporally "dense" waves allow narrow time windows, which can discriminate against overlapping but less dense arriving waves from other latitudes.

We also note that because the best-fit TSCFs for the flaperon are zero for latitude bins between -33° and -38°, one should favor those latitudes for the MH370 POI based on this flaperon drift speed match alone.

8.7. Superiority of flaperon

The flaperon is the best debris for assessing POI latitude. There are three reasons for this:

1. we know the exact date on which it arrived,

2. the CSIRO model drift speed is calibrated using a surrogate flaperon, allowing us to restrict the TSFC to being zero (for the flaperon only), and

3. its proximity to Arc 7 minimizes the spatial and temporal dispersion of the arriving wave of drifters.

Thus, for the flaperon we need to fit only two parameters for the time and distance window widths, since both the reporting delay and the TSCF are known to be zero. The flaperon results indicate two likely POI latitudes: -34° and -38°. The primary peak at -34° is also seen in many other debris PDFs. However, the secondary flaperon peak at -38° does not appear in the PDFs for generic debris found at other locations. This demonstrates the benefit of spatial diversity in finding locations, because some peaks will be rendered undetectable in the joint PDF even though they are significant in one or even several single-debris PDFs.

For use in computing the joint PDF of all debris, we used the special case of Method III for the flaperon, with both the reporting delay and the TSCF fixed at zero, as discussed previously. This result is shown in Figure 8.7-1 below which differs only slightly from Figure 8.6-1.
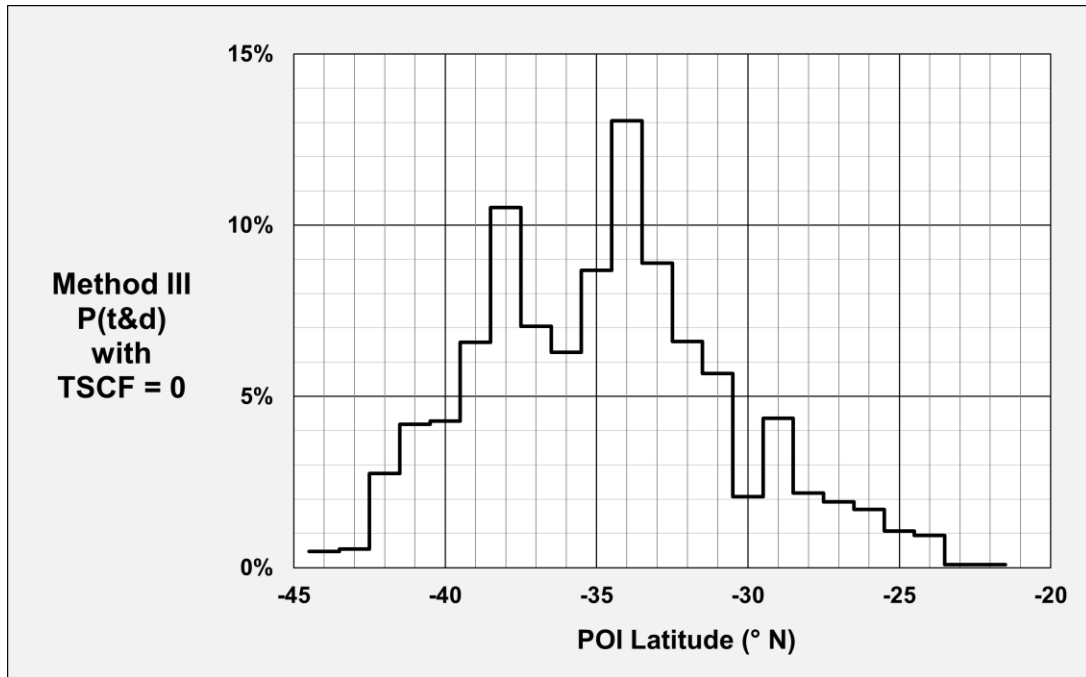

Figure 8.7-1 Method III flaperon PDF with zero reporting delay and zero TSCF

8.8. Latitude dependence on average TSCF

We also tested the assumption that non-zero TSCFs would shift the best-fit latitude in a systematic way when using all 17 debris in the joint PDF. Figure 8.8-1 shows the result when we <u>assumed</u> the same value of TSCF for all 17 debris and solved for the latitude which had the highest probability in the joint PDF (i.e., the peak of the product of all 17 PDFs).

In Figure 8.8-1 we see a systematic shift in the predicted most-likely crash latitude using Method III depending on an assumed transit speed adjustment to the CSIRO drift model. Note that TSCF = 0 corresponds to -34° crash latitude. The slope is about -5% / °. More northerly latitudes require negative TSCFs, and more southerly latitudes require positive TSCFs, as expected based on the general northerly drift near Arc 7. Figure 8.8-1 represents the averaged dependence on drift speed of all 17 debris. Some debris will show a larger dependence, and some debris, such as the flaperon, will show a smaller slope or even a zero slope (as demonstrated previously in Figure 8.6-1 for the flaperon).
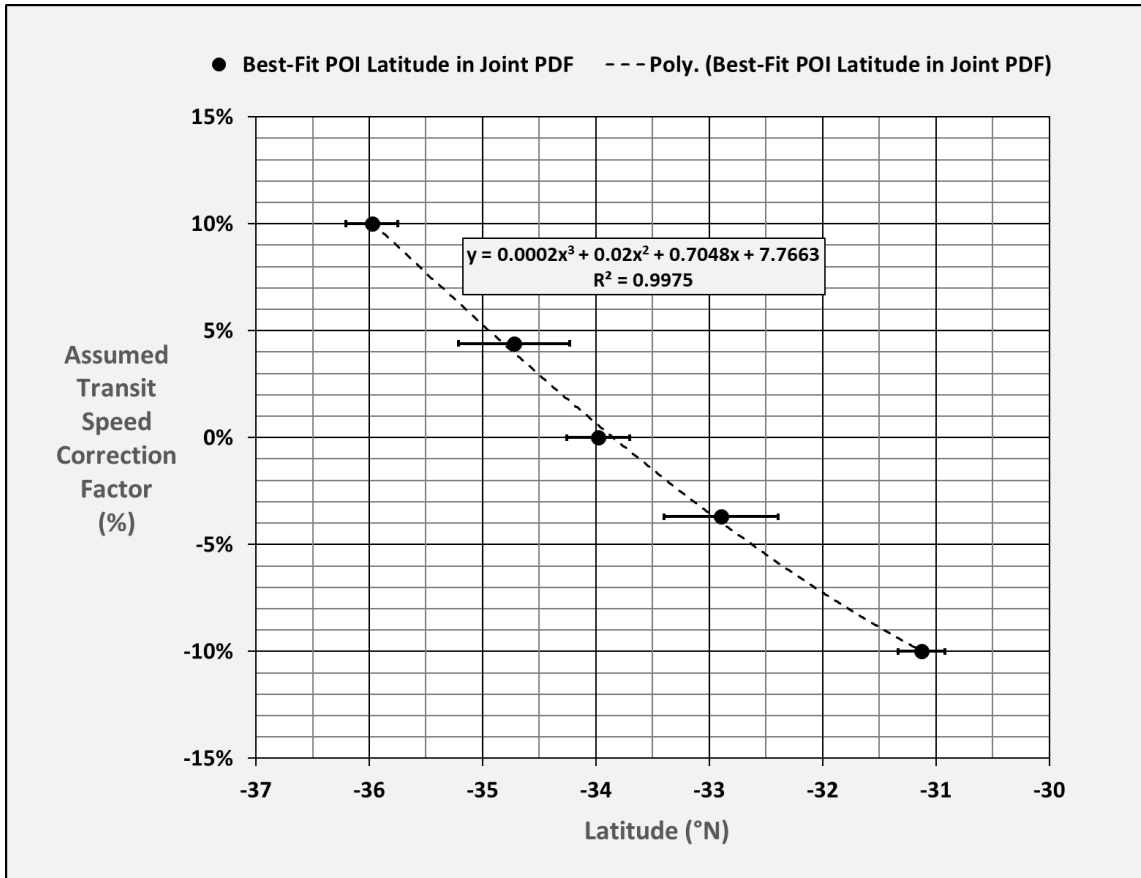
Figure 8.8-1 Latitude dependence on transit speed correction factor of joint PDF using 17 debris

8.9. Best-fit TSCF values

As indicated in Figure 8.9-1 below, fitting the TSCF using Method III was needed in only four of the twelve generic debris which met the SNR threshold.
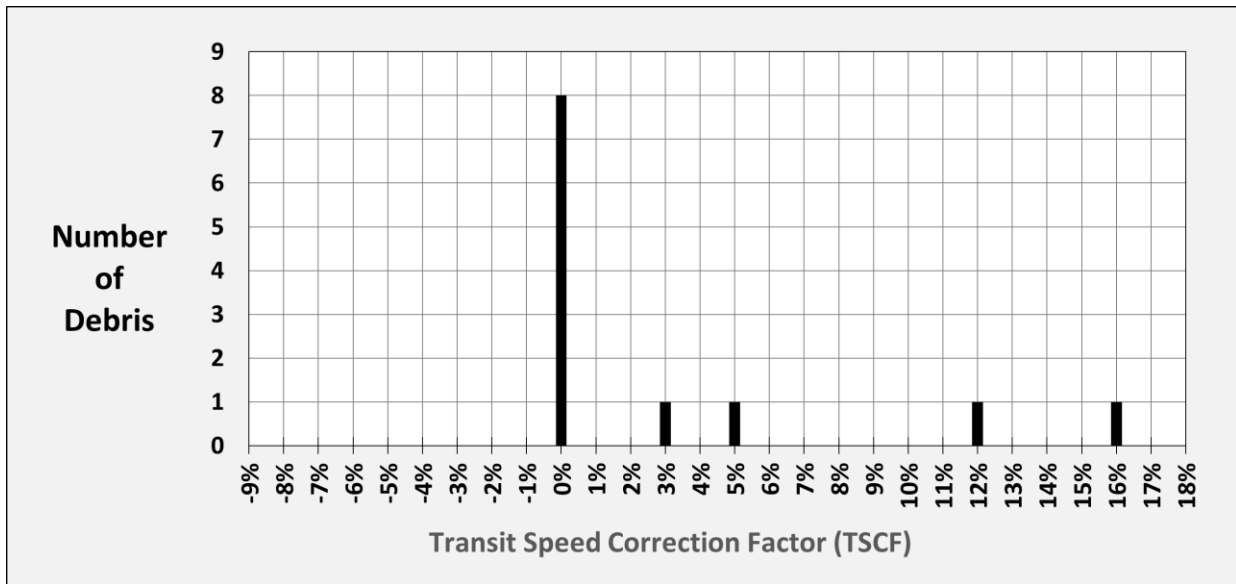

Figure 8.9-1 Best-fit TSCF values at -34° latitude for non-flaperon MH370 debris

Bobby Ulich and Victor Iannello   June 6, 2023   Improved Prediction of MH370 Crash Location Based on Drift Modeling of Floating Debris

Figure 8.9-1 is a plot of the occurrence frequency of TSCF values at one latitude bin (-34°). Most debris are well fitted with TSCF = 0 (13 out of 17 debris favored this). In all four cases of non-zero TSCFs, the debris when found were free of barnacle encrustations. Thus, it appears that the windage value used by CSIRO in predicting generic drift tracks is a good approximation for many (but not all) of the MH370 non-flaperon debris. None of the debris with many barnacles (the right flaperon found in La Réunion) or with a few barnacles (the storage closet door found in Rodrigues and the outboard flap found in Pemba, Tanzania) needed a non-zero TSCF to achieve good consistency between the drift model predictions and the debris reports.

Note the four non-zero TSCFs in Figure 8.9-1 above are all positive. It is possible this is partly because the 1.2% windage used by CSIRO for the non-flaperon debris is slightly below the actual average windage. However, there is a bias in the fitted TSCF values to be positive, because many of the debris have a very large range of acceptable reporting delays. Negative TSCFs are not allowed unless the estimated arriving date occurs prior to the earliest date allowed by the largest value of the reporting delay. So, we can't tell the difference between a long reporting delay or a modest reporting delay plus a negative TSCF. In both cases the time window dates and counts can be almost identical. Thus, we won't always find negative TSCFs when they occur, because even at zero TSCF the best arriving wave is often accessible by means of the reporting delay parameter.

Fitting the TSCF in Method III has several effects:

1. The error introduced by using an incorrect average drift speed in the model is significantly reduced.

6. A somewhat larger signal-to-noise ratio in predicted probability is required for accommodating the third fitted variable (i.e., either the reporting delay or the TSCF). This SNR requirement (we used a threshold of 6.5 per bin) eliminates four marginal cases. Those debris with too few predicted arrivals to be used in the joint PDF included the engine right fan cowl, the upper fixed panel forward of the left flaperon, the wing-to-body fairing, and the right engine inner vortex generator. It is noted that including these four debris in the joint PDF does not alter any of the conclusions presented in this paper. Reliable detection of a PDF feature requires a SNR of at least 1 in each PDF and at least 4 overall. The minimum detectable contrast in the joint PDF is roughly the inverse of the SNR. Therefore, with SNR = 6.5 per bin per PDF, the minimum detectable contrast is about 17% per debris when using 13 debris.

7. Secondary peaks of significant probability now appear in the Method III joint PDF at nearby POI latitudes, because the global peak is reduced in probability and the secondary peaks are increased in probability. by the two accuracy enhancements we incorporated in Method III compared to Method I:

   a. maximizing the likelihood at each POI-latitude bin, and

   b. allowing the average drift speed to be adjusted if needed.

By studying the fitted TSCF values in Method III, we found that, while the average transit speed was important in discriminating POI latitude, it was generally not dominant. A comparable degree of discrimination is provided by the proximity of the predicted tracks of trial drifters to the finding locations. Thus, both spatial and temporal discriminations are significant, and their relative strengths depend on both the assumed POI latitude and on the debris finding location.

8.10. Best-fit window dimensions

The values of all the best-fit Method III parameters for each debris at -34° latitude are listed in Section 3 in Table 3.2-1. Figure 8.10-1 below is a plot of the best-fit window widths at one latitude bin (-34°) using Method III.
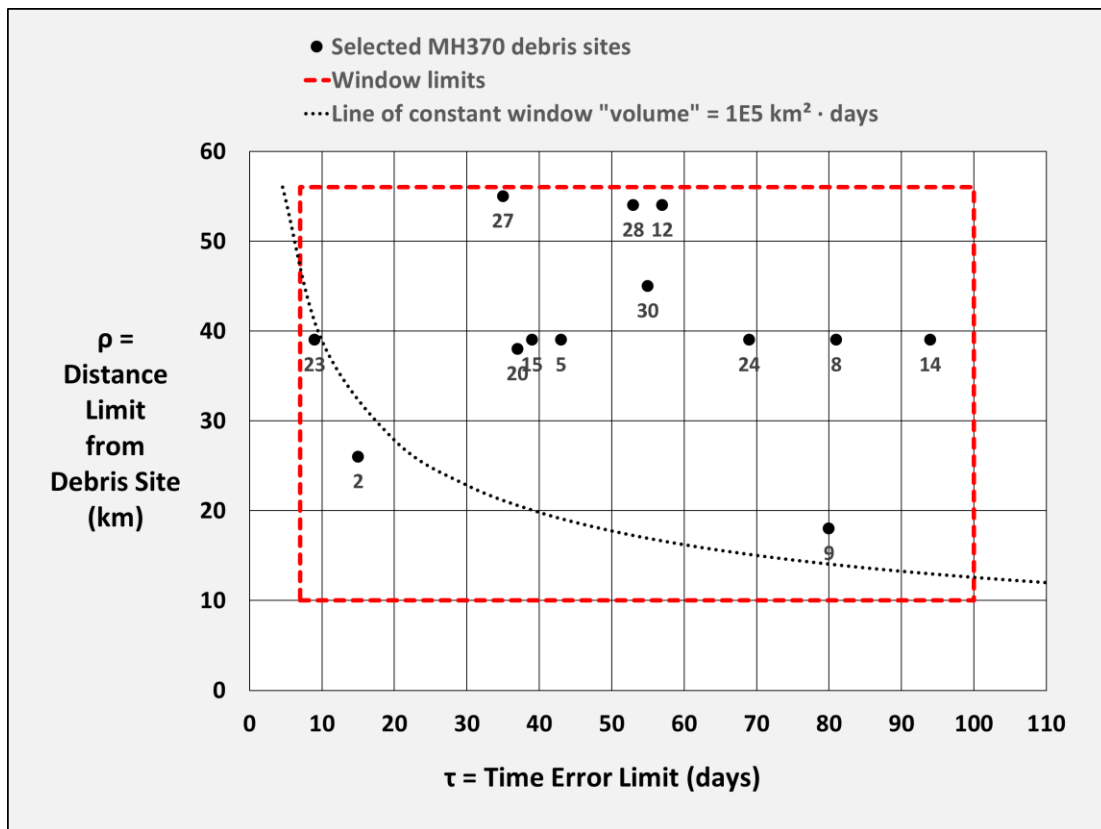
Figure 8.10-1 Method III window dimensions for MH370 debris at -34°

The red dashed lines in Figure 8.10-1 indicate we allowed 10-56 km for the distance limit and 7-100 days for the half-width of the time window. The label below each plotted point is the identification number of the debris. For example, D2 is the flaperon. Due to its finding location and its proximity to Arc 7, it has the sharpest windows with the smallest "volume" (surface area times duration). Therefore, we expect the flaperon to be superior among MH370 debris for crash-latitude discrimination because the high density of trials near the debris site and close to the arriving date allows smaller, and more discriminating windows to be used while maintaining a sufficiently high number of counts to meet the SNR threshold.

9. Joint Probability Density Function

9.1. MH370 Joint PDF

The MH370 single-debris PDFs using prediction Method III, and their joint PDF (i.e., their product), are shown in Figure 9.1-1 below. Note the latitude scale (the abscissa) only extends northward to -22° in this plot because between -22° and -8° the joint probability is negligibly small.

The seventeen black lines in Figure 9.1-1 are the PDFs (each normalized for plotting so the peak probability = 1) for the seventeen MH370 debris we analysed. The individual PDFs are plotted here so that 0% probability is at the debris site number (from 1 to 30), and 100% probability is at the next higher number. For example, the PDF for the flaperon, which is D2, is plotted between 2 and 3 on the ordinate scale. Four of the seventeen individual PDFs are flat lines at 100%, because D10, D11, D13, and D29 had inadequate statistics to be processed using Method III (i.e., their SNRs were too low). The red line in Figure 9.1-1 is the joint PDF of the ensemble, which is the product of the 13 individual PDFs, scaled so its area is unity. We use the product rather than the sum because

the joint probability is conditional upon all the debris matching their reported sites and dates. The conditional joint probability is the product of all the single-debris probabilities when the condition is that all are TRUE.
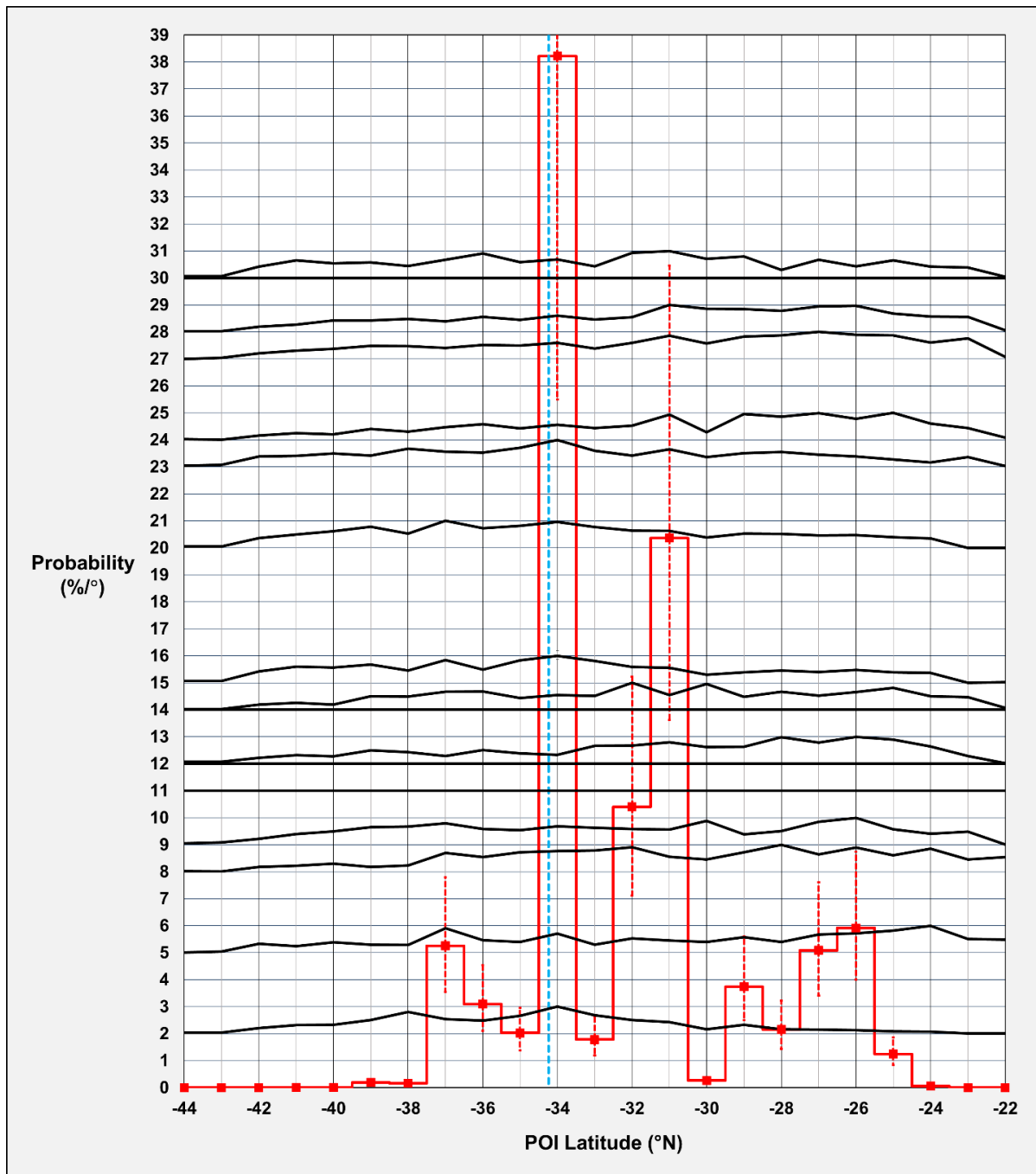

Figure 9.1-1 Individual and joint PDFs for MH370 debris probability

Note the ± 1σ error bars (the vertical dashed red lines) on the joint PDF values (the red dots) in each POI-latitude bin. Note the vertical error bars at -34° and at -31° overlap, so it is likely, but not nearly certain, that -34° has a higher probability than -31°. The vertical dashed blue line is the latitude of the LEP from UGIB (2020). Note the secondary peak in the joint PDF at -31° using Method III is about half the probability at -34°. Method I does not show this secondary peak at a significant probability.

Inspection of the plot above reveals that the highest peak in the joint PDF is at -34° POI latitude, very close to that of the UGIB LEP at -34.23°. However, only three debris (D2, D15, and D23) have their individual PDF peaks at -34°. The error bars on the joint PDF in Figure 9.1-1 are a relatively constant percentage of the joint PDF value. Hence, the highest peak also has the largest uncertainty, and the SNR is relatively constant across the POI-latitude bins. Figure 9.1-1**Error! Reference source not found.** is not our final prediction of the debris probability b ecause systematic localization errors in the ocean drift model have not yet been included (this is done in Section 11 later in this paper).

10. Maps of Trial Drifter Tracks

10.1. Trial drifter tracks from -34° reaching MH370 debris sites

Figure 10.1-1 illustrates trial drifter tracks originating from the vicinity of Arc 7 near -34° and reaching all the MH370 debris sites we analysed. In this figure we selected the one trial per debris site which gave the closest match in the time and distance windows.
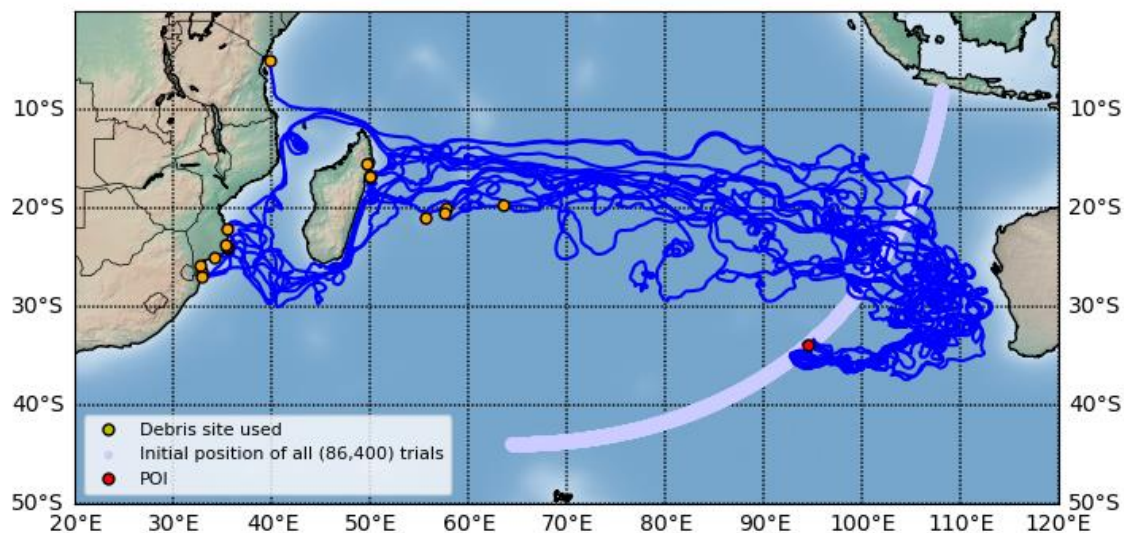

Figure 10.1-1 Trial drifters from -34° arriving at all debris locations analysed

In Figure 10.1-1 above all the debris initially drift eastward away from the 7th Arc and then turn northward, but none make landfall in Western Australia. Then the South Equatorial Current sends the floating debris westward toward Madagascar and the intervening islands. Figure 10.1-1 demonstrates that the paths of those trials which best matched the MH370 debris finds generally passed about 200 km or more to the west of the West Australia coastline.

10.2. Trial drifter tracks from -34°

Figure 10.2-1 below shows a larger number (75) of randomly selected trial paths which originated near -34° close to Arc 7.

Note in Figure 10.2-1 that some of those trial paths pass very near the Western Australia coastline. Some trials are also predicted by CSIRO to reach very shallow water there, although no MH370 debris were reported (other than possibly the towelette packet).

Figure 10.2-1 Seventy-five CSIRO-predicted drift tracks originating near -34°
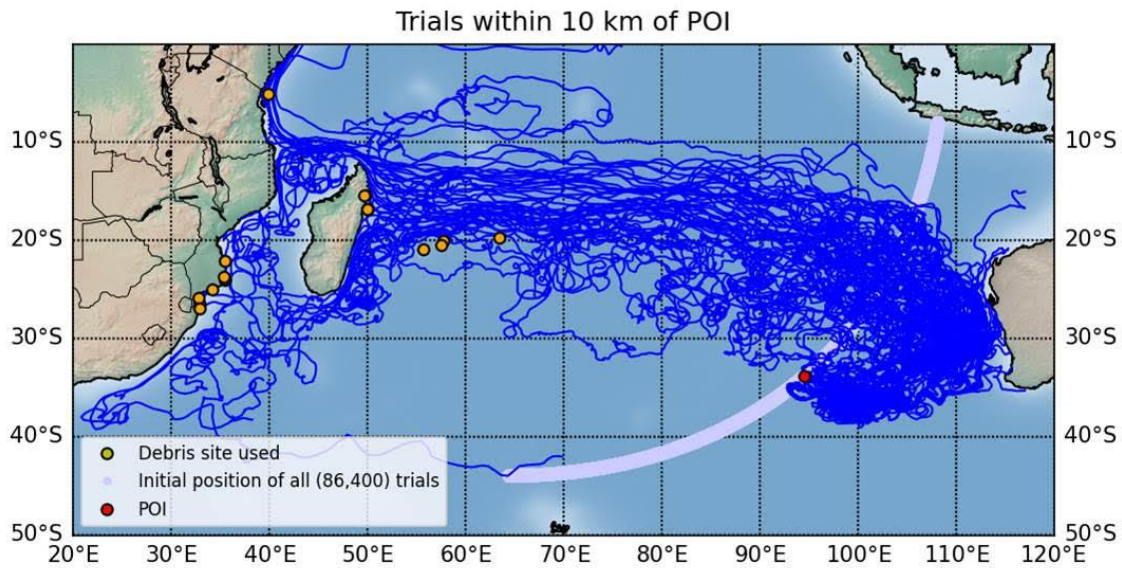
10.3. Flaperon trial drifter tracks reaching La Réunion

Figure 10.3-1 below shows flaperon trial drifter tracks from the entire range of latitudes on Arc 7 which reach La Réunion (where the flaperon was found) within the distance and time windows.

Figure 10.3-1 Trial drifter tracks in both distance and time windows for the flaperon at La Réunion
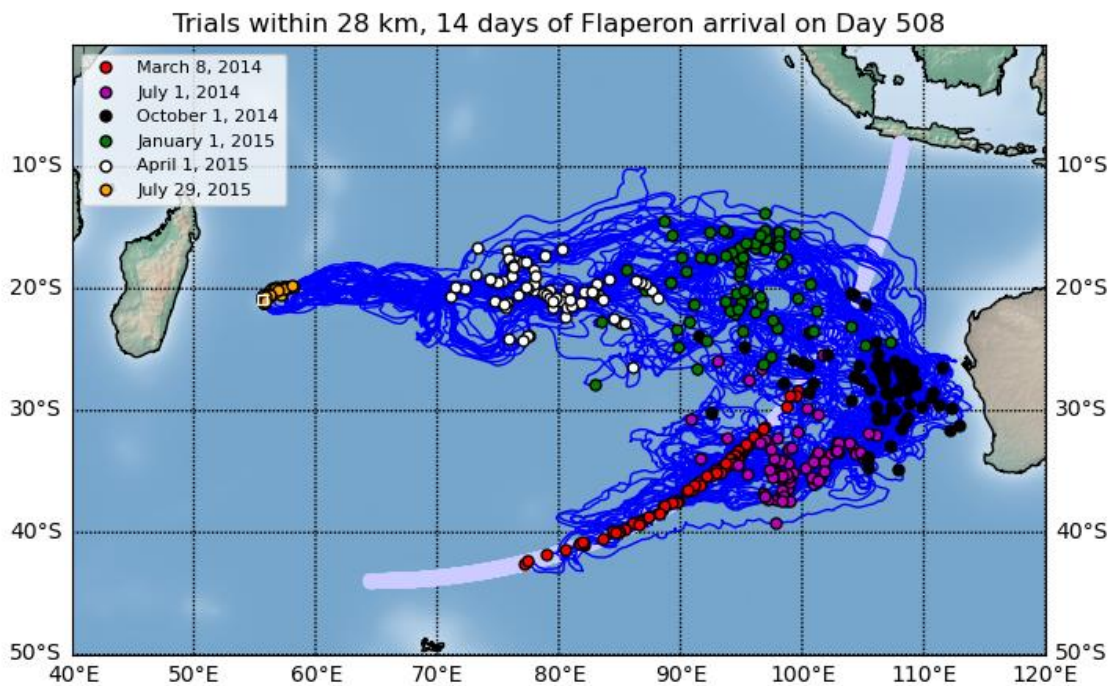
The red dots in Figure 10.3-1 indicate the starting locations near Arc 7 of the selected trials. The remaining sets of colored dots indicate the trial drifter locations at intervals of 3 months. Halfway through the drift, the trials are widely diverged spatially in longitude and less diverged in latitude. During the remainder of the transit, the spatial divergence gets compressed into a narrow latitude range by the strong westerly current, and the

divergence in longitude creates the divergence in arriving date at La Réunion. Figure 10.3-1 demonstrates that trial drifters from a wide range of locations on Arc 7 can arrive in La Réunion, but there they can be somewhat discriminated by their arriving dates. Figure 10.3-1 also shows that very few flaperon trials that fall within the time and distance window at La Réunion start north of -30° latitude.

10.4. Trial drifter tracks for Debris # 15

Figure 10.4-1 is a similar plot for Debris #15, the seat back trim panel, which was found at Riake Beach in Madagascar.
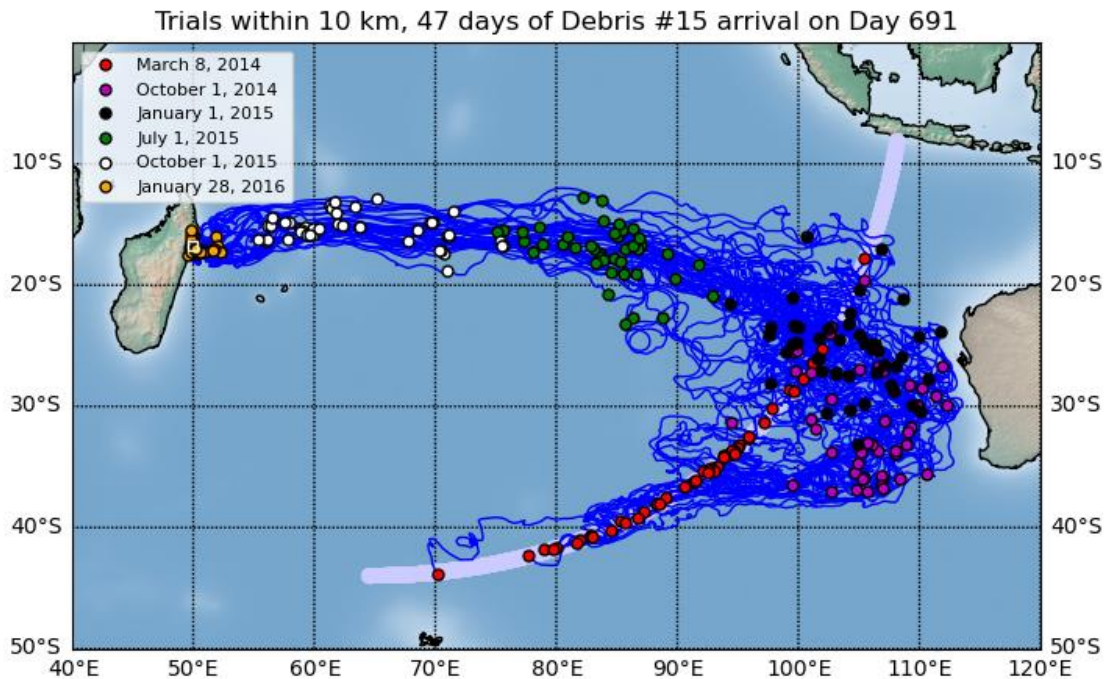

Figure 10.4-1 Trial drifter tracks in both distance and time windows for Debris 15 at Madagascar

The non-flaperon debris like D15 take more northerly tracks across the SIO when travelling westward (because of their zero leeway angle). The flaperon was experimentally found to drift to the left of the non-flaperon debris paths, based on the CSIRO drift tests [Griffin et al. (2017)] which used a model of the recovered flaperon. Therefore, the non-flaperon debris tend to miss La Réunion on the north side, heading toward Madagascar.

11. Ocean Model Localization Error

Dr. David Griffin of CSIRO has estimated the BRAN2015 relative location error to be at most ± 1.0° of arc [private communication (2022)].

11.1. Bayesian PDF of BRAN2015 localization error

We assumed the 1.0° of arc to be 2σ of a gaussian probability density function. The relative location error (or "localization" error) is the uncertainty (relative to the origin) in the position of a drift track (i.e., a trial-day location) after a lengthy transit, such as occurred for the MH370 debris crossing the Southern Indian Ocean. The same localization error may be applied when predicting the origin based on knowing the finding location. Figure 11.1-1 below shows the Bayesian localization error PDF.
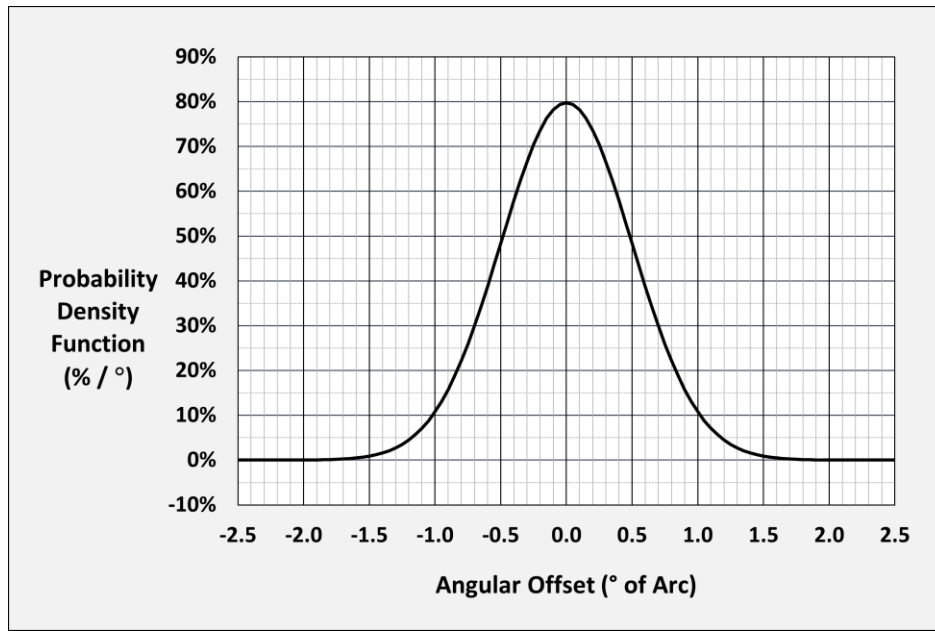
Figure 11.1-1 PDF of BRAN2015 localization error

12. Drift Probability

12.1. Joint PDF with localization error included

We incorporated the estimated BRAN2015 localization error by convolving the joint PDF in Figure 9.1-1 with the localization error PDF shown in Figure 11.1-1 above. This convolution has the effect of blurring the joint PDF such that peaks are reduced in probability and valleys are increased in probability. Our result for the "drift probability" with the localization error included is shown in Figure 12.1-1 below.

Figure 12.1-1 MH370 drift probability

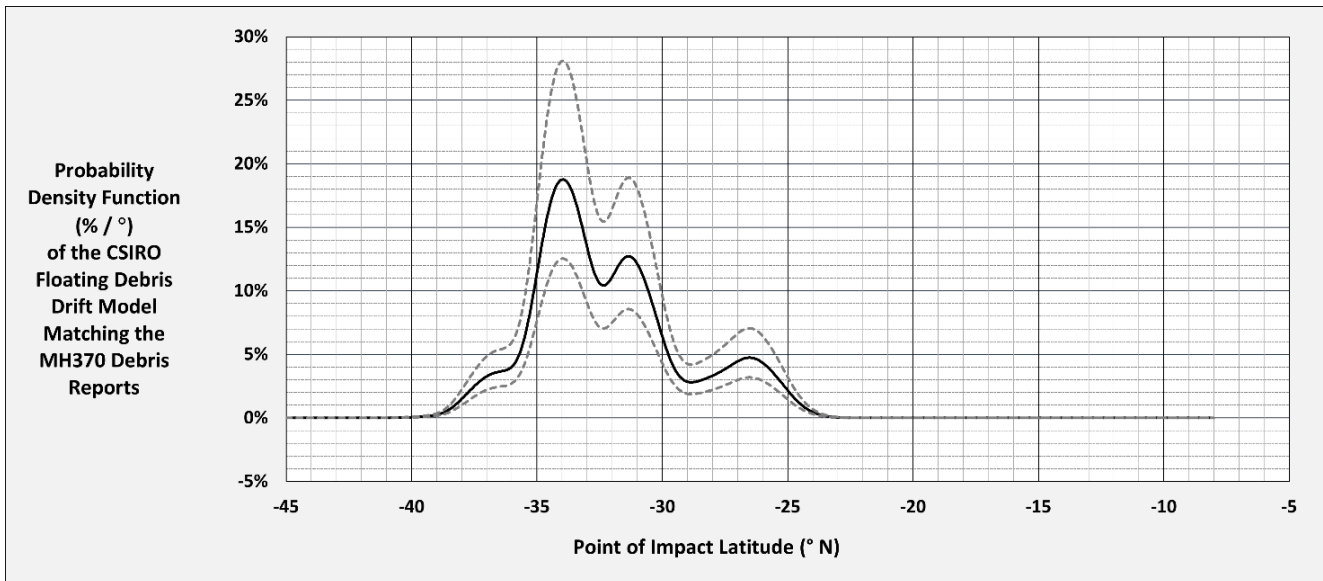The solid black line in Figure 12.1-1 above is the joint drift PDF (i.e., the MH370 drift probability) including consideration of the model localization errors. The two black dotted lines indicate the ± 1σ errors in the drift probability.

Figure 12.1-2 below is an enlarged plot of the drift probability covering the latitude range of non-zero probability.
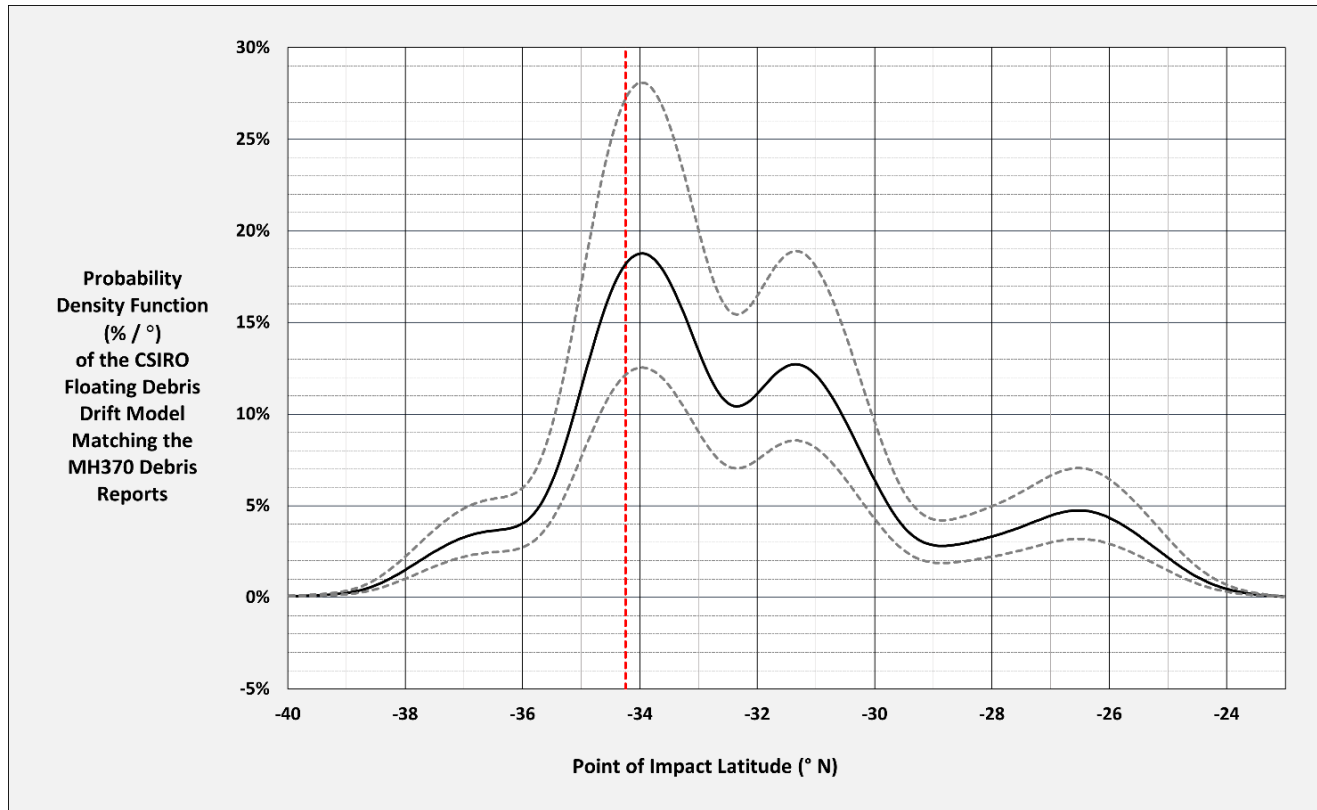

Figure 12.1-2 MH370 drift probability and ± 1σ uncertainties

Considering the systematic BRAN2015 localization errors, the most likely POI is at -34.00 ± 0.54°N, 94.07 ± 0.65°E. This new estimated impact position prediction is only 41 NM northeast of the Arc 7 location (= -34.23 ± 0.5°N, 93.79°E) previously predicted by UGIB (2020) as the "Last Estimated Position" based on the satellite and weather data (and indicated by the vertical dashed red line in Figure 3.34-2 above). The proximity of the peak drift probability to the LEP implies the post-fuel-exhaustion glide distance may be less than 50 NM. The asymmetry in the drift probability in Figure 12.1-2 implies the course deviation after flame-out was more likely to the left of the autopilot course.

Arc 7 Latitudes between 29.9° and 35.7° constitute all locations which are within a factor of 4X lower than the peak value of the debris probability. This is the latitude zone for the debris field location which is indicated by the drift analysis alone. However, portions of this latitude range are effectively nullified by other considerations, primarily the fuel modeling and the post-crash aerial search for floating debris, producing a smaller latitude range when all factors are considered.

13. Comparisons with Prior Drift Studies

13.1. Comparisons with previous predictions using CSIRO drift tracks

In Section 1 we summarized the CSIRO prediction for the MH370 POI as being between 32-36°S, with the most likely latitude being 35°S. Our new result is consistent with the CSIRO latitude range, although our northern limit is slightly farther north at -31°. This difference is partly caused by our inclusion of the localization error, which broadens our drift probability. Our most likely POI latitude (-34°) is slightly to the north of CSIRO's most likely POI latitude (-35°).

In UGIB (2020) we performed a crude analysis of the fraction of trials with predicted arrivals in the same geographical area and within a wide time window of the debris reports. That result (Figure H-1 in that paper) is shown below in Figure 13.1-1
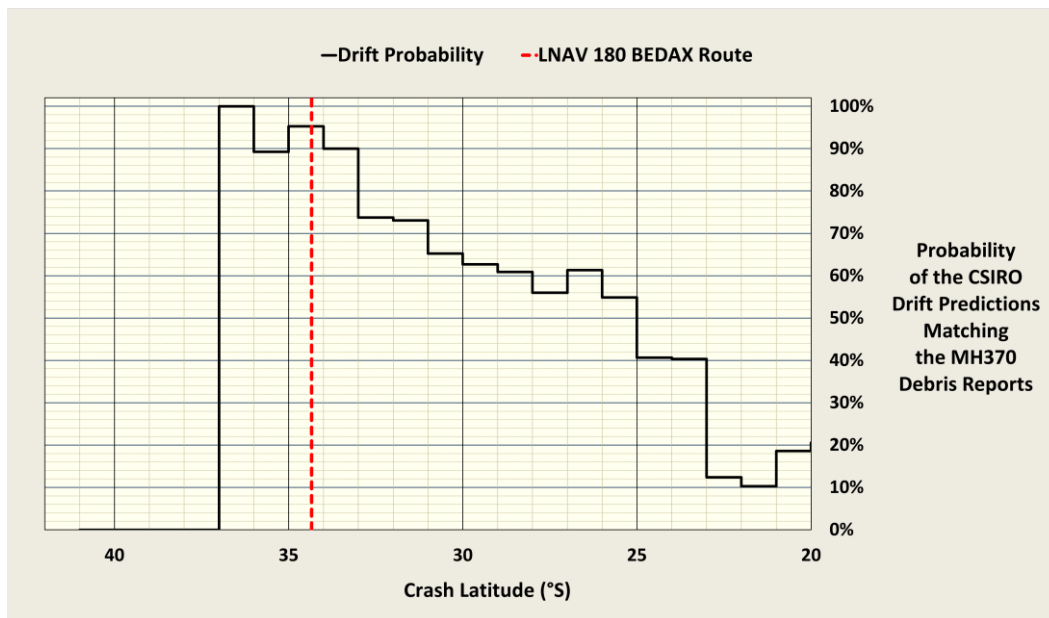

Figure 13.1-1 Figure H-1 from UGIB (2020) for comparison with new prediction

This initial result indicated a POI latitude of 33-37°S as being more likely. Our new result is consistent with, but more precise and more accurate than, our initial 2020 prediction.

Godfrey (2020) analysed the CSIRO drift tracks and predicted a POI at 34.13 ± 1.06°S (this error is a precision estimate only without any allowance for drift speed error or localization error). Godfrey's prediction method has multiple limitations, including the following:

a) It uses the number of trials arriving at a location within fixed distance and time windows from a given crash latitude [i.e., $N(D,\phi,\rho,\tau,\delta)$, as a probability. That is not a probability, because the number of trials per latitude bin is not a constant. This processing error introduces a slight latitude bias error, and it suffers from the deficiencies inherent in Method I. Since the single-debris-site PDFs are not probabilities, neither is their joint PDF product.

b) It excludes several debris sites which showed results that appeared inconsistent with the Flaperon PDF. No adequate justification is given for their exclusion.

c) It excludes multiple probability peaks at various latitudes. However, this behavior is to be expected. It is quite possible that debris from different latitudes can arrive at the same location and at the same time.

d) It ignores systematic errors in the BRAN2015 model and in the predicted CSIRO drift tracks.

e) There are no validation tests of the method.

Godfrey's prediction method is unvalidated and slightly degraded in accuracy. His result depends almost solely on the large peak at 34°S for the flaperon at La Réunion. The error estimation is overly simplified (for instance, it does not use the width of the joint PDF) and incomplete (because systematic model errors are not included). Despite these drawbacks, Godfrey's prediction of the most probable crash latitude is consistent with our new result, although his PDF overestimates its probability relative to nearby latitudes.

13.2.   Comparisons with other drift studies

Rydberg (2015) analysed the Flaperon track to La Réunion using the drift model of Erik van Sebille et al. (2012) incorporated in the online calculator at adrift.org.au (2015). Rydberg concluded "the most likely origin of the Flaperon is currently a 2 by 2-degree area, centered at (34S, 94E)." The precision of Rydberg's estimate is coarser than our new result because of fewer trials. It appears not to consider localization error or the difference in the windage and drift angle parameters which Griffin et al. (2017) measured to be significantly different for the flaperon than undrogued drifters. Nonetheless, it is impressive what Rydberg accomplished with the relatively coarse tools and simple methods available in 2015.

Triananes et al. (2016) studied MH370 floating debris drift and said: "Our results indicate that areas within the Indian Ocean subtropical gyre, including the search area, could be a source of the debris found on La Réunion Island. We also identify zones that can be excluded as potential crash sites and provide estimated travel times and probable ashore positions of plane debris through an analysis of the historical surface drifter dataset." They made no specific prediction of crash latitude.

Wijeratne and Pattiaratchi (2017) also modeled the drift of MH370 floating debris. They said: "Of the 22 pieces of debris found the location of 18 were predicted by our UWA model. Those not predicted were in Mauritius and Rodrigues Islands which may not be well represented in the oceanographic model. The debris origin for this was at 96.5°E and 32.5°S along the 7th arc." The error in their latitude prediction is quoted by Thomas (2017) as being 40 km (or 0.4°), but no explanation of its derivation is provided. We also do not know whether the effects of Stokes drift and leeway were included. Neglecting these effects would under-predict the mean drift speed and bias the POI prediction to the north. Wijeratne and Pattiaratchi's prediction for the MH370 POI latitude at 32.5 ± 0.4°S is within our predicted range. We expect our result to be more accurate because we have used:

  a)   more matching debris predictions (twenty-two debris sites when the redundant cases are included),

  b)   many trials (86,400) to reduce the statistical noise,

  c)   compensation if needed for the unknown windage of each debris,

  d)   the measured leeway and drift angle parameters to predict the Flaperon tracks, and

  e)   a prediction method which is validated to be accurate over a wide range of POI latitudes.

Corrado et al. (2017) used four undrogued drifter tracks to predict a POI latitude of 35 ± 5°S.

Gao et al. (2018) concluded: "The results suggest that the north part of the UWSA is the most likely area to be the crash site of MH370."

Nesterov (2018) also studied the MH370 crash location as follows: "The drift study of MH370 debris was conducted by means of numerical modelling using a forward particle tracking technique. A total of 40 hypothetical locations of the crash site along the seventh arc were screened. Three major aspects were considered: (1) the efficacy of the aerial search; (2) ambient water temperatures along the path of the Flaperon to La Réunion; (3) the spatial distribution of the debris washed ashore . . . . Obtained results indicate the likelihood of the crash site to be located between 25.5°and 30.5°S, with the segment from 28° to 30°S being the most promising." Nesterov discounted the region from 30.5°S to 34.5°S because "Excellent aerial coverage of the debris cloud originating from this segment makes the crash site unlikely to be located within it." We disagree

with this conclusion because Figure 13.2-1 below demonstrates the aerial coverage there was incomplete. We took Figure 13.2-1 from Figure 4.1 in Griffin et al. (2016), which was also used as Figure 20 in ATSB (2017).
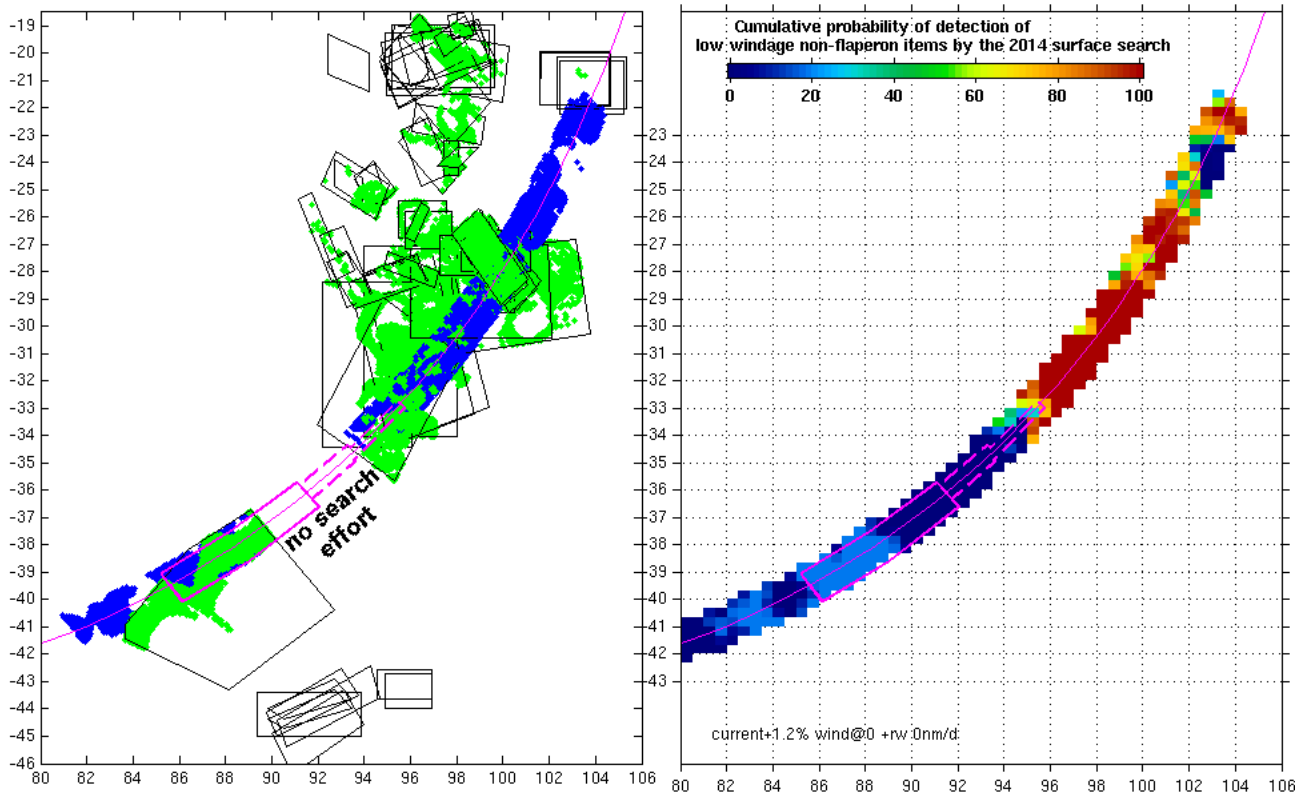

Figure 13.2-1 Probability of detection of the surface search [Figure 4.1 from Griffin et al. (2016)]

The right panel in Figure 13.2-1 shows the probability of surface debris detection for origins near the 7th Arc. It indicates the probability was extremely high, close to 100%, for POI latitudes north of -32.7°. Between -32.7° and -34.0°, the probability declines rapidly to near zero. Close to the arc the probability is extremely low from -37.7° up to -33.3°. Thus, the region between -33.3° and -34.5°, which Nesterov (2018) excluded, has a low to extremely low probability of detection of surface debris based on the aerial search. Therefore, it cannot be excluded on this basis. Also, the POI latitude predicted by Wijeratne and Pattiaratchi (2017) of -32.5°S lies in the area where the aerial search had an extremely high probability of detecting surface debris, so it is an unlikely location.

Durgadoo et al. (2021) considered drift trajectories which originated within the maximum aircraft range and within 550 km of the 7th Arc. There they found ". . . the most probable region for the crash site around the Arc lies between 30–35°S . . . ." This result is entirely consistent with our prediction.

The previously published drift predictions discussed in this section are all consistent with our more accurate drift PDF. The prediction by Wijeratne and Pattiaratchi (2017) is within our drift probability range, but it is unlikely because it falls in the area where the aerial search was highly effective in determining a negative result.

14. Other MH370 Crash Latitude Discriminators

14.1. Route probability

Figure 14.1-1 below shows the route probability from UGIB (2020). This is the probability that an autopiloted post-19:41 route matches the SATCOM and GDAS data. The most probable route is the LNAV 180° BEDAX route at LRC at FL390, but many other routes are possibilities.
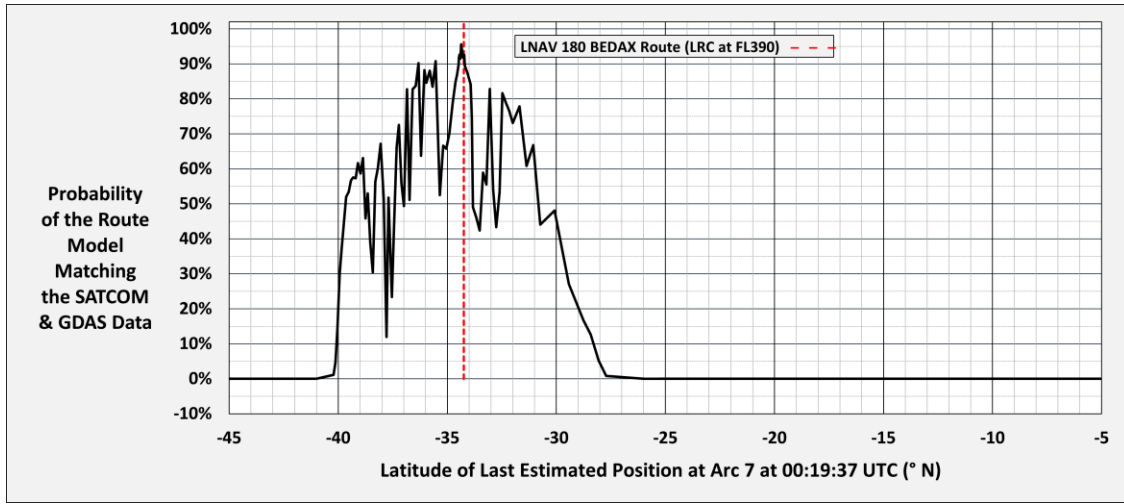

Figure 14.1-1 Probability of the UGIB (2020) route model matching the SATCOM/GDAS Data

14.2. Fuel probability

Figure 14.2-1 below shows the fuel probability. UGIB (2020) estimated the fuel required to achieve main engines fuel exhaustion (MEFE) circa 00:17:30 UTC (as implied by the SATCOM data) for each of the routes found otherwise plausible and therefore included in the route probability.
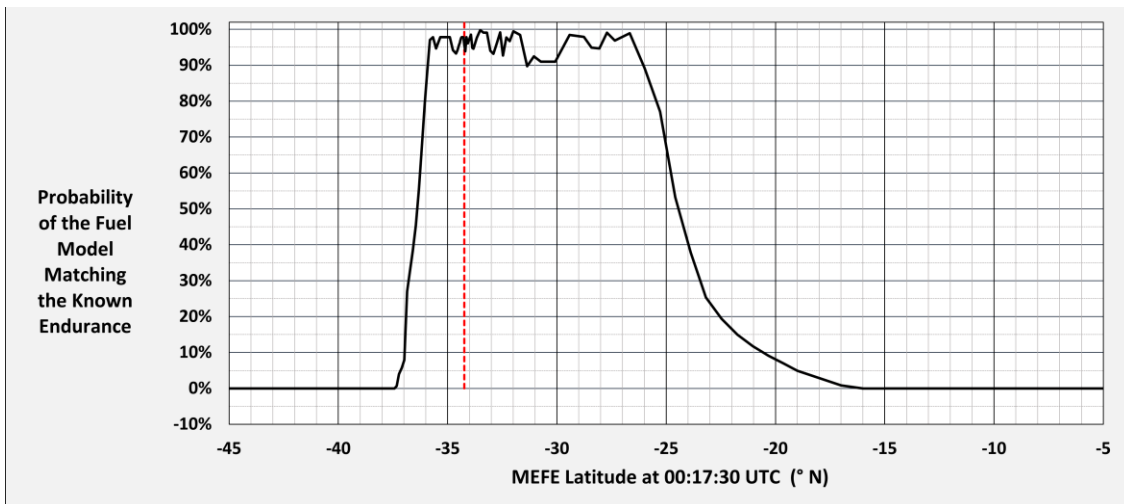
Figure 14.2-1 Revised probability of the UGIB (2020) fuel model matching the known endurance

We revised the fuel probability from UGIB (2020) by including additional routes intersecting Arc 7 between -35° and -36° which were subsequently identified as being acceptable matches to the SATCOM and GDAS data, including main engines fuel exhaustion (MEFE) circa 00:17:30 UTC. Therefore, this revised fuel probability extends the acceptable range of Arc 7 latitudes to about -36.5°.

The product of the route and fuel probabilities is shown in Figure 14.2-2. Note that the compound probability (i.e., the product of route X fuel) retains the fine structure of the route probability.
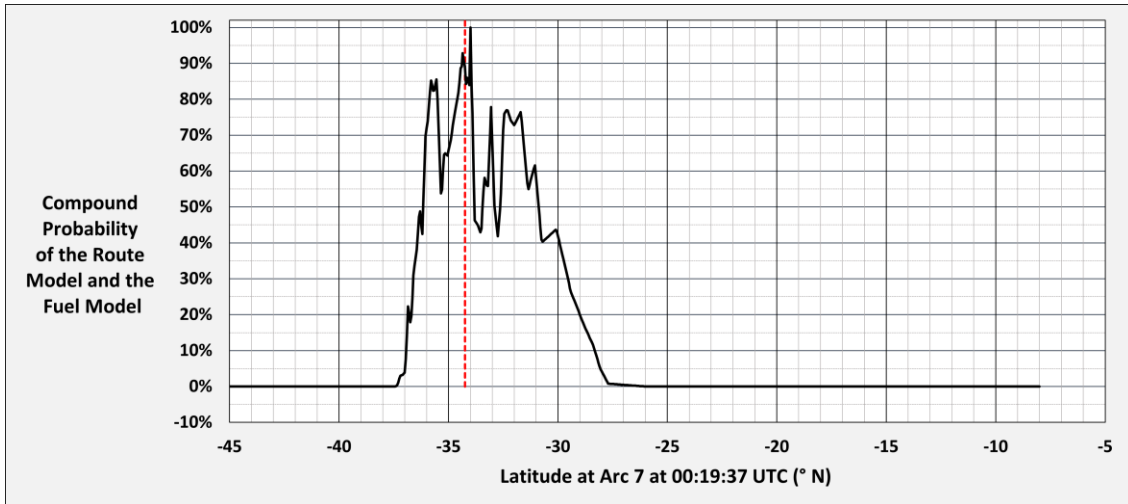
Figure 14.2-2 Product of the route and fuel probabilities

14.3. Glide range probability

To process the compound route/fuel probability in Figure 14.2-2 above with the aerial search and drift probabilities, we must modify Figure 14.2-2 so it corresponds to the time of impact, not the time of MEFE. While we don't know the exact time of impact, except that it must be at least several minutes later than MEFE and probably prior to 00:44 UTC, we can accomplish this by adding an unpowered "glide" from cruising altitude to the sea surface. We parameterize this glide by the horizontal distance (i.e., the glide range) covered during the descent from the MEFE altitude and position to the POI.

Figure 14.3-1 presents our assumed glide range probability as a function of the horizontal distance traveled.

Figure 14.3-1 PDF of glide range after fuel exhaustion

We model the glide range probability as a Bayesian statistic. We assume a gaussian distribution with 3σ = 140 NM, which is the maximum glide range possible for a Boeing B777-200ER if ideally flown by an experienced pilot maintaining maximum lift-to-drag ratio. This glide range probability would have a range of 1σ = 47 NM = 0.78° of arc or less 68% of the time, 2σ = 94 NM or less 95% of the time, and 3σ = 140 NM or les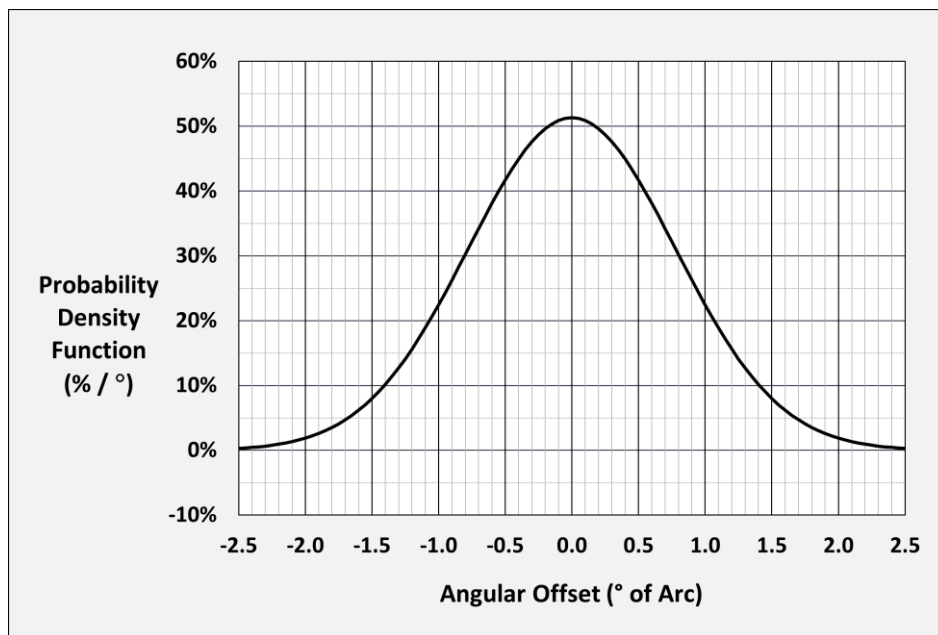s 99.2% of the time. We apply this glide range in the N-S latitude direction, as a worst case, understanding that glides at other bearings would shift the crash latitude by a smaller projected distance on the latitude axis.

14.4. Route/fuel/glide range probability

Because the glide range applies to all points on Arc 7, we convolve the glide probability in Figure 14.3-1 above with the route/fuel probability from Figure 14.2-2 above to obtain the route/fuel/glide range probability at impact, as shown below in Figure 14.4-1.
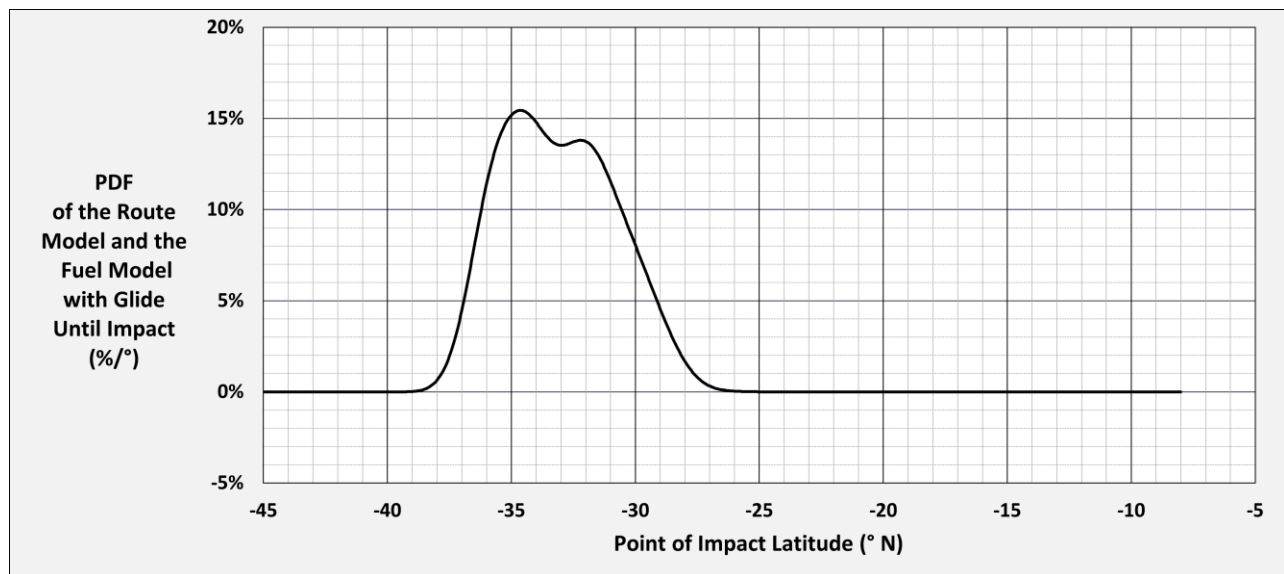
Figure 14.4-1 PDF of POI latitude using route/fuel/glide probabilities

The glide range probability blurs the fine structure in the route probability, so what remains is a broader, smooth function with two blended peaks. The larger peak is near -35° and the slightly smaller peak is near -32°. The probability is within a factor of 3X of the peak from -29° to -37°, which is quite a large range. Incorporating the glide range increases the extent of acceptable impact latitudes, as expected.

14.5. Aerial search probability

The next step is to incorporate the aerial search probability, which is shown below in Figure 14.5-1. This is the probability that the aerial search <u>did not detect</u> the floating debris field in the vicinity of Arc 7 within a few weeks after the crash [private communication from David Griffin (2019) as published by UGIB (2020)].

We calculated the one-dimensional aerial search PDF shown here as Figure 14.5-1 based on the two-dimensional probability map shown previously as Figure 13.2-1. Note the lack of aerial search coverage south of -33° results in a high estimated probability MH370 could have crashed there.
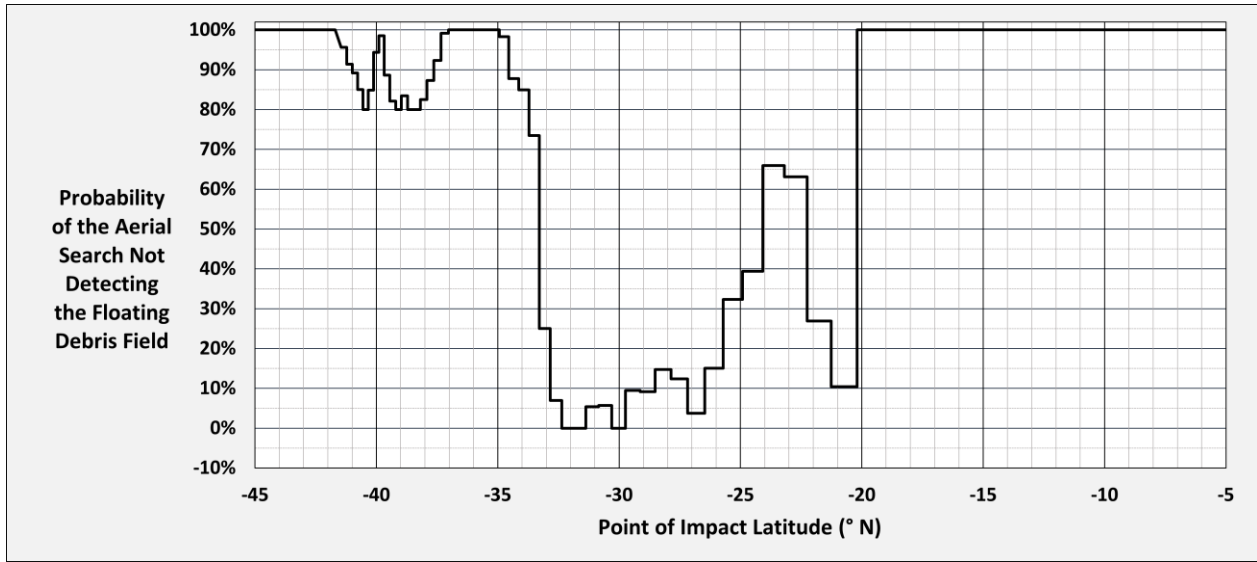
Figure 14.5-1 Aerial search probability of MH370 crash latitude

15. Overall Probability of MH370 Crash Latitude

15.1. Joint PDF including all factors

To obtain our final compound PDF, we use the product of the route/fuel/glide probability (in Figure 14.4-1), the aerial search probability (in Figure 14.5-1), and the debris drift probability (in Figure 12.1-2). This compound route/fuel/glide range/aerial search/drift probability is the joint PDF shown below in Figure 15.1-1.
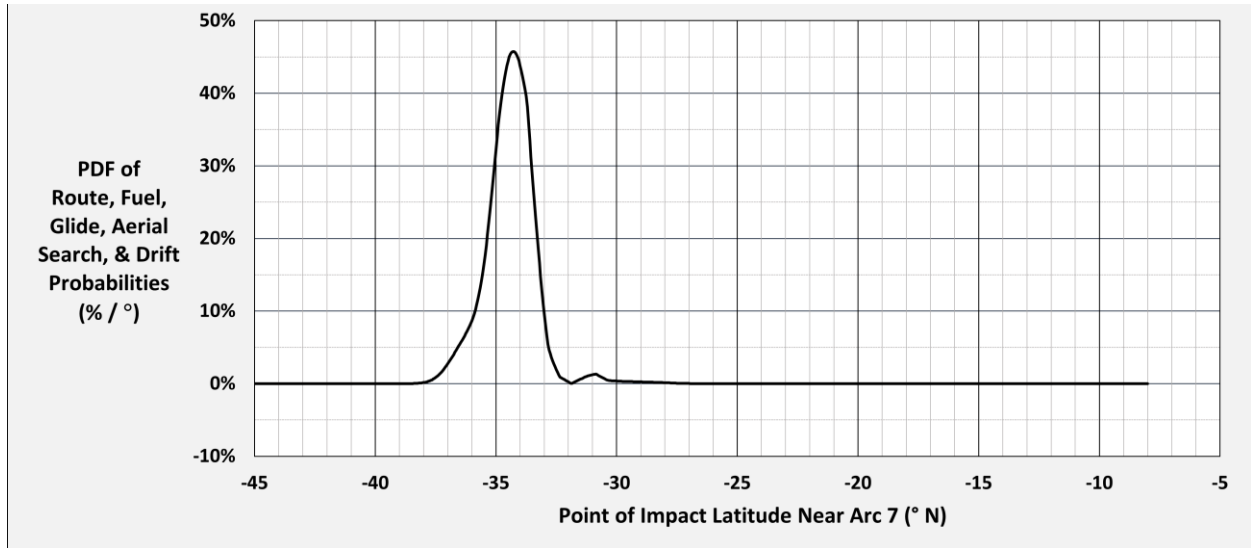
Figure 15.1-1 Probability of MH370 crash latitude near Arc 7

It is interesting to note that this result hardly changes if one excludes the route probability. The southern edge of the acceptance zone of latitudes is set by the fuel/glide range probability. The northern edge is set primarily by the aerial search probability. The drift probability is aligned with the zone between those limits and enhances it.

We effectively have three independent indicators of a crash in the vicinity of -34°:

a. the combination of the fuel/glide range/aerial search probabilities,

b. the peak route probability, and

c. the drift probability.

Their agreement is a good indication that the aircraft crashed not too far from -34°. How else could all three be substantially wrong and by the same amount?

An expanded view of the compound PDF over the latitude range of interest is shown in Figure 15.1-2.
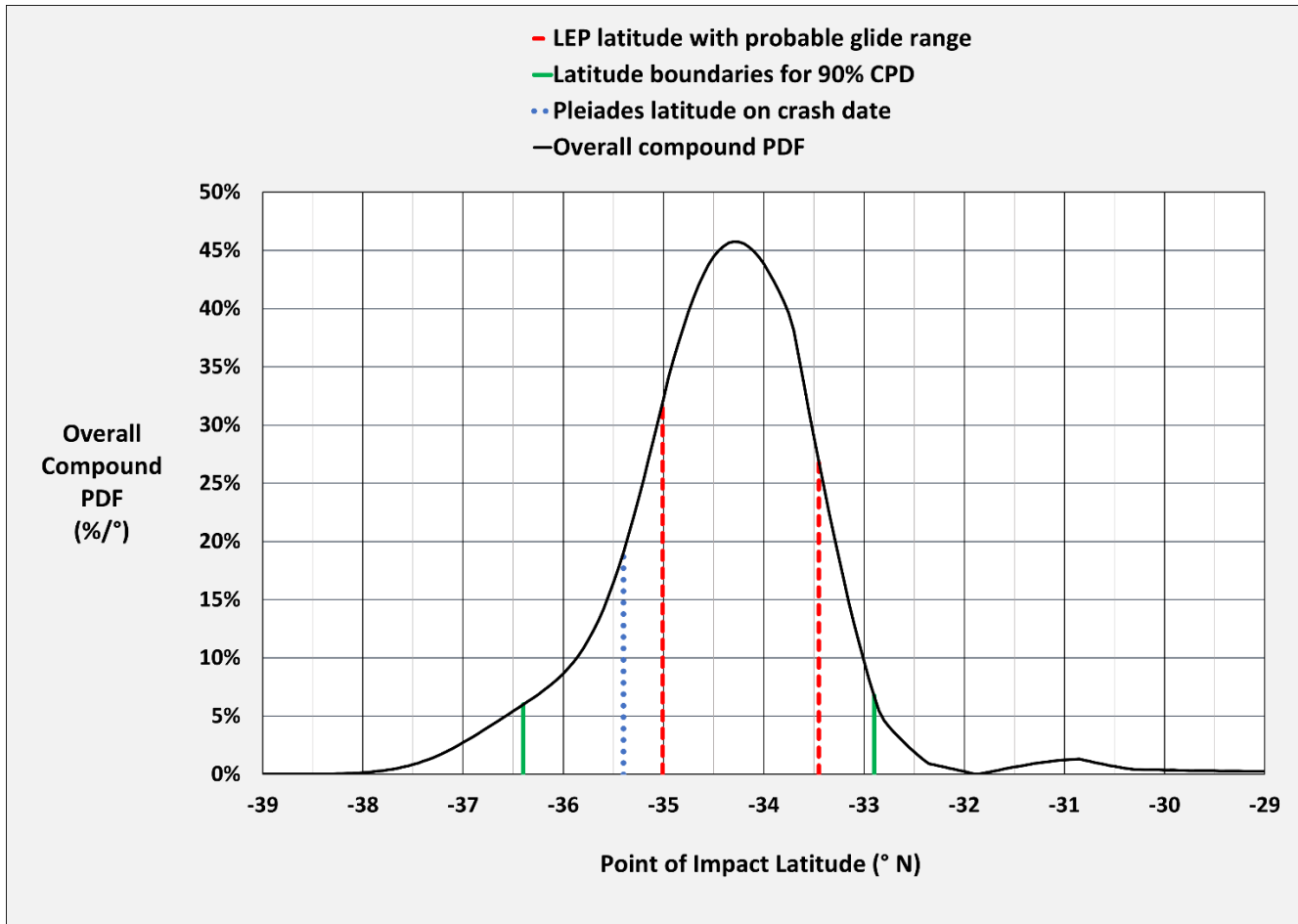
Figure 15.1-2 Probability of MH370 POI latitude near Arc 7

The solid black line is the compound probability that the 9M-MRO point of impact was at a given latitude near Arc 7 considering route, fuel, glide range, aerial search, and debris drift probabilities.

The latitudes from -32.9° to -36.4° (as indicated by the two vertical solid green lines) are within about 8X of the peak probability (which occurs at -34.3°). This latitude region, with a width of ± 94 NM from Arc 7, contains about 90% of the cumulative probability distribution (CPD).

The two vertical dashed red lines in Figure 15.1-2 are the boundaries of the latitude range of the Last Estimated Position (LEP) predicted by UGIB (2020) plus and minus the estimated probable glide range of 47 NM (i.e., ± 1σ). The close agreement shown in Figure 15.1-2 implies the post-fuel-exhaustion glide range is more likely than not to be less than 47 NM.

The estimated location on the crash date of the COSMO-SkyMed/Pleiades objects at -35.4°N, 92.8°E [Iannello (2021a)] is not ruled out by Figure 15.1-2. This location is shown by the blue dotted line in Figure 15.1-2.

16. Impact Zones with Assumed Course

We estimated the boundaries of MH370 locations at the times of various events in the vicinity of Arc 7, assuming the route from BEDAX to the UGIB LEP was flown. This assumption is not certain, but there is evidence in the route fitting results that its probability is the highest among all the routes we analysed. Therefore, we use these location predictions, based on the LEP route, to prioritize searching within our recommended zones (which make no assumption regarding this particular route).

16.1.   LEP Route Boundaries

Our predictions of the MH370 locations at various times near fuel exhaustion, assuming the UGIB LEP route was flown, are shown in Figure 16.1-1 below.

LEP Route

The black dashed vertical line is the best-fit southbound track from UGIB (2020). This course passes through waypoint BEDAX and has a true bearing of 180°. The blue diamond is where that auto-piloted course intercepts Arc 7 (shown by the blue line) circa 00:19:29. This is the Last Estimated Position (LEP) from UGIB (2020).

Arc 6 at 00:11:00 UTC

The green diamond is the estimated aircraft position at Arc 6 (the curved green line) at 00:11:00 UTC. The green parallelogram is the 2-sigma boundary of the aircraft location at 00:11:00. The "width" of this parallelogram is derived from the uncertainty in the fitted route longitude (as indicated by the pair of vertical black dotted lines). The "height" of the parallelogram (i.e., the range error perpendicular to Arc 6) is due to the noise present in BTO readings. Thus, if the route assumption is correct, there is a 90% probability the aircraft was inside the green parallelogram at 00:11:00 UTC. We therefore have a fairly precise estimate of the aircraft location at 00:11:00. However, the location error grows with time thereafter.

Fuel Exhaustion at 00:17:30 UTC

The next time of interest, in the end-of-flight timeline for MH370, is the fuel exhaustion at 00:17:30 UTC. The aircraft location at that time is inside (at 2-sigmas) the gray parallelogram. Note that its width in longitude is the same as the width at 00:11:00 (the green box). That's because the autopilot was maintaining the track in the interim, although the ground speed is somewhat uncertain. The uncertainty in average ground speed between 00:11:00 and 00:17:30 makes the gray box larger in the direction parallel to the course. We know the aircraft probably suffered one engine flame-out prior to 00:17:30 (which is when the second engine flamed out), but we don't know exactly when the first engine flamed out. Therefore, the 00:17:30 box dimension along the track allows the first engine fuel exhaustion to occur at any time between 00:11:00 (our earliest estimate) and 00:17:30 (our latest estimate). If the first engine flamed out nearer 00:11:00 (which we think is more likely), then the aircraft would have slowed more and would be nearer the northern end of the gray box. If the first engine flamed out close to 00:17:30, the aircraft would be nearer the southern end of the gray box. Note that it is possible, but not likely in this scenario, for the aircraft to have already crossed Arc 7 at 00:17:30.

Boeing Splash Point Simulations

The pink dots in Figure 16.1-1 are the splash points of the Boeing simulations, when their starting courses are aligned in time and also shifted to be due south on the assumed track from BEDAX. Note most of the Boeing splash points are to the "left side" of the autopilot track.
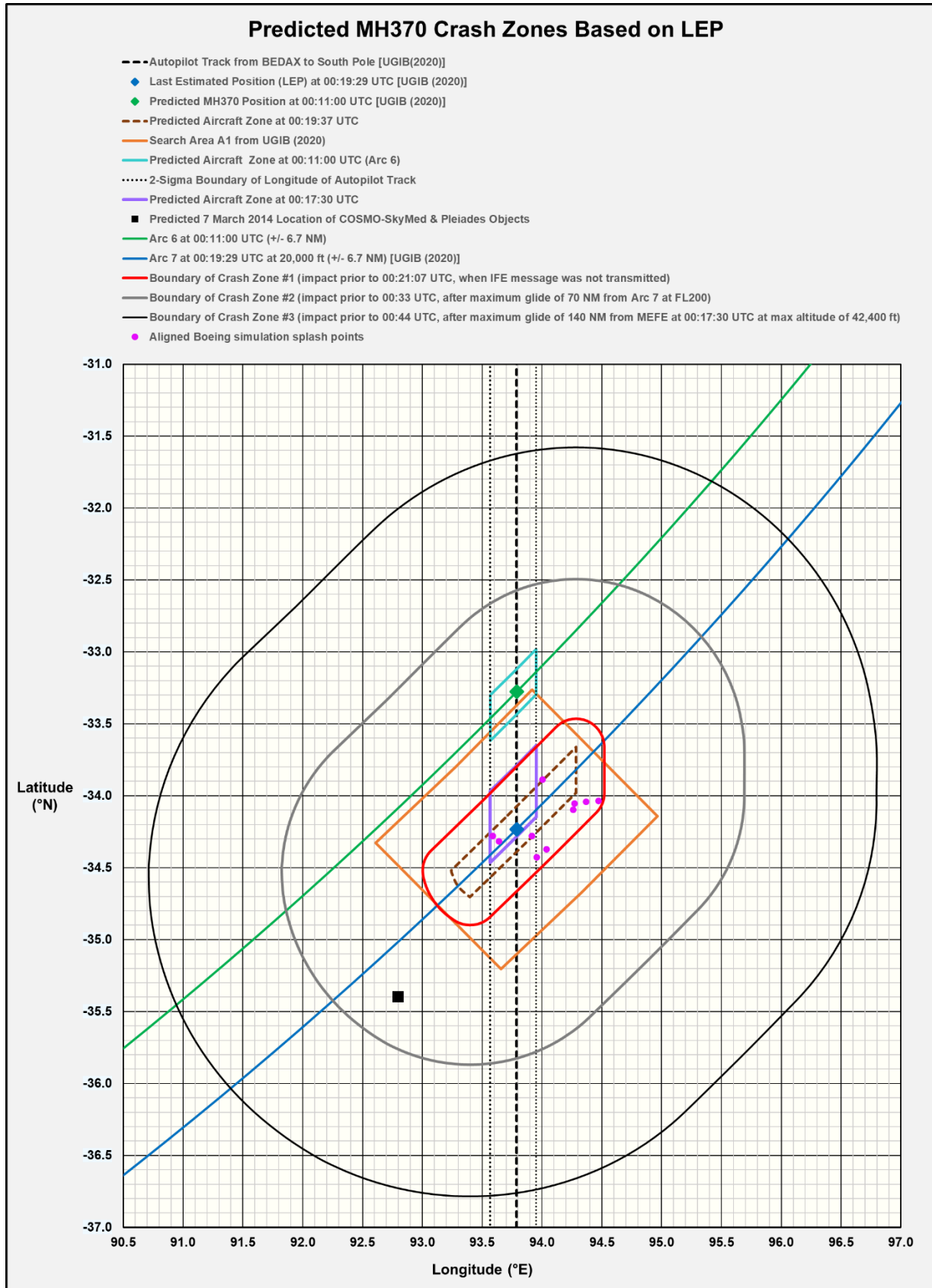
Figure 16.1-1 MH370 locations assuming the LEP Route

Arc 7 at 00:19:30 UTC

The aircraft location at 00:19:30 is shown by the black dashed "box" centered on Arc 7. Its width perpendicular to the 7th Arc is set by the BTO noise. Its width along Arc 7 is set by the maximum distance the aircraft could have flown from all points within the 00:17:30 box in the 2-minute interim (which is 16.6 NM). Now we know the boundary of the aircraft position at 00:19:30 (the black dashed boundary).

Missing SATCOM Transmission at 00:21:07 UTC

The time of the expected, but not detected, In-Flight Entertainment (IFE) transmission is 00:21:07 UTC. It appears that either the aircraft crashed before that time, or possibly it was in an unusual attitude such that the SATCOM antennas on the aircraft did not have a clear view of the satellite, or possibly the APU ran out of fuel. The solid red line bounds the aircraft location at 00:21:07 UTC, using the maximum possible ground speed for the 1:37 elapsed time between Arc 7 and the IFE transmission. So, if the aircraft had crashed by 00:21:07 in this scenario, the POI should be inside the red zone. In this case there would have been no piloted, extended glide.

70 NM Glide until 00:33:00 UTC

The large brown "racetrack" boundary shows an additional 70 NM glide range (from Arc 7 at FL200). We believe it is highly probable in this scenario that the MH370 debris field is within this 70-NM-glide zone.

140 NM Glide until 00:44:00 UTC

The very large black racetrack indicates the 140 NM maximum glide boundary from the maximum possible altitude (43,200 feet) at MEFE at 00:17:30 UTC, and with an impact not later than 00:44:00 UTC. This boundary provides close to 100% certainty of containing the POI if the BEDAX route were flown.

16.2. Search Area A1 from UGIB (2020)

The orange rectangle in Figure 16.1-1 above is the proposed Search area A1 from UGIB (2020). It encompasses almost all of the newly predicted 00:21:07 zone and extends farther from Arc 7.

17. Search Recommendations

17.1. Prioritised search zones

Our prioritised recommendations for a future sea-floor search for the MH370 debris field are as follows:

1. Closely inspect those portions of the area from -32.9° to -36.4°, and within the previously searched width along Arc 7, which are:

    a. holidays (i.e., unsearched areas),
    b. areas with difficult terrain,
    c. areas with lower-quality sonar data, and
    d. previous contacts by GO Phoenix and Ocean Infinity which could be misclassified.

    This Zone 1 is the area enclosed by the white rectangle in Figure 17.1-1 below. When those portions listed above are completed, Zone 1 includes 22% of the cumulative detection probability (CDP). We recommend prioritising the portion of this Zone 1 which is also within the predicted 00:21:07 boundary, which is shown by the red racetrack (i.e., Zone 1A). Zone 1B is that portion of Zone 1 which is outside the 00:21:07 boundary (i.e., outside the red racetrack), and this area is lower in priority than Zone 1A.

2. If #1 is unsuccessful, then widen the search to ± 70 NM from the UGIB Arc 7. This Zone 2 achieves a 90% CDP, and it is indicated by the purple racetrack in Figure 17.1-1.

3. If #2 is unsuccessful, then widen the search to ± 140 NM from the UGIB Arc 7. This Zone 3 achieves a 98% CDP, and it is indicated by the very large green racetrack in Figure 17.1-1.

These three recommended search zones (Zones 1-3) and the possible 00:21:07 boundary (which segregates Zone 1A from Zone 1B) are shown in Figure 17.1-1.

We hope future searches for the aircraft debris field will be successful, allowing the potential recovery of the flight data and voice recorders, which may assist in the determination of the cause of the crash and define the exact route flown.
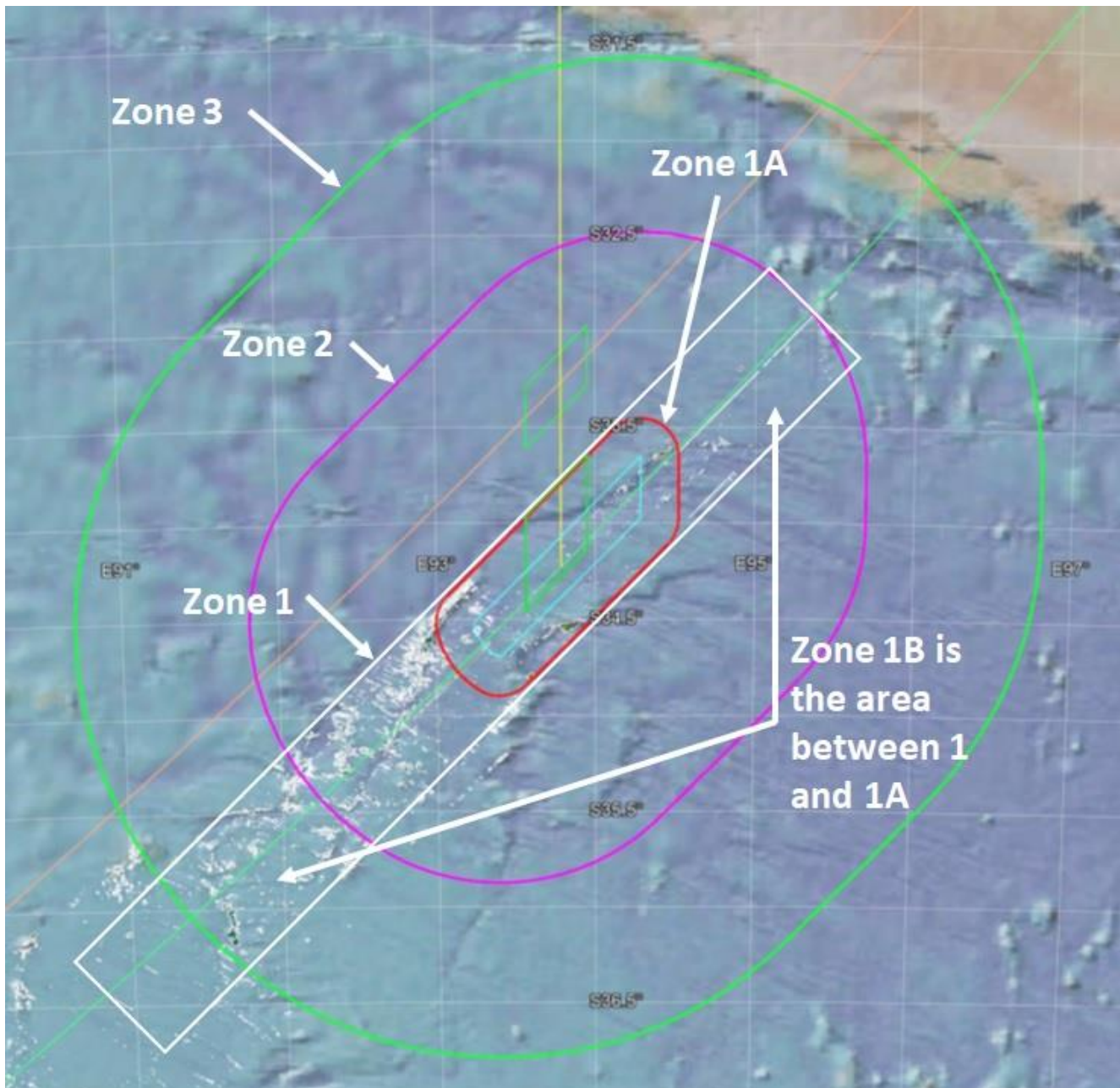
Figure 17.1-1 Map of recommended search zones

18. Acknowledgements

19. List of Appendices

We provide additional details of our work and results in the attached Appendices as follows:

Appendix A – Drift Probability Theory

Appendix B – Description of Processing Method

Appendix C - Probability Equation for Validation Tests

Appendix D - Comparison of Positive and Negative Debris Reports

20. Bibliography

Safety Investigation Report

Malaysia Ministry of Transport (2018)
Malaysia Ministry of Transport (2018). "Safety Investigation Report: Malaysia Airlines Boeing B777-200ER (9M-MRO) 08 March 2014"; Malaysian ICAO Annex 13 Safety Investigation Team for MH370, Report MH370/01/2018; 2 July 2018.
http://www.airsafe.com/events/reports/mh370-malaysia-government-final-report-2018.pdf

Aerial Debris Search

AMSA (2014)
Australian Maritime Safety Authority (2014). "Search for Malaysia Airlines flight MH370" and "MH370 Search – Media kit."
https://www.amsa.gov.au/safety-navigation/search-and-rescue/search-malaysia-airlines-flight-mh370
https://www.amsa.gov.au/news-community/media-library/mh370-search-media-kit

JACC (2014)
Joint Agency Coordination Centre (2014). "Search for MH370" and "Timeline of significant actions—Search for missing airline MH370".
https://www.infrastructure.gov.au/infrastructure-transport-vehicles/aviation/aviation-safety/aviation-accident-investigations/Joint-agency-coordination-centre
https://www.infrastructure.gov.au/infrastructure-transport-vehicles/vehicles/aviation/Joint-agency-coordination-centre/timeline

Griffin et al. (2016)
Griffin, David, Oke, Peter, and Jones, Emlyn (2016). "The search for MH370 and ocean surface drift"; CSIRO Oceans and Atmosphere; Report Number EP167888; 8 December 2016.
https://publications.csiro.au/publications/publication/PIcsiro:EP167888

ATSB (2017)
Australian Transport Safety Bureau (2017). "The Operational Search for MH370"; ATSB Transport Safety Report, External Aviation Investigation AE-2014-054; 3 October 2017.
https://www.atsb.gov.au/sites/default/files/media/5773565/operational-search-for-mh370_final_3oct2017.pdf

Sea Bottom Search

ATSB (2014a)
ATSB Transport Safety Bureau (2014). "MH370 - Definition of Underwater Search Areas"; ATSB Transport Safety Report, External Aviation Investigation AE-2014-054; issued 26 June 2014, updated 18 August 2014 and 30 July 2015.
https://www.atsb.gov.au/sites/default/files/media/5668327/ae2014054_mh370__search_areas_30jul2015.pdf

ATSB (2015)
ATSB Transport Safety Bureau (2015). "MH370 - Definition of Underwater Search Area Update"; ATSB Transport Safety Report, External Aviation Investigation AE-2014-054; issued 3 December 2015, updated 10 December 2015.

https://www.atsb.gov.au/sites/default/files/2022-12/AE-2014-054_MH370-Definition%20of%20Underwater%20Search%20Areas_3Dec2015.pdf

ATSB (2016g)
Australian Transport Safety Bureau (2016). "MH370 – Search and Debris Examination Update"; ATSB Transport Safety Report, Aviation External Investigation, AE-2014-054; 2 November 2016. https://www.atsb.gov.au/sites/default/files/media/5773389/ae-2014-054_mh370-search-and-debris-update_aug2017.pdf

ATSB (2016h)
Australian Transport Safety Bureau (2016). "MH370 – First Principles Review"; ATSB Transport Safety Report, Aviation External Investigation, AE-2014-054; 20 December 2016. https://www.atsb.gov.au/sites/default/files/media/5772107/ae2014054_final-first-principles-report.pdf

ATSB (2017)
Australian Transport Safety Bureau (2017). "The Operational Search for MH370"; ATSB Transport Safety Report, External Aviation Investigation AE-2014-054; 3 October 2017. https://www.atsb.gov.au/sites/default/files/media/5773565/operational-search-for-mh370_final_3oct2017.pdf

CSIRO Debris Drift Studies

Griffin et al. (2016)
Griffin, David, Oke, Peter, and Jones, Emlyn (2016). "The search for MH370 and ocean surface drift"; CSIRO Oceans and Atmosphere; Report Number EP167888; 8 December 2016. https://publications.csiro.au/publications/publication/PIcsiro:EP167888

Griffin et al. (2017)
Griffin, David, Oke, Peter, and Jones, Emlyn (2017). "The search for MH370 and ocean surface drift – Part II"; CSIRO Oceans and Atmosphere; Report Number EP172633; 13 April 2017. https://publications.csiro.au/publications/publication/PIcsiro:EP172633

Griffin and Oke (2017a)
Griffin, David and Oke, Peter (2017a). "The search for MH370 and ocean surface drift – Part III"; CSIRO Oceans and Atmosphere; Report Number EP177204; 26 June 2017. https://publications.csiro.au/rpr/download?pid=csiro:EP174155&dsid=DS3

Griffin and Oke (2017b)
Griffin, David and Oke, Peter (2017b). "The search for MH370 and ocean surface drift – Part IV"; CSIRO Oceans and Atmosphere; Report Number EP17415526; 3 October 2017. https://publications.csiro.au/publications/publication/PIcsiro:EP177204

Malaysia Ministry of Transport Debris Analyses

Malaysian Ministry of Transport (2017a-2017r)
Malaysia Ministry of Transport (2017a). "Summary of Possible MH370 Debris Recovered"; Malaysian ICAO Annex 13 Safety Investigation Team for MH370, Ministry of Transport, Malaysia; updated 30 April 2017.

http://www.mh370.gov.my/phocadownload/3rd_IS/Summary%20of%20Debris%20300417.pdf

Malaysia Ministry of Transport (2017b). "Identification of Debris (Item 6 in the "Summary of Possible MH370 Debris Recovered") recovered south of Chidenguele, Mozambique on 24 April 2016"; Malaysian ICAO Annex 13 Safety Investigation Team for MH370, Debris Examination Report Ref: DB/01/17; issued on 28 February 2017, updated on 30 April 2017.
http://mh370.gov.my/phocadownload/3rd_IS/Debris%20Examination%20300417.pdf

Malaysia Ministry of Transport (2017c). "Identification of Debris (Item 7 in the "Summary of Possible MH370 Debris Recovered") recovered at Anvil Bay, Chemucane, Mozambique on 30 April 2016"; Malaysian ICAO Annex 13 Safety Investigation Team for MH370, Debris Examination Report Ref: DB/02/17; issued on 28 February 2017, updated on 30 April 2017.
http://mh370.gov.my/phocadownload/3rd_IS/Debris%20Examination%20300417.pdf

Malaysia Ministry of Transport (2017d). "Identification of Debris (Item 8 in the "Summary of Possible MH370 Debris Recovered") recovered at Gris Gris Beach, Mauritius on 24 May 2016"; Malaysian ICAO Annex 13 Safety Investigation Team for MH370, Debris Examination Report Ref: DB/03/17; issued on 28 February 2017, updated on 30 April 2017.
http://mh370.gov.my/phocadownload/3rd_IS/Debris%20Examination%20300417.pdf

Malaysia Ministry of Transport (2017e). "Identification of Debris (Items 9 and 15 in the "Summary of Possible MH370 Debris Recovered") recovered at Macenta Peninsular, Mozambique on 22 May 2016 and Riake Beach, Nosy Boraha Island, Madagascar on 06 June 2016, respectively"; Malaysian ICAO Annex 13 Safety Investigation Team for MH370, Debris Examination Report Ref: DB/04/17; issued on 28 February 2017, updated on 30 April 2017.
http://mh370.gov.my/phocadownload/3rd_IS/Debris%20Examination%20300417.pdf

Malaysia Ministry of Transport (2017f). "Identification of Debris (Item 11 in the "Summary of Possible MH370 Debris Recovered") recovered at Riake beach, Nosy Boraha Island, Madagascar 0n 06 June 2016"; Malaysian ICAO Annex 13 Safety Investigation Team for MH370, Debris Examination Report Ref: DB/05/17; issued on 28 February 2017, updated on 30 April 2017.
http://mh370.gov.my/phocadownload/3rd_IS/Debris%20Examination%20300417.pdf

Malaysia Ministry of Transport (2017g). "Identification of Debris (Item 11 in the "Identification of Debris (Item 12 in the "Summary of Possible MH370 Debris Recovered") recovered at Riake Beach, Nosy Boraha Island, Madagascar on 06 June 2016"; Malaysian ICAO Annex 13 Safety Investigation Team for MH370, Debris Examination Report Ref: DB/06/17; issued on 28 February 2017, updated on 30 April 2017.
http://mh370.gov.my/phocadownload/3rd_IS/Debris%20Examination%20300417.pdf

Malaysia Ministry of Transport (2017h). "Identification of Debris (Item 13 in the "Summary of Possible MH370 Debris Recovered") recovered from Riake Beach, Nosy Boraha Island, Madagascar on 12 June 2016"; Malaysian ICAO Annex 13 Safety Investigation Team for MH370, Debris Examination Report Ref: DB/07/17; issued on 28 February 2017, updated on 30 April 2017.
http://mh370.gov.my/phocadownload/3rd_IS/Debris%20Examination%20300417.pdf

Malaysia Ministry of Transport (2017i). "Identification of Debris (Item 14 in the "Summary of Possible MH370 Debris Recovered") recovered from Riake Beach, Nosy Boraha Island, Madagascar on 12 June 2016";

Malaysian ICAO Annex 13 Safety Investigation Team for MH370, Debris Examination Report Ref: DB/08/17; issued on 28 February 2017, updated on 30 April 2017.
http://mh370.gov.my/phocadownload/3rd_IS/Debris%20Examination%20300417.pdf

Malaysia Ministry of Transport (2017j). "Identification of Debris (Items 16 and 17 in the "Summary of Possible MH370 Debris Recovered") recovered from Antsiraka Beach, Madagascar on 12 June 2016"; Malaysian ICAO Annex 13 Safety Investigation Team for MH370, Debris Examination Report Ref: DB/01/16; issued on 4 October 2016, updated on 30 April 2017.
http://mh370.gov.my/phocadownload/3rd_IS/Debris%20Examination%20300417.pdf

Malaysia Ministry of Transport (2017k). "Identification of Debris (Item 18 in the "Summary of Possible MH370 Debris Recovered") recovered from Antsiraka beach, Madagascar on 12 June 2016"; Malaysian ICAO Annex 13 Safety Investigation Team for MH370, Debris Examination Report Ref: DB/09/17; issued on 28 February 2017, updated on 30 April 2017.
http://mh370.gov.my/phocadownload/3rd_IS/Debris%20Examination%20300417.pdf

Malaysia Ministry of Transport (2017l). "Identification of Debris (Item 20 in the "Summary of Possible MH370 Debris Recovered") recovered from Kosi Bay mouth, Northern Kwa Zulu Natal, South Africa on 21 June 2016"; Malaysian ICAO Annex 13 Safety Investigation Team for MH370, Debris Examination Report Ref: DB/10/17; issued on 28 February 2017, updated on 30 April 2017.
http://mh370.gov.my/phocadownload/3rd_IS/Debris%20Examination%20300417.pdf

Malaysia Ministry of Transport (2017m). "Identification of Debris (Item 21 in the "Summary of Possible MH370 Debris Recovered") recovered from Northern Kwa Zulu Natal, South Africa on 18 July 2016"; Malaysian ICAO Annex 13 Safety Investigation Team for MH370, Debris Examination Report Ref: DB/11/17; issued on 28 February 2017.
http://mh370.gov.my/phocadownload/3rd_IS/Debris%20Examination%20300417.pdf

Malaysia Ministry of Transport (2017n). "Identification of Debris (Item 22 in the "Summary of Possible MH370 Debris Recovered") recovered at Linga Linga beach, Mozambique on 26 August 2016"; Malaysian ICAO Annex 13 Safety Investigation Team for MH370, Debris Examination Report Ref: DB/12/17; issued on 28 February 2017, updated on 30 April 2017.
http://mh370.gov.my/phocadownload/3rd_IS/Debris%20Examination%20300417.pdf

Malaysia Ministry of Transport (2017o). "Identification of Debris (Item 23 in the "Summary of Possible MH370 Debris Recovered") recovered from Riake Beach, Nosy Bohara Island, Madagascar in October 2016"; Malaysian ICAO Annex 13 Safety Investigation Team for MH370, Debris Examination Report Ref: DB/13/17; issued on 28 February 2017, updated on 30 April 2017.
http://mh370.gov.my/phocadownload/3rd_IS/Debris%20Examination%20300417.pdf

Malaysia Ministry of Transport (2017p). "Identification of Debris (Item 25 in the "Summary of Possible MH370 Debris Recovered") recovered from Riake beach, Nosy Boraha Island, Madagascar in July 2016"; Malaysian ICAO Annex 13 Safety Investigation Team for MH370, Debris Examination Report Ref: DB/14/17; issued on 28 February 2017, updated on 30 April 2017.
http://mh370.gov.my/phocadownload/3rd_IS/Debris%20Examination%20300417.pdf

Malaysia Ministry of Transport (2017q). "Identification of Debris (Item 26 in the "Summary of Possible MH370 Debris Recovered") recovered from Nautilus Bay, South Africa on 23 December 2016"; Malaysian ICAO

Annex 13 Safety Investigation Team for MH370, Debris Examination Report Ref: DB/15/17; issued on 30 April 2017.
http://mh370.gov.my/phocadownload/3rd_IS/Debris%20Examination%20300417.pdf

Malaysia Ministry of Transport (2017r). "Identification of Debris (Item 27 in the "Summary of Possible MH370 Debris Recovered") recovered from Mpame Beach, South Africa on 27 January 2017"; Malaysian ICAO Annex 13 Safety Investigation Team for MH370, Debris Examination Report Ref: DB/16/17; issued on 30 April 2017.
http://mh370.gov.my/phocadownload/3rd_IS/Debris%20Examination%20300417.pdf

ATSB Debris Analyses

ATSB (2016a-2016f)

ATSB (2016a). "Debris examination – update No. 1, Missing aircraft, Boeing 777, 9M-MRO, 8 March 2014: Identification of two items of debris recovered from beaches in Mozambique"; Australian Transport Safety Bureau, Australia Technical Examination Report, Aviation, AE-2014-054; 19 April 2016 (amended 17 August 2017).
https://www.atsb.gov.au/sites/default/files/media/5773385/debris-examination-update-1_amended.pdf

ATSB (2016b). "Debris examination – update No. 2, Missing aircraft, Boeing 777, 9M-MRO, 8 March 2014: Identification of two items of debris recovered from beaches in South Africa and Mauritius; Australian Transport Safety Bureau, Australia Technical Examination Report, Aviation, AE-2014-054; 12 May 2016 (amended 24 May 2016 and 17 August 2017).
https://www.atsb.gov.au/sites/default/files/media/5773386/debris-examination-update-2_amended.pdf

ATSB (2016c). "Debris examination – update No. 3, Missing aircraft, Boeing 777, 9M-MRO, 8 March 2014: Identification of large flap section recovered off the Tanzanian coast"; Australia Transport Safety Bureau, Australian Technical Examination Report, Aviation, AE-2014-054;15 September 2016 (amended 17 August 2017).
https://www.atsb.gov.au/sites/default/files/media/5773387/debris-examination-update-3_amended.pdf

ATSB (2016d). "Debris examination – update No. 4, Missing aircraft, Boeing 777, 9M-MRO, 8 March 2014: Preliminary examination of two items of debris recovered near Sainte Luce, Madagascar"; Australian Transport Safety Bureau, Australia Technical Examination Report, Aviation, AE-2014-054; 2016.
https://www.atsb.gov.au/sites/default/files/media/5771521/debris-examination-report-4.pdf

ATSB (2016e). "Debris examination – update No. 5, Missing aircraft, Boeing 777, 9M-MRO, 8 March 2014: Identification of wing trailing edge debris recovered from Mauritius"; Australian Transport Safety Bureau, Australia Technical Examination Report, Aviation, AE-2014-054; 6 October 2016 (amended 17 August 2017).
https://www.atsb.gov.au/sites/default/files/media/5773388/debris-examination-update-5_amended.pdf

Australian Transport Safety Bureau (2016f). "MH370 – Search and Debris Examination Update"; Australian Transport Safety Bureau, Transport Safety Report, Aviation External Investigation, AE-2014-054; 2 November 2016.
https://www.atsb.gov.au/sites/default/files/media/5773389/ae-2014-054_mh370-search-and-debris-update_aug2017.pdf

Reports of Blaine Gibson Debris Finds

Bowker and Gelineau (2016)

Tom Bowker and Kristen Gelineau (2016). "It was so light': Man finds possible MH370 debris";
CTV News, The Associated Press; 3 March 2016.
https://www.ctvnews.ca/world/it-was-so-light-man-finds-possible-mh370-debris-1.2801918

BBC News (2016)
BBC News (2016). "MH370 search: New debris found on Madagascar beach"; BBC News; 10 June 2016.
https://www.bbc.com/news/world-asia-36495617

Thomas (2021)
Geoffrey Thomas (2021). "MH370; The Extraordinary Debris Trail Across the Indian Ocean "; Airline Ratings;
1 December 2021.
https://www.airlineratings.com/news/mh370-extraordinary-debris-trail-across-indian-ocean/

Flight Path Analyses

ATSB (2014b)
ATSB Transport Safety Report (2014). "MH370 – Flight Path Analysis Update"; ATSB Transport Safety Report,
External Aviation Investigation AE-2014-054; 8 October 2014.
https://www.atsb.gov.au/sites/default/files/2023-03/AE-2014-054_MH370%20-
FlightPathAnalysisUpdate.pdf

Davey et al. (2016)
Sam Davey, Neil Gordon, Ian Holland, Mark Rutten, and Jason Williams (2016). "Bayesian Methods in the
Search for MH370"; Springer Verlag ISSN 2191-8112; 2016.
https://link.springer.com/content/pdf/10.1007%2F978-981-10-0379-0.pdf

ATSB (2016g)
ATSB (2016). "MH370 – Search and Debris Examination Update"; ATSB Transport Safety Report, External
Aviation Investigation, AE-2014-054; 2 November 2016, updated 18 August 2017.
https://www.atsb.gov.au/sites/default/files/media/5773389/ae-2014-054_mh370-search-and-debris-
update_aug2017.pdf

Holland (2018)
Ian D. Holland (2018). "MH370 Burst Frequency Offset Analysis and Implications on Descent Rate at End-of-
Flight"; IEEE AES Mag., v. 33, no. 2, pp 24-33 (2018); issued 7 February 2017, updated 15 January 2018.
https://arxiv.org/pdf/1702.02432.pdf

Ulich et al. or UGIB (2020)
Bobby Ulich, Richard Godfrey, Victor Iannello, and Andrew Banks (2020). "The Final resting Place of MH370";
7 March 2020.
https://drive.google.com/file/d/1mAAVLdxjvaukhRJzL0i5BFvT34vTuHp4/view
https://mh370.radiantphysics.com/2020/03

Other Drift Studies

Ashkenazy and Gildor (2011)
Yosef Ashkenazy and Hezi Gildor (2011). "On the Probability and Spatial Distribution of Ocean Surface
Currents"; Ben-Gurion University, 2011.
https://www.bgu.ac.il/~ashkena/Papers/JPO11.pdf

Van Sebille et al. (2012)
Eric Van Sebille, Matthew H. England, and Gary Froyland (2012). "Origin, dynamics and evolution of ocean garbage patches from observed surface drifters"; Environmental Research Letters 7:044040, 19 December 2012.
https://pdfs.semanticscholar.org/11d0/cb20f29d5045bdfe0a7968430936aad17667.pdf

Adrift (2015)
Ocean drift model by Erik van Sebille, David Fuchs, and Jack Murray.
https://www.sciencedirect.com/science/article/abs/pii/S0022098114002445
and
https://plasticadrift.org/

Rydberg (2015)
Henrik Rydberg (2015). "MH370: Finding the Debris Origin"; published August 2, 2015, updated August 5, 2015.
http://bitmath.org/mh370/debris-origin.pdf

Trinanes et al. (2016)
Joaquin A. Trinanes, M. Josefina Olascoaga, Gustavo J. Goni, Nikolai A. Maximenko, David A. Griffin, and Jan Hafner (2016). "Analysis of flight MH370 potential debris trajectories using ocean observations and numerical model results"; Journal of Operational Oceanography; 2016.
https://www.aoml.noaa.gov/phod/docs/MH370_Trinanes_etal.pdf

Wijeratne and Pattiaratchi (2017)
Sarath Wijeratne and Charitha Pattiaratchi (2017). "Where is MH370? Scientists Say They Have 'Credible Information' for Location"; Newsweek; 28 April 2017.
https://www.newsweek.com/mh370-search-location-591708

Thomas (2017)
Geoffrey Thomas (2017). "UWA pinpoints MH370 crash site"; The West Australian; 7 March 2017.
https://thewest.com.au/news/mh370/uwa-pinpoints-mh370-crash-site-ng-b88407234z

Corrado et al. (2017)
Raffaele Corrado, Guglielmo Lacorata, Luigi Palatella, Rosalia Santoleri, and Enrico Zambianchi (2017). "General characteristics of relative dispersion in the ocean"; Nature Scientific Reports | 7:46291 | DOI: 10.1038/srep46291re; 2017.
https://www.nature.com/articles/srep46291.pdf

Nesterov (2018)
Oleksandr Nesterov (2018). "Consideration of various aspects in a drift study of MH370 debris"; Ocean Science, 14, 387–402; 2018.
https://os.copernicus.org/articles/14/387/2018/os-14-387-2018.pdf

Gao et al. (2018)
Jia Gao, Lin Mu, Xianwen Bao, Jun Song, and Yang Ding (2018). "Drift analysis of MH370 debris in the southern Indian Ocean"; Frontiers of Earth Science volume 12, pages 468–480; 2018.

https://www.researchgate.net/publication/325275156_Drift_analysis_of_MH370_debris_in_the_southern
_Indian_Ocean

Godfrey (2021)
Richard Godfrey (2021). "MH370 Floating Debris – Drift Analysis"; published 1 January 2021, updated 12 January 2021.
https://www.dropbox.com/s/kwp4qm0e08lg487/MH370%20Floating%20Debris%20Drift%20Analysis%20-%2012th%20January%202021.pdf?dl=0

Durgadoo et al. (2021)
Jonathan V. Durgadoo, Arne Biastoch, Adrian L. New, Siren Rühs, Aylmer J. G. Nurser, Yann Drillet, and Jean-Raymond Bidlot (2021). "Strategies for simulating the drift of marine debris"; Journal of Operational Oceanography, 14:1, 1-12, DOI: 10.1080/1755876X.2019.1602102; 2021.
https://www.tandfonline.com/doi/pdf/10.1080/1755876X.2019.1602102

Pleiades Image Analyses

Minchin et al. (2017)
S. Minchin, N. Mueller, A. Lewis, G. Byrne, and M. Tran M. (2017). "Summary of imagery analyses for non-natural objects in support of the search for Flight MH370: Results from the analysis of imagery from the PLEIADES 1A satellite undertaken by Geoscience Australia"; Geoscience Australia Record 2017/13; 2017.
https://ecat.ga.gov.au/geonetwork/dashboard/api/records/96f5e354-8ed8-4ffe-a947-3a6c786a6d65

Iannello (2021a)
Victor Iannello, (2021). "Italian satellite may have detected MH370 floating debris"; MH370 and Other Investigations blog; posted 23 July 2021.
https://mh370.radiantphysics.com/2021/07/23/italian-satellite-may-have-detected-mh370-floating-debris/

Appendix

Table of Contents

Appendix A - Drift Probability Theory

A.1. Type classification of MH370 debris reports

There are three possible types of MH370 debris reports:

1. Type I is a <u>positive</u> debris report with a specific finding <u>location</u> but <u>no specific finding date</u>. An example of a Type I Report is that a MH370 spoiler panel (D35) was found in Ferreira Town, South Africa.

2. Type II is a <u>positive</u> report with a specific <u>location</u> and a specific finding <u>date</u>. An example of a Type II report is that the MH370 flaperon (D2) was found in La Réunion on 29 July 2015.

3. Type III is a <u>negative</u> report with a broad location and a very broad time window. An example of a Type III Report is that no MH370 debris were found in Western Australia.

The difference in the Type I and Type II positive reports is having a specific finding date. All but one of the debris listed previously in Table 3.2-1 are Type II reports, because they have a specific finding location and date.

For Type I Reports (of a debris being reported at a specific location only), the crash latitude probability is simply the fraction of total trials per crash latitude bin that are predicted to arrive multiplied by the fraction of predicted arrivals which are reported. That second fraction (the conditional probability of being reported given that a trial was predicted to arrive = $P_{r/pa}$) only appears in the numerator of the PDF for Type I Reports. So, one cannot compute a PDF for Type I Reports unless one knows or assumes the time dependence of $P_{r/pa}$. It is unnecessary to know the location dependence of $P_{r/pa}$ for a Type I Report, since there is only one location (not a broad zone) and the area under the PDF must equal unity (since one debris was reported with 100% probability). An unknown constant is normalized anyway by the area constraint. Thus, one must assume the time dependence of $P_{r/pa}$, or assume there is no time dependence, to compute a PDF for a Type I Report.

<u>The unique and significant advantage of a Type II report is that no knowledge of additional parameters is required</u>. For a Type II Report, the probability is the fraction of the trials (from a given POI-latitude bin) predicted to arrive within a distance limit from the reporting site which also arrive in a time window (centered on the estimated arriving date). For Type II reports, it does not matter what the conditional probability of being reported is, given that a debris was predicted to arrive, because it is the same for all POI-latitude bins. We don't have to know its value, or how it varied with finding location, or how it varied with time, to compute the Type II PDF, because that conditional reporting probability is the same value for all POI-latitude bins.

We also assessed the utility of a Type III (negative) Report for Western Australia for refining the predicted MH370 POI. That depends on the information content of the report and on the knowledge of additional parameters needed to compute the probability density function (PDF) over the POI-latitude range.

The Type III (negative) Reports have a significant disadvantage compared to Type II (positive) Reports because, to compute the PDF of crash latitude, we must know or assume the conditional reporting probability as a function of arriving location and time. In addition, for Type III Reports we must know the total number of findable debris created by the crash.

For Type III reports, the PDF is the $\mathcal{N}th$ power of one minus the probability a debris was reported, for each crash latitude bin, where $\mathcal{N}$ is the total number of debris which existed during the period of the non-report. So, for Type III reports, one must know the value of $P_{r/pa}$, and how it varies with location within the non-reporting zone, and how it varies with time. Assuming it is a constant is not sufficient (as was the case for Type I Reports) to compute a PDF. The PDFs for negative reports also don't have known areas (because no debris were found).

To summarize, for Type II reports (with a finding location and date), we do not need to know or assume anything about $P_{r/pa}$ to compute the crash latitude PDF. For Type I Reports (giving a finding location but no date), we do not need to know the <u>value</u> of $P_{r/pa}$, but we must know if and how it varies with time. For Type III Reports (a

negative report for a broad zone and a very broad time window), we must know the value of P$_{r/pa}$ over the broad zone and over time and we must know the number of debris $\mathcal{N}$. Therefore, the information content is the highest in Type II Reports, and the lowest in Type III Reports.

A.2. Probability considerations

From a theoretical point of view, one must first understand that the list of debris locations we have are based on an impact at the <u>actual</u> MH370 POI. That is, the MH370 debris sites will have generally favorable probabilities, on average, of arriving from the true MH370 POI latitude. <u>Tests from other assumed POI latitudes will have different, and generally lower, average probabilities of arriving at those same sites</u>.

In our prediction method, for MH370 only, we compute the probability that a trial drifter is predicted to arrive at the given debris site (within a distance limit) <u>and</u> at the specified arriving date (within a time error limit). This is the probability that a trial drifter is predicted to arrive at the given MH370 debris site <u>and</u> at the given time (i.e., both <u>there</u> and <u>then</u>). It is conditional, based on knowing the location of the MH370 debris site. This specific type of conditional probability is applicable to the MH370 case, but not to the other validation tests at different crash latitudes, because the MH370 debris sites are not typically representative of the likely distribution of debris reporting sites from crashes at other POI latitudes. This difference means that we must use a different equation for predicting the probability of the validation tests than the equation we use for the MH370 case. The MH370 finding locations are known to be compatible with the geographical dispersion of MH370 debris, but those same sites may not be representative of the typical geographical dispersion of debris from different locations on Arc 7. Ignoring this difference necessarily leads to biased predictions of crash latitude.

For test latitudes which are quite different from the actual MH370 POI latitude, using this type of probability (of arriving both <u>there and then</u>), leads to errors and ambiguity in the Joint PDF. A different probability metric is required for POI latitudes which are different from the MH370 POI latitude, and we used a different metric for all non-MH370 test cases. The reason for this change in probability metric is that we do not have any lists of actual debris reporting locations for different crash latitudes than the actual MH370 crash latitude (and we don't yet know that latitude for certain).

The best we can do for non-MH370 tests is to compute the conditional probability that a trial drifter will arrive at the given date, given the condition that the trial drifter did arrive at a MH370 debris site. In simple terms, what is the conditional probability that a trial drifter which arrived at a MH370 debris site did so at the given date? <u>Given</u> that a trial drifter arrived <u>there</u>, how likely is it that it arrived <u>then</u> (i.e., on the given date)?

For non-MH370 tests, we have <u>less </u>information available to us because the debris sites are generally distributed differently for assumed POI latitudes different from the MH370 POI latitude. We have the <u>same</u> number of dates, but there is <u>more</u> information in each of those dates for the non-MH370 tests because they are arriving dates, not finding dates.

For MH370 we have a list of (reasonably likely on average) arriving locations and a list of finding dates. For non-MH370 tests we have a list of arriving dates at the MH370 debris reporting locations. Therefore, the information content is different.

Despite the different information content in non-MH370 tests, we found it possible to make accurate POI predictions over a wide range of assumed crash latitudes. There is generally additional noise as a result having a finite number of trials. With an infinite number of trials, the statistical noise for the non-MH370 test cases would be comparable to the MH370 case. This increase in statistical noise for the non-MH370 test cases is more than compensated by the fact that we have seventeen specific arriving dates, each with zero reporting delay. Not needing to fit an unknown reporting delay improves the precision of the validation test cases compared to the MH370 prediction. To evaluate the impact of using the MH370 debris sites for the non-MH370 test predictions, we analysed the various probability equations and determined the prediction noise.

A.3. Probability equations

We define the various probabilities in the following equations.

Let $N_{trials}(\phi) \equiv$ the number of trials originating in a 1°-wide latitude bin centered at crash latitude ϕ (which is an integer). The sum of $N_{trials}(\phi)$ over the latitude range from -8° to -44° is 86,400. $N_{trials}(\phi)$ varies from 1,596 at -9° to 7,714 at -44° because the density of trials along Arc 7 is nearly constant, but the slope of the arc trends towards east-west as the latitude becomes more negative, allowing a more southern latitude bin to contain more trials.

Let $N_d(D,\phi,\rho) \equiv$ the number of arriving trials from POI-latitude bin ϕ within a distance limit ρ (an integer in km) of debris site D. Thus, these trials arrive (at "best approach") within a circle of radius ρ at any time within the CSIRO calculation window from 0-1,027 DAC. $N_d(D,\phi,\rho)$ is simply the number of trials per POI-latitude bin whose best approaches fall inside the circular "distance limit". Since the trials in the distance window are drawn from the arriving trial-days list, which includes miss distances up to 56 km, the maximum value of the distance limit in our calculations is therefore 56 km. The optimum distance limit is usually smaller, depending on the areal density of the cloud of trial drifters near the debris site. A greater cloud density allows the use of a smaller distance limit, improving the crash latitude discrimination.

Equation (1)   Let $PDF_d(D,\phi,\rho) \equiv constant \cdot N_d(D,\phi,\rho) / N_{trials}(\phi)$

be proportional to the fraction of trials from a given latitude bin ϕ which arrive at a given debris site D within the distance limit ρ. PDF_d is a probability <u>density</u> function, because it has units of probability <u>per degree of POI latitude</u>. It is also a <u>conditional</u> PDF because it varies with the debris site D under consideration. The constant in Equation (1) is determined so the sum of the PDF over all latitude bins is unity. So, the constant in Equation (1) is simply the inverse of the sum of $N_d(D,\phi,\rho) / N_{trials}(\phi)$ over all ϕ.

Let $N_{t\&d}(D,\phi,\rho,\tau) \equiv$ the number of arriving trials from POI-latitude bin ϕ within a distance limit ρ of debris site D and within an integer time-error limit of τ days of the arriving date. These are the trials which are within both the distance and time windows for debris site D from crash latitude ϕ. The time window has an integer half width of τ days and a full width of $2 \cdot \tau + 1$ days. We allow the time-error limit τ to be up to 100 days.

Equation (2)   Let $PDF_{t\&d}(D,\phi,\rho,\tau) \equiv constant \cdot N_{t\&d}(D,\phi,\rho,\tau) / N_{trials}(\phi)$

be proportional to the fraction of trials from a given latitude bin which fall within <u>both</u> the distance and time windows. $PDF_{d\&t}$ is simply the probability per degree (i.e., the probability "density") that a trial from a given latitude bin arrives in both the distance and time windows. We use this equation for the MH370 case. Summing the trials arriving within distance and time windows is equivalent to integrating the discrete probability density function (PDF) between the window limits.

The combination of distance and time windows creates a pseudo-volume for counting trials. The "volume" is the area of the distance window (i.e., a circle of radius ρ) times the duration of the time window ($2 \cdot \tau + 1$ days), with units of km² · days. The larger the volume, the larger is the number of arriving trials inside, and the lower is the noise, but the selectivity in POI latitude decreases. Finding the optimum window dimensions is key to maximizing prediction accuracy, because that occurs when we achieve the best balance between noise and latitude discrimination. The prediction accuracy will be degraded when this is not done or when one uses windows of fixed dimensions for all POI latitudes or for all debris sites.

Equation (3)   Let $PDF_{t/d}(D,\phi,\rho,\tau) \equiv constant \cdot N_{t\&d}(D,\phi,\rho,\tau) / N_d(D,\phi,\rho)$

be proportional to the fraction of trials from a given latitude bin which fall within the time window, given the condition that the trial falls within the distance window. Thus, $PDF_{t/d}$ is the conditional probability density (per

degree) that a trial which is in the distance window will also be in the time window, for a given debris site. We use this equation for the non-MH370 test cases.

One can combine the above three equations as follows:

Equation (4) $PDF_{t/d}(D,\phi,\rho,\tau) = constant \cdot PDF_{t\&d}(D,\phi,\rho,\tau) / PDF_d(D,\phi,\rho)$.

This equation demonstrates that the difference between what we use for the non-MH370 test cases (which is $PDF_{t/d}$) and what we use for the MH370 case (which is $PDF_{t\&d}$) is simply PDF_d. PDF_d is the fraction from each crash latitude which arrives at the debris site. In this case, it does not vary wildly, but it varies sufficiently to create ambiguity in the predicted crash latitude, if one were to use $PDF_{t\&d}$ for non-MH370 test cases (as we demonstrate later in this paper).

A.4. Calculation window

The finite length of the calculation window has no material effect on the prediction accuracy of the MH370 latitude, which is based on the Joint PDF calculated by multiplying the Equation (2) probability densities for each debris site. That is, for Equation (2) there is no systematic bias error so long as the calculation window extends beyond the end of the time window. For the seventeen MH370 debris sites we analysed, the calculation window extends past the optimized time window for each debris. However, for the non-MH370 test cases, we must use Equation (3) for the single-debris-site PDFs. Recall that a PDF is simply the probability density distribution scaled by a constant factor such that its area (when integrated over all POI latitudes) is unity. The denominator in Equation (3) is $N_d(D,\phi,\rho)$, which is the sum of the trials that fall within the distance limit. When the calculation window is of finite length, but longer than the end of the time window, a few late arrivals can be missed which would have arrived in the distance window if the calculation window were sufficiently long. From Figure 7.2-1 we can see that this occurs primarily for latitudes south of -30°. It also depends on the distance from Arc 7 to the debris site, with closer destinations, such as La Réunion, suffering little or no loss of late arrivals, but South Africa being substantially affected. Therefore, in a few encounters, there will be a bias to higher probability at the most southerly POI latitudes caused by the exclusion of late arrivals in the denominator of Equation (3). This bias error tends to accentuate the probabilities near the southern end of Arc 7, especially circa -40°. This limitation, resulting from the CSIRO choice of 1,028 days for the length of the calculation window, does not appear to preclude reliable predictions using our method even to 40°S, although the shape of the PDF in that region is slightly affected and some distant debris sites are excluded, resulting in reduced precision.

A.5. Statistical noise considerations for validation test cases

Note from inspection of Equation (4) above that the fractional standard deviation of the statistical noise in $PDF_{t/d}$ is larger than the fractional standard deviation of the statistical noise in the numerator $PDF_{t\&d}$ by the quadrature addition of the fractional standard deviation of the noise in the denominator PDF_d. Recall that the variance of the statistical noise in a trial counting value is proportional to the number of counts. So, the fractional noise in P_d causes the fractional noise in $PDF_{t/d}$ to be larger than the fractional noise in $PDF_{t\&d}$.

To assure the statistical noise in a PDF (computed using one of the probability equations listed above) is not excessively high, for the non-MH370 validation test cases we applied two conditions using Method I over a 3-degree wide region of interest (ROI) which is centered at a predicted POI latitude:

a) the minimum number of trials simultaneously in both the distance and time windows is at least 2 per latitude bin, and

b) the average number is at least 5.

For a very few debris sites which are unlikely to be reached from the assumed POI latitude, we relaxed these limits to a minimum of 1 and an average of 4 trials in the ROI. This allowed additional single-debris-site PDFs to be used in the Joint PDF in a few marginally adequate encounters.

We found experimentally that having an average number of counts in both windows of at least 5, and typically 6-7, is an effective compromise between statistical noise and obtaining the best available latitude resolution with about seventeen debris sites. Widening the windows to obtain additional counts broadens the Joint PDF peak because of reduced latitude discrimination. Similarly, narrowing the windows to obtain fewer counts also broadens the Joint PDF peak, in this case because of the higher noise level. Adjusting the windows to obtain an average number of counts per bin in the ROI of 5-7 produces the narrowest Joint PDF peak, which has the best POI-latitude selectivity for the validation test cases.

In order not to eliminate certain latitude bins which may have low, or extremely low, probabilities, we assume that latitude bins for a given encounter with zero counts in the time window have one count. Since any latitude bin with zero counts in the time bin in any of the single-debris-site PDFs will have zero probability in the joint PDF, we want to prevent a single noisy result from eliminating a latitude bin altogether (by forcing a zero-probability product). The result of setting the minimum number of counts to one instead of zero is to overestimate extremely low probabilities. In this case, with only a handful of counts in many bins, we choose to accept that bias in order not to call a low-probability bin as being of zero probability. In other words, in this situation the uncertainty in zero counts is sufficiently large that it can sometimes include one count, so one cannot say with certainty that zero counts is zero probability, only that the probability is very low.

Similarly, when the number of trials in the distance window is one or zero, it is difficult to estimate the probability because the relative statistical noise is very large. In this case we set the probability to the inverse of the total number of trials in both the distance and time windows over all latitudes. This substitutes a low probability when the statistical noise is so large that the low probability value is impossible to estimate with any degree of accuracy.

Neither of these low-probability substitutions can occur in the region of interest (which is centered at the predicted latitude) because of the minimum and average count requirements in that zone. They can only slightly affect the low-probability wings of a PDF, to prevent any probability from having a value of zero (which should not occur anyway if the number of trials were sufficiently large).

A.6. Distance and time window optimizations for validation tests using Method I

We optimize the widths of the distance and time windows for each encounter using an evolutionary maximization process in EXCEL. The FOM to be maximized is the output of the convolution of a matched filter (MF) with the single-debris-site PDF. The matched filter has values of 1/3, 1/3, and 1/3 across the 3-bin wide ROI. So, the center-bin PDF value is equally weighted with the values in the two neighboring bins. This flat-topped matched filter is needed to avoid biasing the latitude prediction for the general test case in which the assumed crash latitude is not an integer number of degrees. The ROI location process is such that its central latitude will converge to be one of the two integer latitudes nearest the true POI latitude, the true latitude being either on the higher side or the lower side of the center bin in the ROI (if not in the center bin). We used a 3-bin wide "top-hat" matched filter, assuring that the two nearest bins to the correct latitude are always in the ROI and therefore are used in the window optimization FOM. In addition, averaging three bins rather than using just one bin reduces the noise in the FOM.

Using a ROI allows finding the POI region that is most sensitive to POI location, because over that ROI the probability functions are similar in shape, being primarily different by a shift in arriving time, and narrower in time than when at more-distant POI regions. Note that the maximum likelihood estimator of the POI location is not simply the bin within the ROI with the highest probability. Instead, we use the ROI to identify the POI bins

near the probability peak, to which we then fit a continuous probability function, the central-peak latitude of which is the maximum likelihood estimator of the POI latitude.

Typically, the separation of peaks in a single-debris-site PDF is 3-5°. Using a 3°-wide ROI excludes all the peaks but one, minimizing the bias which would be introduced if multiple peaks occurred within the matched filter. Thus, the FOM filter is "matched" to the typical width of one peak in the PDF.

We did not use a matched filter narrower than 3° in latitude because it can optimize a noise peak in a single bin, which is undesirable because it results in bias error in the predicted latitude.

We excluded encounters with very wide windows having distance limits larger than 56 km and time limits greater than 100 days. Those predictions would have poor origin discrimination and would degrade the latitude resolution of the Joint PDF.

The time window width is typically less than half the duration of one arriving wave when the trial density is high at the debris site. When the trial density is low, the time window width approaches the duration of an arriving wave to achieve adequate statistics.

Note that, because the PDF is constrained by scaling to have unity area, the window optimization process can increase the PDF in the ROI by two means. First, it can increase the number of trials in both the distance and time windows inside the ROI. Second, it can reduce the number of trials in both windows at other latitudes outside the ROI. When the latter occurs, the PDF values in the ROI are increased by the scaling to maintain unity area. Thus, the window optimization effectively maximizes the difference in the average probabilities inside and outside the ROI.

For the validation tests using Method I, we find initial guesses for the window dimensions by first increasing the distance limit so that we get an average of about fifteen trials in the distance window per latitude bin in the ROI. Then we increase the time error limit so that we get an average of slightly more than five trials in both windows per latitude bin in the ROI. This starting point assures the minimum threshold values are met, and typically we find the optimum solution is not far away.

Because various combinations of distance and time-error limits can result in similar numbers of trials being in both windows, the optimization of the Method I window sizes is complicated by the presence of multiple local peaks in the FOM we are maximizing. Therefore, one must use an optimization method which can, by trial and error, locate the global maximum and exclude other local maxima, within the allowable ranges of the two fitted window sizes. This wide area search of the solution plane (implemented using the "evolutionary" method in EXCEL) is quite time consuming, even when allowing only integer values of the distance and time error limit, because there are thousands of combinations of the two window dimensions. On a 64-bit personal computer with 8 cores at 2.89 GHz, a single evaluation of the FOM takes 8 seconds, and the window optimization process typically takes about 15 minutes to converge for one encounter, depending on the initial guesses of parameter values.

Note this initial analysis using Method I fits window dimensions which are assumed to be independent of POI latitude for a given debris. Making that simplification allows the processing to be completed in a conveniently short time over the entire latitude range. However, it introduces small errors in the PDF values because at some different latitudes the ROI-based window dimensions are not close to the optimum values. As discussed previously in this paper, Methods II and III avoid this error and were used in the MH370 case. This slightly improves the PDF prediction accuracy, but at a very high cost in processing time. Thus, we used the initial, approximate Method I to predict the POI latitude and to validate the general approach. Then we used the more accurate Method III to obtain our MH370 result.

A.7. Encounter exclusion rules

We exclude encounters from the joint PDF calculation when any one of the following rules is not met:

a) As described above, in all test cases we exclude encounters from inclusion in the joint PDF which do not have a have minimum number of trials in both the distance and time windows of at least two and an average number of at least five per latitude bin in the ROI. Otherwise, the PDF is too noisy because of inadequate trials for this debris site and arriving date.

b) We also exclude any encounters for which the end of the best-fit time window exceeds the calculation window of 1027 days after crash. Eliminating these debris sites avoids biasing the predicted latitude due to clipping different portions of the arriving frequency distribution of each latitude bin which would have arrived after the end of the calculation window. We note here that this rule does not exclude any of the debris sites in the MH370 test, because CSIRO set the calculation window sufficiently long to include the trials from those seventeen debris sites we used. However, it does exclude a few non-MH370 single-debris-site PDFs because some of the randomly selected dates fall too close to the end of the calculation window to avoid the time window extending beyond the end of the calculation window during the optimization process. We found that, despite having fewer dates for the non-MH370 test cases, we were still able to make precise predictions. One could ensure that no dates were excluded by this rule by limiting the range of dates over which an arriving date is randomly selected for a test case, but we found this to be unnecessary. However, the additional noise for POIs near -40° results from the calculation window limiting both the number of trials in the distance window as well as excluding a few trials with late arriving dates. This additional noise increases the uncertainty in the POI-latitude prediction of validation test cases circa -40° by a factor as large as two or three compared to POIs near -34°.

A.8. Joint probability distribution function

The overall probability that the test case origin is at a given POI latitude is the "joint" PDF of the appropriate single-debris-site PDFs. The Joint PDF is simply the product of all the individual PDFs for each debris site (up to seventeen of them), because the overall probability is based on the condition that a trial debris arrived at each of the seventeen sites. So, the joint probability is the probability that a debris arrived at Site 1, and a debris arrived at Site 2, and a debris arrived at Site 3, etc. This is computed by taking the product of the PDFs at Site 1, Site 2, Site 3, etc.

The joint PDF is therefore the product of the 17 selected single-debris-site PDFs:

Equation (5)   Joint PDF$(\phi,\rho,\tau) \equiv$ Constant $\cdot \Pi_D$ PDF(D,ϕ,ρ,τ),

where the single-debris-site PDF(D,ϕ,ρ,τ) is given by Equation (2) as PDF$_{d\&t}$ for MH370 and by Equation (3) as PDF$_{t/d}$ for all non-MH370 test cases. We use the product in Equation (5) because the Joint PDF is the conditional probability that all the events are true. Therefore, the combined probability is the product of the individual probabilities that each of the events are true. The constant in Equation (5) is chosen so that the area under the joint PDF is unity (i.e., the cumulative joint probability is 100% over crash latitudes from -8° to -44°):

Equation (6)   Constant $\equiv 1 / \Sigma_\phi [\Pi_D$ PDF$(D,\phi,\rho,\tau)]$.

The peak value of the joint PDF indicates the POI-latitude bin which is nearest the true latitude.

Every set of debris locations and every POI has a unique joint PDF. No two joint PDFs are the same.

A.9. Iterating the region of interest (ROI) when using Method I

The process of estimating the POI latitude to locate the ROI is iterative. First, we view the seventeen single-debris-site PDFs, calculated using fixed time and distance windows, to identify one or more common peaks. Then, we set the latitude of the ROI so its center is aligned with the latitude of the most common peak. Next, we compute the single-debris-site PDFs (each with unique optimized window dimensions) and the joint PDF. If the joint PDF has its two largest adjacent values within the ROI, we consider the ROI to be converged. We repeat

this process, if needed, by adjusting the center of the ROI to include the peak bin and its higher-valued neighbor. If there are multiple peaks in the joint PDF which have amplitudes of the same order, then we repeat the joint PDF calculation with the ROI located at the other peaks. In all cases we found that one peak is clearly higher-valued by a large factor. The latitude of the actual joint PDF peak is then approximated by the latitude of the central bin in the ROI, as an initial value, when fitting the joint PDF (with a gaussian) to obtain the maximum likelihood estimator.

A.10.   Interpolating the peak latitude

Once the ROI is converged and the joint PDF has been determined, we perform an "interpolation" using the joint PDF values of the 1° latitude bins near the peak. We fit two parameters of an assumed gaussian "true Joint PDF", which is then binned to 1° to match the 1°-wide POI-latitude bins. We fit the central latitude and width (σ) as free parameters. The amplitude is then computed so the area is always unity. We minimize the sum of the squares of the residuals within the ROI. We use fractional residuals for the fitting errors when the binned joint PDF value is greater than 1% because the fractional noise of the Joint PDF values is relatively constant over the principal peak. For binned joint PDF values less than 1%, we use the unmodified fitting residual.

We do not fit the peak amplitude of the gaussian Joint PDF as a free parameter because it can be calculated directly from the fitting parameters and the sum over the ROI of the joint PDF. Note that the areas of the discrete, binned gaussian and the unbinned gaussian Joint PDFs are identical over the ROI. We constrain the "binned" gaussian area to be one minus the sum of the (binned) Joint PDF values outside the ROI. This area constraint assures the sum of the binned gaussian area inside the ROI and the integral (i.e., sum) of the joint PDF binned values outside the ROI is unity. In many cases the area inside the 3°-wide ROI is 98-99% of the total area (which is 100% by definition). In addition, since the gaussian area = constant X peak amplitude X width, the area constraint allows the peak amplitude to be directly calculated based on the value of the (free) width parameter and the joint PDF area inside the ROI. Thus, we do not need to fit the peak amplitude as a free parameter.

The best-fit POI latitude of the unbinned gaussian joint PDF at its peak amplitude is the final, interpolated POI-latitude prediction (i.e., the maximum likelihood estimation) using Method I.

Empirically, we find the binned gaussian fit in the validation test cases is excellent. This interpolation method allows estimating the POI latitude between bin centers to within a fraction of 1°.

The 1-σ width of the best-fit (unbinned) gaussian Joint PDF indicates the 1-σ uncertainty in the POI-latitude prediction when the number of trials is very large. Thus, the estimated standard deviation of the POI-latitude prediction is at best the 1σ width of the best-fit gaussian joint PDF. The area of the joint PDF between the +1σ and -1σ latitude limits is 68%, so 68% of the time the peak location is within 1σ of the true value. The width of the peak in the joint PDF depends on the statistical noise (more noise = broader peak) as well as on the latitude selectivity of the ocean drift processes and our prediction method, which varies by test case. Less latitude selectivity (i.e., less discrimination) results in a broader peak. Each test case has a unique width, and therefore a unique value of standard error limit in the estimated POI latitude. The noise level in the joint PDF varies from test case to test case, because the number of usable single-debris-site PDFs varies from 14-17. The assumed POI locations farther from the true MH370 crash location have fewer usable single-debris-site PDFs, because a few MH370 debris sites are unlikely destinations for the assumed test case POI. These unlikely destinations do not always have an adequate number of arrivals to compute a meaningful single-debris-site PDF, and the statistical noise for that debris site would then be unacceptably high. In addition, some randomly selected arriving dates occur after the end of the calculation window, and those PDFs are excluded.

A gaussian function was selected for the model of the actual joint PDF because many noise processes have gaussian probability distributions. In addition, the convolution of several functions, even with different PDFs, tends to become gaussian. Our choice of gaussian is validated by the excellent fits of the Joint PDFs, using only two free parameters to fit three data points with extremely small residuals.

Appendix B - Description of Processing Method

B.1. Selection of debris recovery sites

We used seventeen of the MH370 floating debris recovery sites for the POI-latitude prediction. These selected locations have a high probability of recovered debris being from MH370, and all are unique reports. We did not use the additional reports, when multiple debris were reported at the same place and at the same time. Those reports are redundant because we only have one reporting date at such places for the MH370 case. Thus, if we used multiple random arriving dates at the same place for the test cases, they would have an unfair advantage compared to the MH370 case. We use the same number of random arriving dates for the test cases as we have available for MH370 (seventeen locations and seventeen dates). Thus, the accuracy demonstrated in the test cases will approximately correspond to the MH370 case.

The accuracy of the MH370 POI-latitude prediction is improved compared to the test cases at different assumed POI latitudes because the MH370 debris sites statistically represent likely destinations for MH370 debris, but less likely (on average) destinations for origins at other POI latitudes. As a result of this fact, not all the seventeen debris sites can be used to figure the probability when the assumed POI latitude differs markedly from the actual MH370 POI latitude. Some MH370 debris sites have a sufficiently low probability of arriving, or a sufficiently late arrival, that they cannot be used to predict the probability of origin from different latitudes using the available CSIRO drift tracks. As a result of having fewer usable debris sites, the noise in the overall predicted POI latitude is increased. In addition, the noise in the probability density function (PDF) equation is increased for the non-MH370 tests than for the MH370 PDF calculation, because a different probability equation must be used. However, those noise increases are offset by the fact that the non-MH370 test cases have zero reporting delays, which improves the latitude discrimination.

For the POI-latitude retrieval process, we use the 86,400 "trial drifter" paths calculated by CSIRO [*Griffin et al (2016 and 2017)*]. These paths are computed using the CSIRO's "BRAN2015" ocean reanalysis and the European Centre for Medium-Range Weather Forecasts' reanalysis of the ocean surface winds. BRAN2015 comprises daily estimates of the ocean currents (and other properties) at 0.1° (latitude and longitude) resolution, relying on satellite data for day-to-day accuracy. For this application, CSIRO assessed the accuracy of the model's sea-surface velocities for the period of interest using satellite-tracked drifters (drogued and undrogued drifters being treated appropriately), resulting in an estimate of the regional time-mean model bias which was removed to compute trajectories more accurately. CSIRO computed the flaperon (D2) trial paths separately from other debris, using a windage parameter and drift offset angle which were empirically determined by CSIRO [*Griffin et al (2017)*] using a genuine 777 flaperon in field tests. Each of the 86,400 trial paths begins within 25 km of the CSIRO 7th Arc with an areal density which is constant per unit arc length, but which varies with latitude.

David Griffin of CSIRO has kindly provided the predicted daily location of each trial drifter up to 1,027 days after crash (DAC). Counting the crash date, we call this 1028-day duration for the CSIRO predictions the "calculation window". We call each daily position of a trial drifter a "trial-day" position. Thus, we have a unique predicted position for each of the 1,028 days for each of the 86,400 trials. The CSIRO predictions of trial-day positions are fully determined by the starting conditions. That is, repeating the same calculation, using the same origin and crash date, always produces the same predicted drift path. What produces the randomness of the predicted drift paths are very minor changes in the origins. Thus, a tight cluster of assumed starting positions produces a "cloud" of trial drifters, mimicking the dispersion of the hundreds, if not thousands, of floating MH370 debris created by high-speed impact of aircraft 9M-MRO with the ocean.

B.2. Computations

The CSIRO trial paths (a series of latitude and longitude positions) contain 86,400 X 1,028 X 2 = 177.6 E6 numbers. In 64-bit Microsoft EXCEL, each number requires 64 bits or 8 bytes, so the storage required just for the CSIRO trial drifter tracks is 1.42 E9 bytes, or 1.3 GB. To make the necessary data manipulation possible to run in EXCEL on an extremely fast PC in an acceptable amount of time and within memory limits, we first use a Python filtering script to preselect those "arriving trial-days", for each trial, which are near (within 56 km of) each debris site. This radial distance is 30 NM, or ½ degree of arc on the sea surface. So, the diameter of the circle around each debris site which contains all the members of this "arriving trial-days" list is 1° of arc at the sea surface, the same as the 1° wide latitude bins we chose for the trial origins. Thus, all the arriving trial-days in a latitude bin start within a ± 0.5° wide band in POI latitude and arrive within 0.5° of arc from each debris site.

Next, from the list of arriving trial-days (that fall within 56 km of a debris site), we select the earliest date on which the trial-day distance from the debris site is equal to the minimum distance for that trial, using only days that fall within both the distance and time window limits. This date of closest approach is the most likely predicted arriving date, which we call the "best approach trial-day", for each trial at that debris site and within those distance and time windows. Note that the date of a best approach for a given trial can vary with both the distance and time window dimensions.

We further segregate the counted drift trials by starting location into 1° wide bins centered on integer POI latitudes between -8° and -44°.

In summary, we do the following:

a) We make a list of those trial-days whose positions are within 56 km of each debris site. This is done only once. Each debris site distance list of "arriving trial-days" contains many trials, and each trial may include numerous trial-days. That is, typically a trial track is within the distance limit for several to dozens of days because of the low average drift speed. In addition, the same trial may be on the distance lists for multiple debris sites.

b) We call each combination of test case (29) and debris site (17) an "encounter". For each of the 29 X 17 = 493 encounters, we optimize the time and distance window sizes to maximize a Figure of Merit (FOM) based on a calculated PDF.

c) For each encounter (i.e., the unique combination of test case and debris site), we first count the number of trials with origins in each POI-latitude bin which have at least one trial-day within the distance limit without regard to when this occurs. This is the number of trials in the distance window (per POI-latitude bin).

d) For each trial and considering all included trial-days that are within the distance limit, we find those trial-days which are also within the time error limit, if any. We use integer days for both the DAC and the time error limit. Among those trial-days, we find the (integer) day on which the closest approach occurs, which is the "best-approach trial-day". Then we count how many trials have a best-approach trial-day which falls within both (time and distance) windows. So, for each pair of values of the distance limit and the time error limit, we count the number of trials which have a day falling within both the distance limit and the time error limit, from each POI-latitude bin. If this occurs on more than one day, we select the first day on which the distance is minimized (among those trial days in both windows).

e) For each encounter, we find the distance and time error limits which maximize a PDF FOM using (a) the number of trials per POI-latitude bin, (b) the number of trials per POI-latitude bin which are within the distance window and (c) the number of trials per POI-latitude bin which are within both the distance

and time windows. In some instances, a narrow distance window optimizes the POI-latitude selectivity (by maximizing the PDF FOM). At other encounters a narrow time window is superior. In many situations, modest windows for both distance and time provide maximum POI-latitude selectivity.

f)   The ratio of the distance-window counts to the total trials originating in that POI-latitude bin is the probability for a trial drifter to arrive "there" (i.e., at that debris site) at any time in the calculation window.

g)   The ratio of the "distance and time" counts per POI-latitude bin to the total trials starting in that POI-latitude bin is the probability for a trial drifter to arrive "there and then". This type of probability is used to analyse the MH370 test case only.

h)   The ratio of the "distance and time" counts to the distance counts tell us how likely a trial drifter is to arrive "then", given that it arrived "there". This type of probability is used for all non-MH70 test cases.

Altogether, we processed 493 encounters comprising twenty-nine test cases, each with seventeen single-debris-site PDFs.

The probability density function is simply the probability per POI-latitude bin. The sum of the PDF over all bins is 100%, because it is virtually certain (i.e., 100% probability) that MH370 debris arrived at each of the seventeen debris sites we process, from somewhere near Arc 7. Therefore, we accumulated 29 X 17 = 493 optimized PDFs for computing the twenty-nine Joint PDFs, one per test case. The peak value in the Joint PDF is in the most-likely POI-latitude bin.

B.3. Characteristics of trial drifter arrivals

To assess how well a method for retrieving the POI latitude can work in principle, it is useful to understand the drift characteristics of floating debris in the SIO. Figure B.3-1 shows an example of the predicted arriving dates at one debris site, from each POI-latitude bin, which are within a distance window only (shown as black dots) and within both the distance window and a time window centered on the arriving date (shown as red dots).
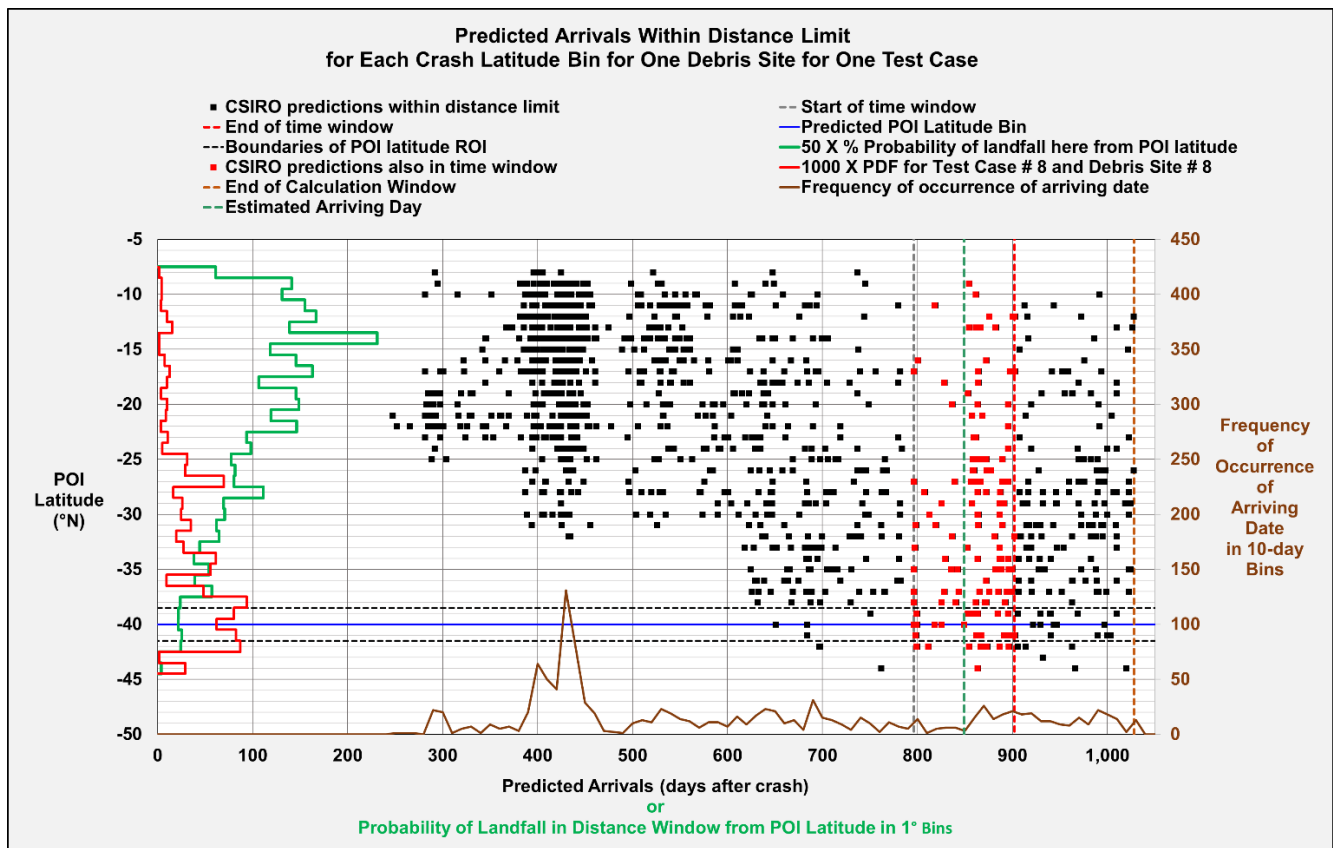
Figure B.3-1 Arriving times for each POI latitude bin

We show the density functions versus latitude on the left side (the latitude axis) of Figure B.3-1 and at the bottom along the horizontal (time) axis. We found the common drift characteristics of floating debris in the SIO (illustrated in the 493 plots we computed like Figure B.3-1 to be as follows:

a) Drift trials from the same POI vicinity arrive at a debris site over a wide range in time of months to years in duration. Note the horizontal time axis in Figure B.3-1 spans about three years.

b) The arriving frequency at a debris site fluctuates semi-periodically. That is, the debris arrives in "waves", caused by water circulation patterns (eddies) near the debris site. Typically, there are 3-9 arriving waves.

c) Each arriving wave has a period of typically 80-200 days, depending on the debris site and on the elapsed time. There is evidence that the duration of an arriving wave increases with drift time. That is expected, since the longer a field of debris drifts, the more it disperses in space and in time. This characteristic implies that shorter drift durations will be more discriminating in POI latitude.

d) Each arriving wave contains trial drifters from a wide range of POI latitudes.

e) The average (over POI latitudes) arriving frequency of an arriving wave at a debris site tends to have a unique Weibull distribution shape. A Weibull distribution may be used to represent ocean surface current speeds [*Ashkenazy and Gildor (2011)*], and this causes the arriving frequency to also have a Weibull distribution. Ashkenazy and Gildor (2011) concluded the scale and shape parameters of the Weibull distribution could vary over distances as short as a few kilometers. Although the noise in the arriving frequency for a single latitude bin is significant, one can obtain a low-noise average shape by estimating the mode in each latitude bin, shifting the arrivals so the modes align for all latitude bins, and then finding the arriving frequency of the time-aligned arriving dates. We show an example of this

process in Figure B.3-2. Note that this plot is for illustration purposes only, and we do not use the mode-alignment process in our latitude prediction method.
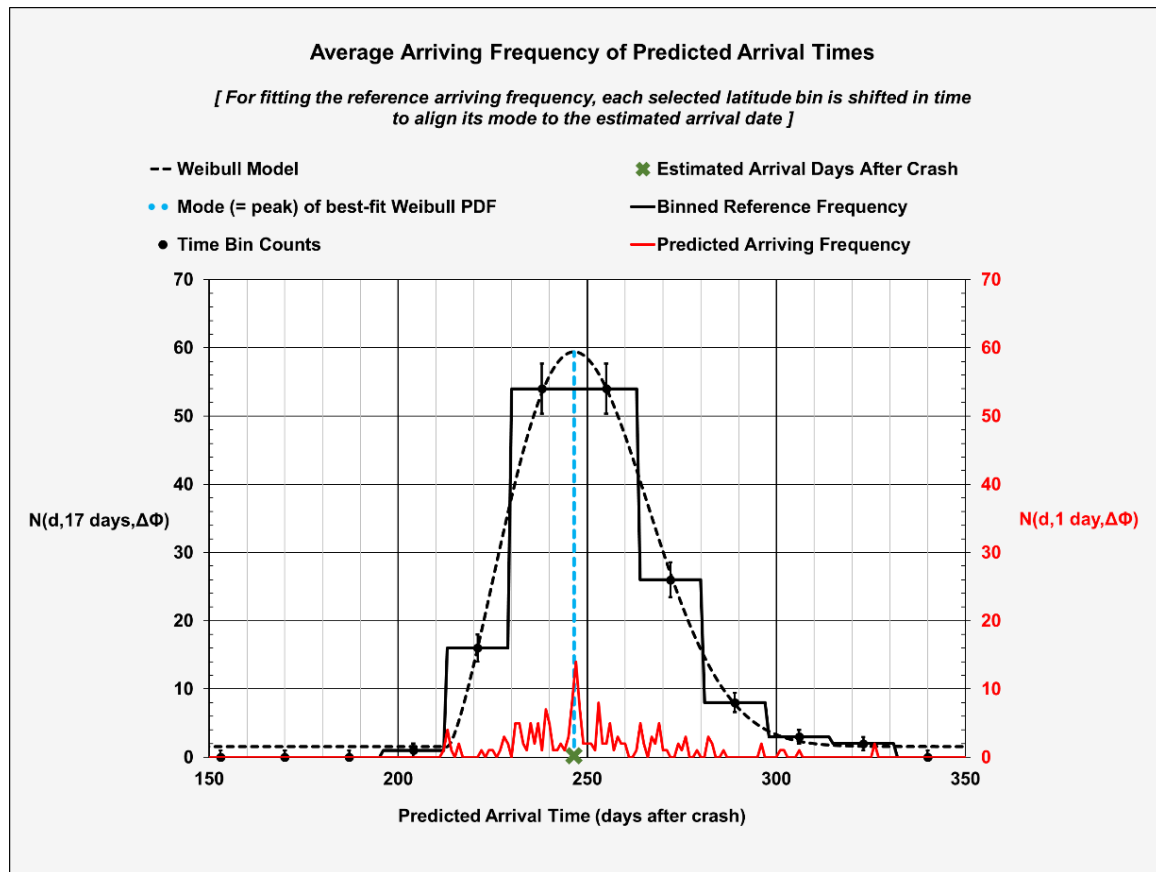

Figure B.3-2 Example of mode-aligned average arriving frequency

The number of arriving trial drifters varies from arriving wave to arriving wave. Waves arriving later in time tend to have fewer members.

f)   The arriving frequency from one POI latitude comprises multiple arriving waves. It tends to have an envelope which is Weibullian. It can be asymmetric.

g)   The median arriving date at a given debris site varies depending on the POI latitude, due to spatially variable drift patterns near Arc 7. This time dependence is not monotonic with latitude on Arc 7. In addition, arrivals from Arc 7 south of about -31° are delayed by almost a year compared to origins north of -31°. This delay may be caused in part by the presence of nearby bottom terrain, including the Ninety East Ridge and Broken Ridge.

h)   The surface areal density and the mean drift speed of the trial drifters in the "cloud" passing by a debris site vary from site to site and with time at a given site. Therefore, one must adjust the acceptance limits for the distance and the time error for each encounter to maximize the discrimination among the POI-latitude bins.

i)   For each debris site, we know only one random arriving date (in "days after crash" or DAC), not the entire arriving frequency distribution, nor even the median or mean or mode of this distribution. Therefore, we only have one date from a unique probability distribution which can be years wide, for each debris site. Obviously, to predict the POI latitude with a high degree of precision, we must analyse numerous debris sites, and we use seventeen.

The question is, given only one arriving date within each unique arriving frequency distribution, how well can one predict the maximum likelihood estimator, which is the POI latitude? We believe the answer is within a fraction of a degree when seventeen debris sites are optimally analysed.

Processing the test cases using our method is quite time consuming. Each of the twenty-nine test cases (two non-blind tests, one partially blind test, and four blind tests, at four cases each per test, plus one test for MH370) requires about 10 hours (for one estimated POI-latitude bin), most of which is high-speed computer processing using a personal computer running Microsoft EXCEL. About one-third of the total time is spent on operator actions. One pass over all test cases, using a given processing method, requires about 290 hours of operator time. More than a dozen variants of our processing method were evaluated and refined as needed until an effective method (presented here) was developed and validated. Using scientific scripting languages such as MATLAB or Python would reduce the processing time, but the need for frequent human interaction would not be eliminated during the development process. In addition, EXCEL has functions and display features which were of great assistance during the lengthy algorithm development process, which took more than 2 years to complete.

All the validation tests were in the POI-latitude range from -27° to -40°. POIs north of -27° and south of -40° are inconsistent with the MH370 debris sites, having too few arriving trials to make meaningful POI-latitude predictions.

Appendix C - Probability Equation for Validation Tests

C.1. Probability equation for non-MH370 test cases

In this section we illustrate the benefit of using a different probability equation for non-MH370 test cases. Figure C.1-1 shows the probability per latitude bin of arriving for Test Case 4, for which our POI-latitude prediction is near -40°. This is a plot of $PDF_d(D,\phi,\rho) = N_d(D,\phi,\rho) / N_{trials}(\phi)$, from Equation (1), for the debris site D2, which is the right Flaperon found in La Réunion.
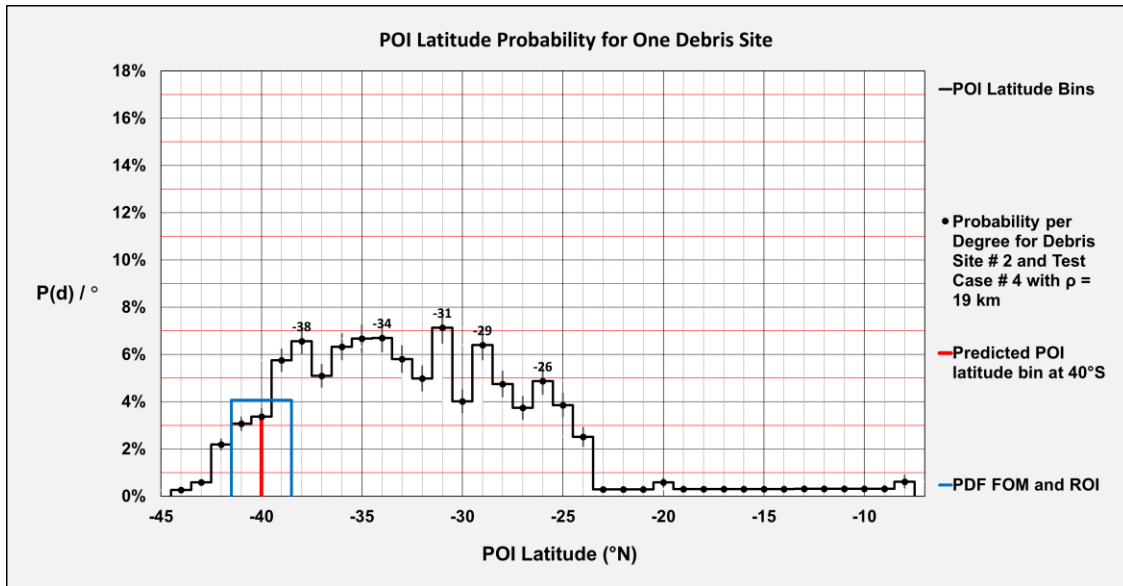

Figure C.1-1 P_d (D=2,φ,ρ=19 km) versus POI latitude

The predicted latitude bin is set to -40°. There is a 3°-wide ROI centered at this latitude and shown by the blue vertical lines. The horizontal blue line indicates the matched filter FOM, which is the average PDF value of the three latitude bins in the ROI. In this example the distance limit ρ = 19 km, which provides an effective compromise between statistical noise and crash latitude selectivity. The fraction of trials arriving within the distance limit is only about half from -40° compared to the fraction from -34° (i.e., our prediction for the most-likely MH370 crash latitude). The variation shown in Figure C.1-1 above is mostly due to real circulation patterns in the SIO and partly due to random noise caused by the limited number of arrivals per latitude bin (typically about 25). The error bars shown in Figure C.1-1 are the 1-σ statistical noise considering the noise in the numerator and denominator of the probability equation. We found empirically that the observed 1-σ noise level in the trial counts of the CSIRO drift model was well modeled by $0.5N^{1/2}$. Because the coefficient (0.5) is < 1, the noise is correlated between adjacent latitude bins. This behavior is expected because there are large-scale features in the ocean current field which have dimensions greater than 1° of arc. These features will correlate the trial counts in 1° bins with their neighbors, resulting in smaller apparent fluctuations over both space and time than $N^{1/2}$. Therefore, with about 25 counts per bin, the typical observed signal-to-noise ratio (SNR) of each PDF value in the peak in Figure 7.1 is about $(25)^{1/2} / 0.5 = 10:1$. Note the PDF shown in **Error! Reference source not found.** imposes the 19-km distance window but does not impose a time window.

Note also that the area under PDF curves is always unity because the sum of all probabilities must be 100%, given the condition that one debris arrived at the debris site.

Figure C.1-1 above demonstrates that trials from -40° are only about half as likely to arrive at La Réunion as trials from -34°. This is a significant factor which must be considered to obtain reliable latitude predictions in the

vicinity of -40°. Another conclusion from Figure C.1-1 is that MH370 crash latitudes north of -23° and south of -43° are strongly excluded.

Figure C.1-2 below shows the probability PDF$_{t\&d}$ (D,φ,ρ,τ) from Equation (2) for the same Test Case 4 and with an arriving date of 524 DAC. Figure C.1-2 is the probability that a trial will arrive at the debris site within both the distance and time windows.
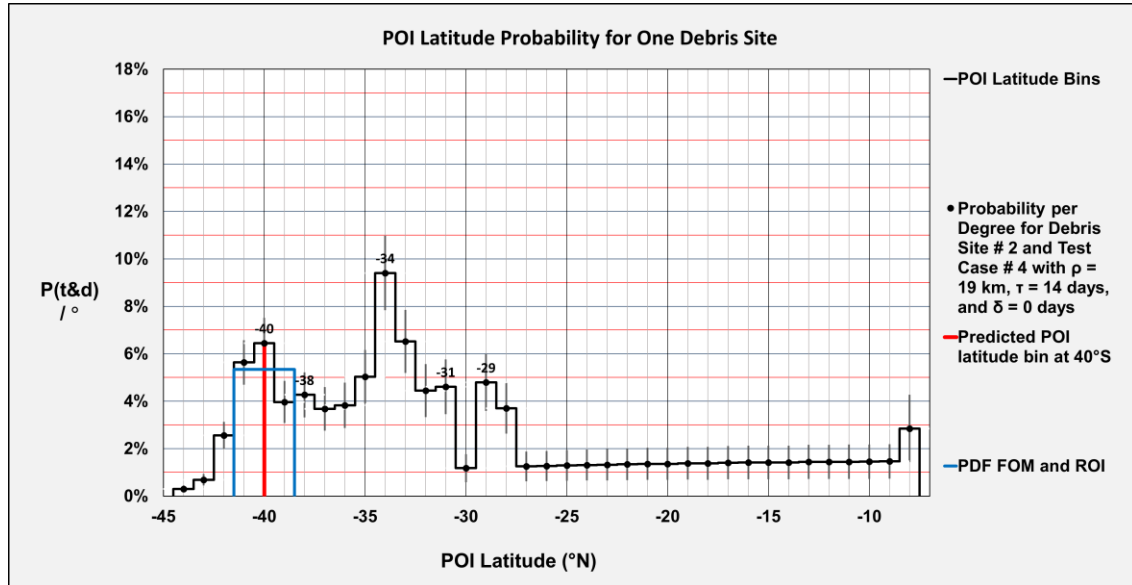

Figure C.1-2 PDF$_{t\&d}$ [D=2,φ,ρ=19 km,τ =14 days] versus POI latitude

Figure C.1-2 demonstrates an ambiguity. There are two major peaks: one at -34°, and one at -40°. Which one is correct? If we pick the slightly higher peak at -34°, that would be incorrect in this instance. Because Figure C.1-2 does not compensate for the fact that the probability of arriving at La Réunion (at any time) is not the same for all latitudes, this PDF contains an over-estimated peak at -34°. The -34° peak appears in Figure C.1-2 because a larger fraction of trials from -34° will arrive at La Réunion than from -40°, as shown previously in Figure C.1-1.

The peak at -34° in these plots is not a random location. It results from the propensity of the MH370 debris sites to match the MH370 POI latitude. So, you can see already in this plot, for only one debris, an indication that MH370 impacted circa -34°.

Figure C.1-3 below shows PDF$_{t/d}$ (D,φ,ρ,τ), which is the conditional probability, using Equation (3), given a flaperon-like debris arrives at La Réunion (which is debris site D2), that it arrives within the time window centered on the given date.

Now the peak at -40° is the largest peak, having been raised relative to the peak at -34° by the factor of two seen above in Figure C.1-1. Figure C.1-3 illustrates the improved probability calculation accuracy for non-MH370 test cases, although the PDF noise is higher in Figure C.1-3 than in Figure C.1-2, as predicted.
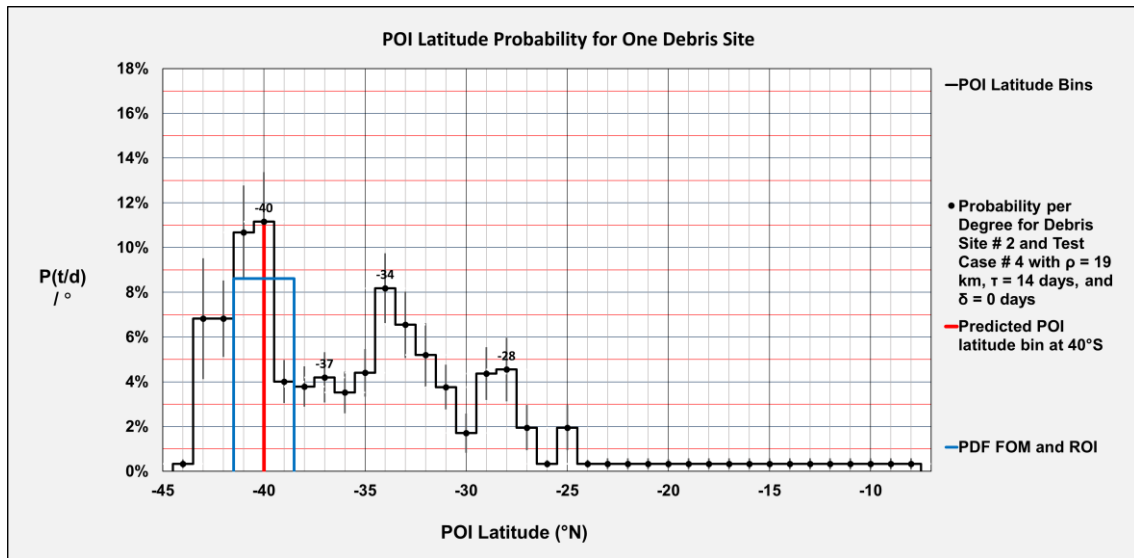
Figure C.1-3 PDF$_{t/d}$ (D=2,ϕ,ρ=19 km,τ =14 days) versus POI latitude

C.2. Latitude dependence of arrival probability

In this section we provide illustrations of the difference in the crash latitude dependence of the arrival probability with debris location. Figure C.1-3 above showed the probability that a flaperon trial arrives in La Réunion (debris site D2) from each latitude bin along Arc 7.

Next, we look at a different debris site, in this case location D24, which is Kosi Bay Mouth in South Africa. Figure C.2-1 is the same plot as Figure C.1-1 except the debris site is different (and the distance limit is 49 km versus 19 km). Note the major differences in probability of arrival in these two plots, especially north of -24°. A comparison of these two plots tells us what we know instinctively, that the map of likely landing spots for debris depends in a significant way on the crash latitude.
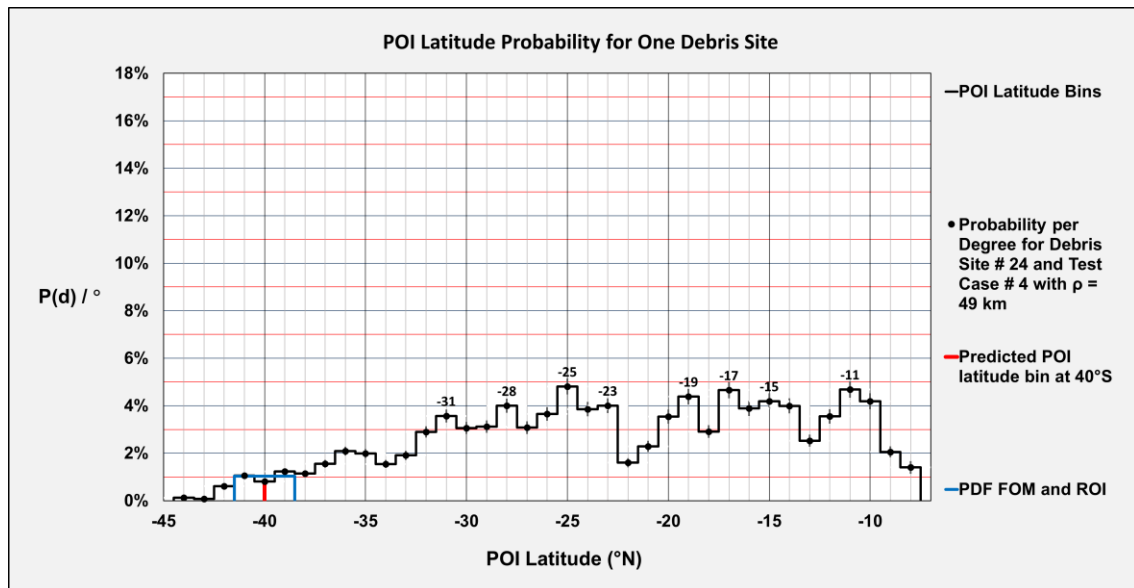

Figure C.2-1 PDF$_d$ (D=24,ϕ,ρ=53 km) versus POI latitude

In addition, because of the expansion of the debris cloud with time and distance, debris sites far from Arc 7 (such as South Africa) are not very discriminating in crash location.

Next, we compare the flaperon/La Réunion probabilities for the -34.2° non-blind Test Case 18 and for the (blind) MH370 case. Figure C.2-2 is the PDF$_{t/d}$ for Test Case 18 and D2 (La Réunion). As expected for an effective method, there is a clear peak, in this case at -34°.
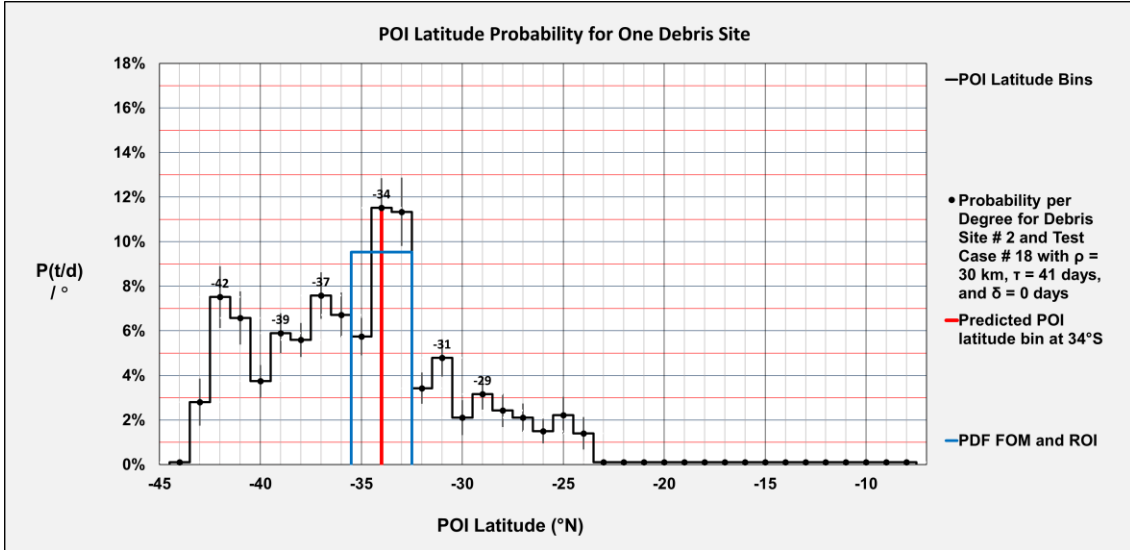

Figure C.2-2 PDF$_{t/d}$ (D=2,φ,ρ=17 km,δ=42 days) versus POI latitude

Figure C.2-3 below is a plot of PDF$_{t\&d}$ for the MH370 Test Case #0 Using Method I for the flaperon at La Réunion. The distance limit is 28 km, and the time limit is 14 days. Note the high degree of similarity of **Error! Reference source not found.** C.2-2 and Figure C.2-3. A POI latitude close to -34° is indicated in both figures.
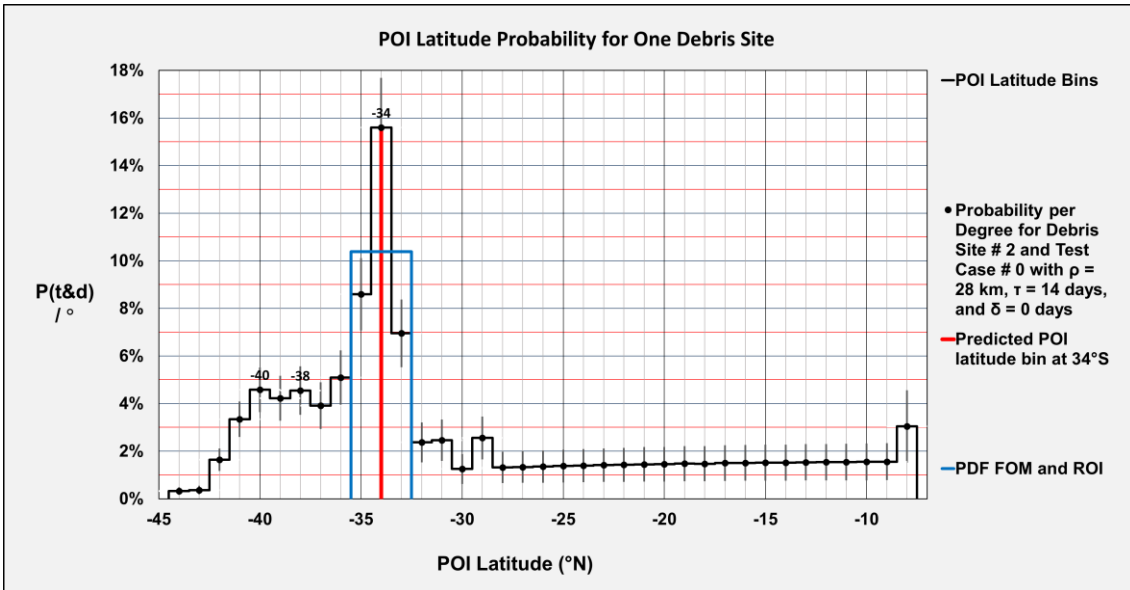

Figure C.2-3 PDF$_{t\&d}$ (D=2,φ,ρ=28 km,δ=14 days) versus POI latitude

A more accurate estimate of MH370 crash latitude is obtained when all seventeen locations are analysed and used to compute the Joint PDF.

All non-MH370 test cases use the PDF$_{t/d}$ metric in Equation (3). It provides unambiguous indicators of POI latitude, although the noise level is slightly increased.

C.3. MH370 latitude prediction using only debris locations

A relevant question is, how well one can estimate the MH370 POI latitude if no arrival dates were known, just locations? Figure C.3-1 shows the equivalent single-debris-site probability for MH370 debris sites when using the probability of arrival PDF$_d$ (D,φ,ρ) from Equation (1) and applying the same prediction method.
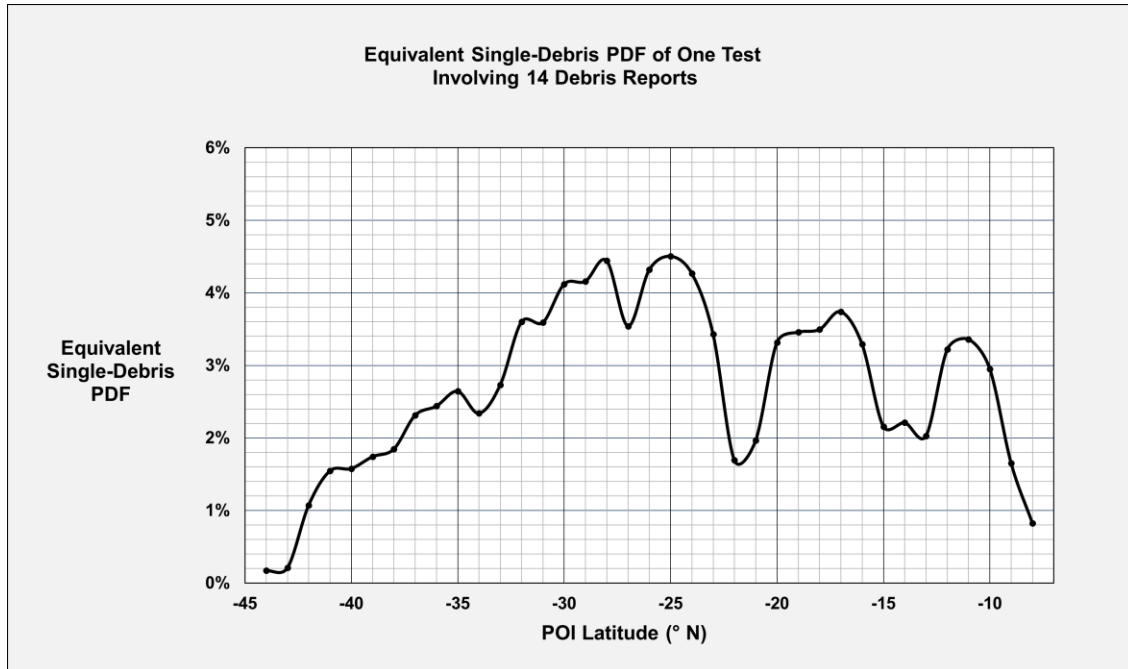

Figure C.3-1 [Joint PDF(φ)]$^{1/M}$ versus POI latitude

The quantity plotted in Figure C.3-1 is the M*th* root of the Joint PDF, when there are M debris sites used. So, this quantity indicates how different the probabilities are among the latitudes for the equivalent of a single debris site. The latitude selectivity is poor and is insufficient in this case to determine a reliable estimate. In addition, the clipping of the finite calculation window significantly lowers the calculated arrival probabilities south of about -30°. That is the cause of the downward slope south of -30°.

The lack of selectivity when using debris reporting locations only is caused by the fact that most debris from Arc 7 are carried westward by the combined West Australia, South Equatorial, and East Madagascar Currents and so end up in mostly the same locations. The more important discriminator is the variable length of time required to reach the westward currents from different parts of the arc. Therefore, the arriving times add significant information which enable a precise POI-latitude determination that is not possible with only several dozen debris recovery locations and no arriving times (as demonstrated in Figure C.3-1 above).

Appendix D - Comparison of Positive and Negative Debris Reports

The list of MH370 debris in Table 3.2-1 contains no verified entry from Western Australia (WA), with the possible exception of the Malaysia Airlines towelette packet (D1). This item could not be verified as being from MH370, and its drift characteristics are unknown but are expected to be quite different from both drogued drifters and undrogued drifters. Its windage is expected to be very high, and at high wind speed it might skip across the sea surface, making a very rapid transit. A potentially useful fact is that no verifiable MH370 debris were reported in WA. One would expect the probability of a debris beaching in WA to depend on the POI location (Griffin et al, 2017). The question is, therefore, can the lack of any debris reports from WA be used to enhance the prediction of POI location?

The seventeen debris reports we analysed are all "<u>positive</u>" findings – in each case a debris <u>was</u> found at a certain place on a certain date. We also know that MH370 debris were <u>not</u> reported elsewhere than the listed locations during the 1,028-day calculation window. Thus, there are potentially very many "<u>negative</u>" reports of locations where MH370 debris were not found. The closer the location of a "negative" (non-finding) debris report is to the POI, the more information it may potentially contain regarding the crash location. The nearest land mass where MH370 debris might have been recovered is WA, and yet no verifiable MH370 debris were reported there. In this section we analyse the negative debris report from WA to determine if it may assist in better defining the POI.

It is instructive first to compare the information contained in positive debris reports and in negative debris reports, because they are quite different in this regard.

D.1. Characteristics of positive debris reports

A positive Type II debris report identifies a MH370 debris being found at a given location on a given date. That positive debris report has the following characteristics:

a) The probability density function of the POI latitude was given previously in Equation (2) as $\text{PDF}_{t\&d}$ $(D,\phi,\rho,\tau) \equiv$ constant $\cdot N_{t\&d}(D,\phi,\rho,\tau) / N_{trials}(\phi)$. Thus, the positive-report PDF at each POI-latitude bin depends on the fraction of trials falling within both the distance and time windows matching the debris report location and arriving date. Thus, the "positive-report" PDF depends only on the relative probability of a trial drifter being predicted to be both "there" and "then". Assuming the probability of finding and reporting a debris (at that location and at that time) is independent of the debris origin, then the PDF of arriving (there and then), which has unity area, is identical to the PDF of a debris being reported.

b) A positive-report PDF does not depend on how many debris existed which were generated by the crash and potentially were findable and identifiable. However, the reporting of an actual MH370 debris does demonstrate the finding location was accessible, it was being visited by persons who might make a MH370 debris report, and that flotsam were not preventing all aircraft debris from being recognized. So, while a debris report does not tell us explicitly the value of the probability of a physically beached debris being reported there, it does tell us that local conditions were then conducive to MH370 debris being reported.

c) The positive-report PDF does not depend on how many trials are predicted by CSIRO to reach very shallow water. We simply used a radial distance to define the distance window, and the number of trials within that distance window does not distinguish between trials passing close by and trials which are predicted by CSIRO to reach very shallow water (i.e., to "beach" in CSIRO nomenclature). The reasons for this choice are (a) the number of predicted "beachings" is generally low compared to passersby (i.e., there are more "flybys" than "beachings"), and the smaller number of beaching trials introduces additional statistical noise, and (b) the beaching probability is less accurately known than are the

offshore drift tracks. For the MH370 drift predictions CSIRO additionally minimized a regional time average of the surface velocity error vector in BRAN2015, using instrumented drifter data [*see Figure 2.4.1 and Section 2.5 in Griffin et al (2016)*]. Each drifter provides a very large number of position measurements, but the limited total number of drifters does not allow accurate determination of actual beaching probabilities with sufficiently high spatial resolution along coastlines to be useful for our purpose. In addition, the CSIRO drift model has no actual beaches in it – the minimum water depth is 15 m [*private communication from David Griffin (2022)*]. The CSIRO model simulates the movement of water – none of which moves onto the land and stays there. The only thing that makes floating debris physically beach is windage. This method is a crude way to simulate beaching quantitatively, but probably not too badly in a relative sense [*private communication from David Griffin (2022)*]. Thus, many modelled trials will be "flybys" rather than "beachings". An accurate beaching model is very difficult to achieve because it cannot be verified or calibrated with existing data. For example, a significant number of undrogued drifters have washed ashore in WA (and a few have also "unbeached"). However, the numbers of instrumented drifters are too low to provide spatial discrimination of their source or their beaching position [*private communication from David Griffin (2022)*]. Therefore, it is not possible to "calibrate" the predicted beaching probability along a shoreline because there aren't enough beachings of instrumented drifters to do so. This was one of the reasons we did not use CSIRO-predicted beachings as a criterion for selecting trials when computing the positive-report PDFs, nor should we use the number of predicted beachings to compute negative-report PDFs without at least applying a scale factor. Whether the relative values of predicted beaching probabilities from different origins are accurately predicted by the CSIRO model is unknown. Knowing the relative values of beaching probabilities is insufficient to predict the relative probabilities of non-reports, although it does indicate whether one POI is more probable or less probable than another POI (see Figure D.3-1 later in this section).

d) The positive-report PDF does not depend on the probability that a beached debris will be found and reported. We already know all that is necessary – that one debris was actually found and reported.

The tremendous benefit of using positive debris reports to compute PDFs is that the only implicit assumption is that the probabilities of beaching there, and then of being found and reported, are independent of the POI. This is generally true for all specific MH370 debris finding sites, which are quite far from the 7th arc and are not spatially extended. In addition, you don't need to know how many debris there were altogether, nor do you need to know any of the beaching/finding/reporting probabilities.

In summary, to optimally extract the information in a single positive debris report, we only need to know the debris report location and (estimated) arriving date and have the set of 86,400 predicted debris trajectories.

D.2. Characteristics of negative debris reports

By comparison, computing a PDF from a negative, "non-finding" debris report is fraught with difficulties. In addition, for locations not very near the POI, a negative debris report generally contains less information about the POI than a single positive finding report. This occurs because (a) the time discrimination is missing altogether in negative reports, and (b) the spatial discrimination is degraded because the locations of negative reports are both extended and necessarily on the periphery of the principal drift patterns. If we analyse just one location or a small range of non-reporting locations, the statistical noise is high because not many trials pass close to or are predicted to beach in that small zone. On the other hand, we can use a large portion, or even the entirety, of a shoreline to increase the number of trials passing nearby. However, the large spatial extent of the arriving zone blurs the crash-latitude dependence, reducing the POI discrimination.

Therefore, there is no guarantee that helpful information can be extracted from negative reports, depending on the distance and time separation of the negative report and the predicted debris trajectories. The closer the report location is to the drift trajectories and to the POI, the greater is the information content and the more

discriminating the negative report becomes. However, a negative-report PDF cannot even be computed unless two additional parameters are known.

Equation (7) is the predicted conditional probability that <u>one</u> debris will <u>not</u> be reported from a crash at latitude ϕ:

Equation (7)   Let $P_{nr}(D,\phi,\rho) \equiv 1 - N_a(D,\phi,\rho) \cdot P_{r/pa}(D,\rho) / N_{trials}(\phi)$,

where $N_a(D,\phi,\rho)$ is the number of trials predicted to arrive and $P_{r/pa}(D,\rho)$ is the conditional probability that a debris predicted to arrive will be reported.

In Equation (7) the expected number of arrived and reported trials from the total $N_{trials}(\phi)$ trials originating in the POI-latitude bin ϕ is $N_a(D,\phi,\rho) \cdot P_{r/pa}(D,\rho)$. Equation (7) demonstrates that one must know $P_{r/pa}(D,\rho)$ along a shoreline in order to predict the probability that one debris from a crash latitude ϕ will <u>not</u> be reported in a potential landing zone.

Note that when both N_a and $P_{r/pa}$ are nonzero in Equation (7), then $P_{nr}(D,\phi,\rho)$ must also be less than unity. Thus, we can say that, in general, the probability of a MH370 debris <u>not</u> being found at a location like Western Australia is between zero and unity, and it could be fairly high if $P_{r/pa}$ is fairly low.

Next, let $\mathcal{N} \equiv$ total number of findable, identifiable debris originating in the crash, each of which floated long enough to potentially reach the negative-report zone within the 1,028-day calculation window. The <u>probability that none of the $\mathcal{N}$ debris would be found and reported</u> is the $\mathcal{N}th$ power of Equation (7) and is given by Equation (8):

Equation (8) $P_{nr\mathcal{N}}(D,\phi,\rho,N) = [\, P_{nr}(D,\phi,\rho) \,]^{\mathcal{N}}$.

From Equation (8) the probability that no debris out of $\mathcal{N}$ were reported is the $\mathcal{N}th$ power of the probability that one debris would not be reported. Because $\mathcal{N}$ is possibly several hundred, then $P_{nr\mathcal{N}}(D,\phi,\rho,\mathcal{N}) < P_{nr}(D,\phi,\rho)$. Thus, the probability that not one out of all the debris was reported cannot be moderately high (to be consistent with the observation that none were reported there) unless $P_{nr}(D,\phi,\rho)$ is <u>very high</u> (i.e., nearly 1).

Combining Equation (7) and Equation (8), we have:

Equation (9) $P_{nr\mathcal{N}}(D,\phi,\rho,\mathcal{N}) = [\, 1 - N_a(D,\phi,\rho) \cdot P_{r/pa}(D,\rho) / N_{trials}(\phi) \,]^{\mathcal{N}}$.

Based on Equation (9), a negative debris report has the following characteristics:

a) The probability of a POI-latitude bin producing no debris report depends on $\mathcal{N}$, the total number of findable, identifiable debris.

b) The probability of a POI-latitude bin producing no debris report depends on $P_{r/pa}$, which is the probability that a predicted arrival is reported.

c) Errors in the $P_{r/pa}(D,\rho)$ and $\mathcal{N}$ values can have a profound effect on the computed PDF $P_{nr\mathcal{N}}$ because of the form of Equation (9).

d) Note the relative probabilities between two different origins depends on the value of $P_{r/pa}(D,\rho)$. So, if one knows only the relative values of $P_{r/pa}(D,\rho)$, and not their absolute values, one cannot predict the relative values of $P_{nr\mathcal{N}}(D,\phi,\rho,\mathcal{N})$.

Thus, to compute a negative-report PDF, it is necessary to know independently the number of findable, identifiable debris and the probability that a debris will arrive and be reported. If the negative reporting zone is spatially extended, such as is the case for WA, one must know the average $P_{r/pa}$ within the non-reporting zone.

Table D.2-1 presents the probability of no debris being reported in a zone depending on the number of findable and verifiable debris and on the probability of one debris arriving from a latitude bin and being reported.

Table D.2-1 Probability of no reports

		Total number of findable, identifiable debris floating long enough to beach in the negative-report zone					
		100	200	400	800	1600	3200
Probability that one debris will arrive and be reported from one crash-latitude bin	0.016%	98.4%	96.9%	93.9%	88.2%	77.9%	60.7%
	0.031%	96.9%	93.9%	88.2%	77.9%	60.6%	36.8%
	0.063%	93.9%	88.2%	77.9%	60.6%	36.8%	13.5%
	0.125%	88.2%	77.9%	60.6%	36.8%	13.5%	1.8%
	0.25%	77.9%	60.6%	36.7%	13.5%	1.8%	0.0%
	0.5%	60.6%	36.7%	13.5%	1.8%	0.0%	0.0%
	1%	36.6%	13.4%	1.8%	0.0%	0.0%	0.0%
	2%	13.3%	1.8%	0.0%	0.0%	0.0%	0.0%
	4%	1.7%	0.0%	0.0%	0.0%	0.0%	0.0%
	8%	0.0%	0.0%	0.0%	0.0%	0.0%	0.0%

With at least 200 total reportable debris, one must have less than a 0.35% probability that one debris will be reported to achieve a 50/50 chance that no debris will be reported from that latitude bin.

For the reasons discussed above, we don't have a verified estimate of how $P_{r/pa}$ (D,ρ) varies with D and ρ, and we don't know the total number of debris, so we can't accurately predict the probability that no debris will be reported for any assumed zone, including WA. However, because no debris were reported in WA, it is likely that the actual single-debris reporting probability was less than 1%.

D.3. Discussion of lack of reported debris in Western Australia

Figure D.3-1 a plot of the fraction of the trials which are predicted by CSIRO to reach very shallow water (not just pass nearby) in Western Australia (WA) during the calculation time window. This is a plot of the value of N_a (D,ϕ,ρ) / N_{trials} (ϕ) in Equation (7), using 0.1 degree bins in POI latitude and assuming an estimated 0.3° of localization error (± 1σ) applied over the shorter transit from Arc 7 to WA. The probability of a washed-up aircraft debris being reported in WA is expected to be higher than other locations because of the lack of flotsam (due to the remoteness from large populations and the lack of persistent onshore winds), the high local interest in MH370, the regularity of beach visits, and the annual beach cleanups. However, the lack of persistent onshore winds also inhibits MH370 debris from being washed up on the WA beaches. So, one can surmise that the probability that MH370 debris which are passing near WA will make landfall is below average, but the probability that a debris making landfall would be found and reported is above average.

Using Figure D.3-1 below, it is not possible to determine a <u>unique</u> POI-latitude bin which is consistent with no debris reports in WA (i.e., having a <u>low</u> beaching probability in Figure D.3-1. For example, there are many peaks in predicted beaching probability in Figure D.3-1 between -30° and -42°, and there are also many "valleys". The multiple peaks and valleys are a result of the complex currents near Arc 7. The reduced information content in negative debris reports can therefore lead to multiple predicted origins, each of which is consistent with the negative observation.
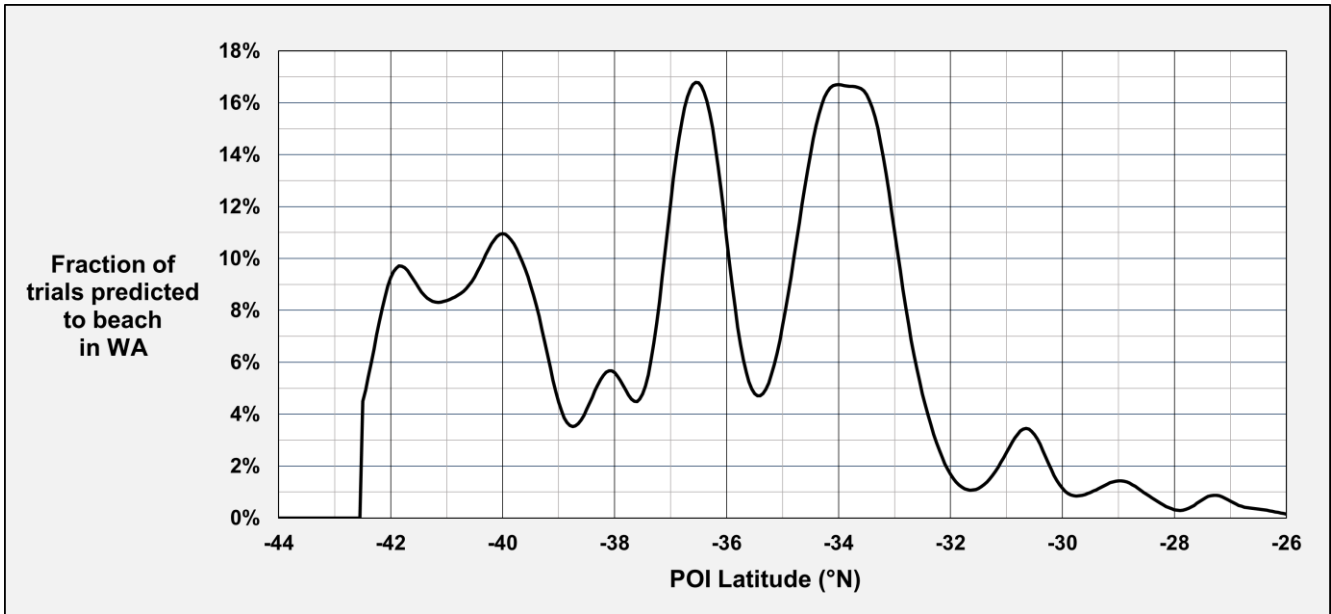
Figure D.3-1 CSIRO-predicted fraction of trials beaching in Western Australia

The minimum in Figure D.3-1 circa -35° was used by CSIRO to predict the most likely POI latitude there [David Griffin, private communication (2022)].

Figure D.3-2 is a map of the origins (blue dots) and beaching locations (red dots) of the trials predicted by CSIRO to beach in WA.
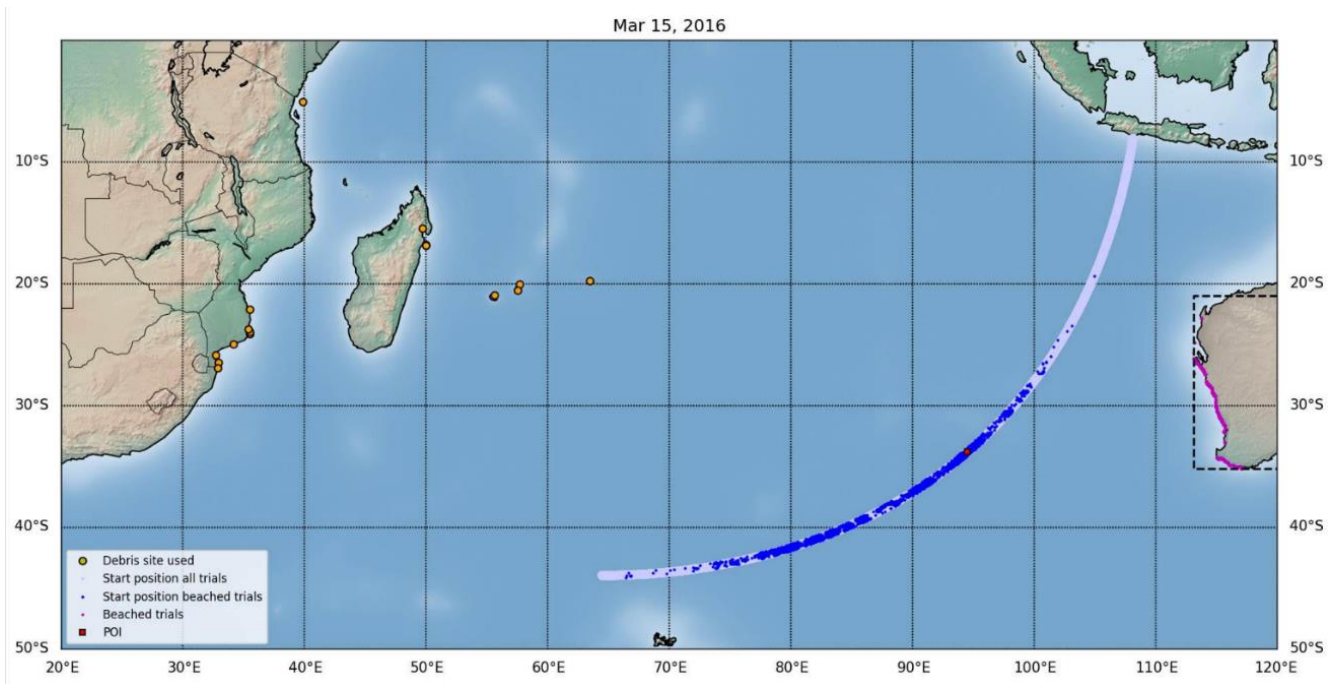

Figure D.3-2 Trial origins and corresponding beaching locations predicted by CSIRO

The trials which are predicted to beach in WA cover the Arc 7 latitude range from roughly -28° to -44°. Similarly, the beaching locations cover extended portions of the WA coastline.

Figure D.3-3 shows the predicted probability that no debris would be reported in WA versus POI latitude using Equation (9) and Figure D.3-1. Each colored line corresponds to a different assumed value of the conditional reporting probability $P_{r/pa}$ which in this case is assumed to be the same as $P_{r/b}$, the probability of being reported given it was predicted to "beach" by CSIRO. All the curves in Figure D.3-3 are compatible with zero debris reports from WA.
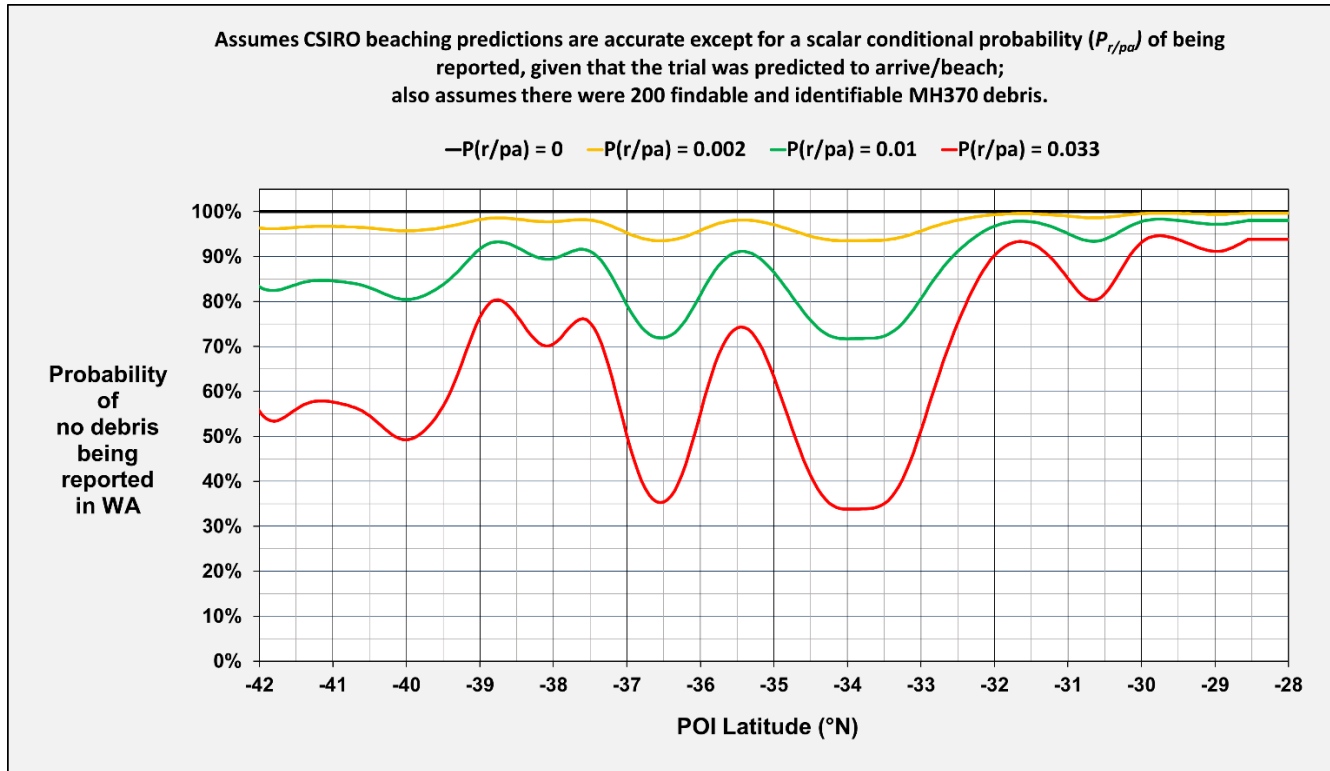

Figure D.3-3 Probability of no debris reports in WA using CSIRO-predicted beachings

Several independent predictions indicate the likely POI zone is between about -32° and -36°. Table D.2-1 demonstrates that if $P_{r/pa} \leq 0.033$, the probability that no debris would be reported in WA is sufficiently high (> ≈ 30%) over this POI-latitude range to be consistent with the observational value of zero reported MH370 debris. Note in Figure D.3-3 the ratio of probabilities for two POI latitudes is not a constant, but rather that ratio depends on both $P_{r/pa}$ and N.

To summarize, making a reliable estimate of the probability of no MH370 debris being reported in WA, as a function of POI latitude, is more difficult than it was for the case when a MH370 debris was reported, and the information content of the debris non-detection is less. There are additional unknown parameters in the probability Equation (9), and we don't have a validated beaching and reporting probability model covering the WA coastline. As a result, we cannot determine the proper value for $P_{r/pa}$, and we cannot know the correct PDF for zero reports in WA. One can make a guess for the value of $P_{r/pa}$, and we must also assume it does not vary along the WA coastline. However, we have not found an objective method to choose the value of $P_{r/pa}$ which avoids potentially biasing the predicted POI latitude.

Figure D.3-4 below shows the combination (i.e., the joint PDF) of the seventeen Type II Reports (positive finds with known locations and dates) from East Africa with the single Type III Report (a negative report) from WA, for the range of assumed values of $P_{r/pa}$ and assuming 200 findable debris were generated by the crash.
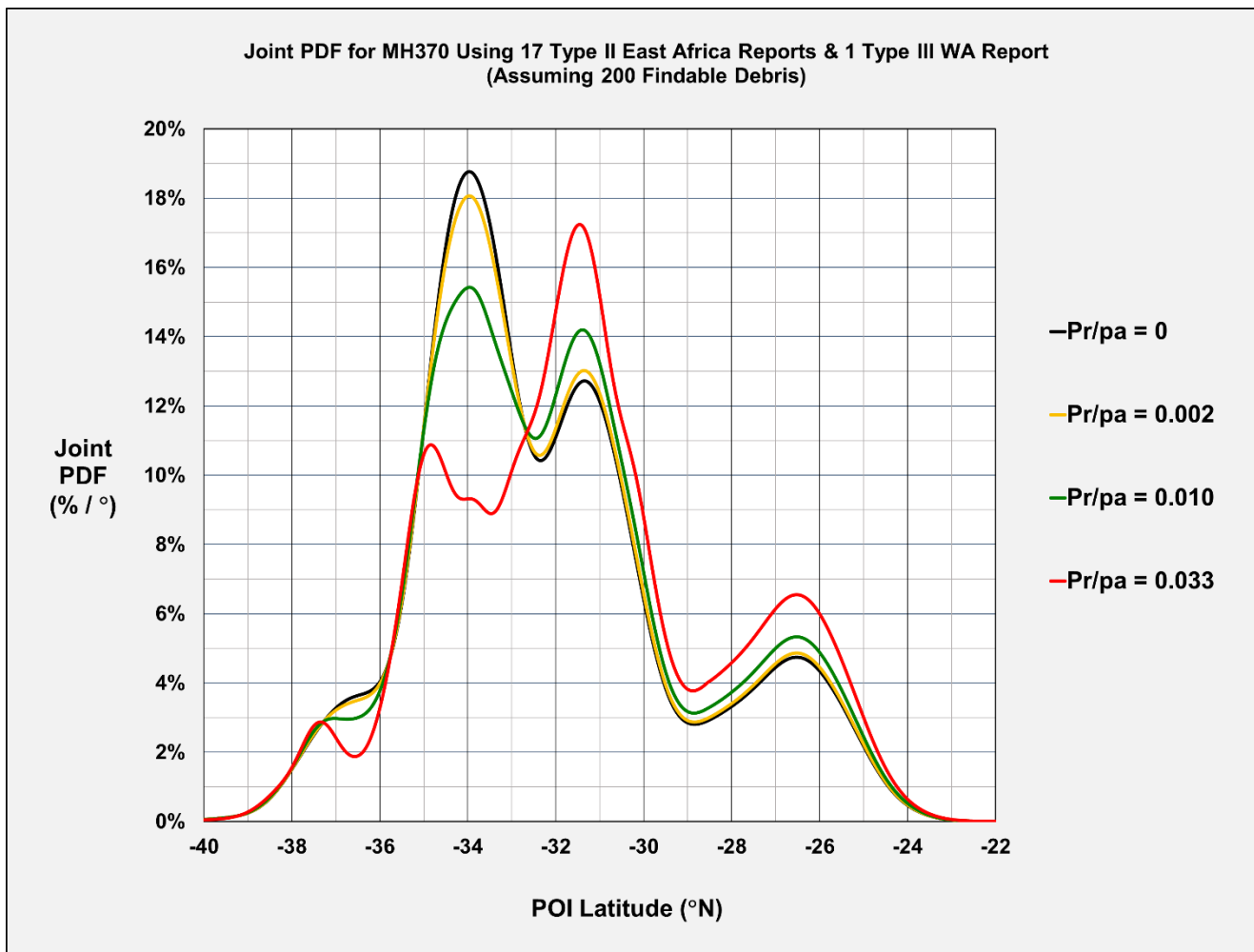
Figure D.3-4 Combined probability of no debris reports in WA with 17 debris reports in East Africa

Figure D.3-4 demonstrates that the primary peak location in the joint PDF (i.e., the product of the two probabilities) remains at -34.0° for low reporting probabilities in WA. However, for higher reporting probabilities in WA, the peak at -34.0° is reduced in amplitude while the peak at -31.4° is increased. With $P_{r/pa}$ = 0.033 (i.e., the red curve in Figure D.3-4) the peak in the joint PDF at -31.4° latitude becomes dominant in the overall drift prediction.

Because the beaching predictions in WA, or anywhere else in the SIO, are not validated or calibrated using statistically significant numbers of instrumented undrogued drifters, it is not possible to compute negative-report probabilities accurately because we don't know $P_{r/pa}$ or N. As Figure D.3-4 demonstrates, the most likely latitude based on debris drift could be in the range from -34.0° to -31.4° and still be consistent with no debris being found in WA.

Whether or not -31.4° latitude should be seriously considered as a plausible MH370 crash location depends on the other estimated MH370 probabilities, including the aerial search (see Figure 14.5-1) and the route/fuel/glide range (see Figure 14.4-1). The route/fuel/glide range probability is about 84% of its maximum value at -31.4°, so a crash there is not excluded by it. However, the aerial search probability is less than 5% of its maximum value at -31.4°. Therefore, unless there are very large, unexpected errors in the aerial search probability, it appears to rule out a crash at -31.4°. In hindsight, it would have been useful to seed the aerial

search areas with a sufficient number of instrumented floating debris surrogates (such as drogued or undrogued drifters, perhaps painted gray to more closely mimic aircraft debris), so the efficacy of the aerial search could have been assessed, with the aerial search crews not being informed in advance of the locations of the instrumented surrogates.

Figure D.3-5 is a plot of the overall probability ignoring the aerial search probability. It is the product of the route / fuel / glide range PDF with the drift PDF (with and without the WA debris non-report).
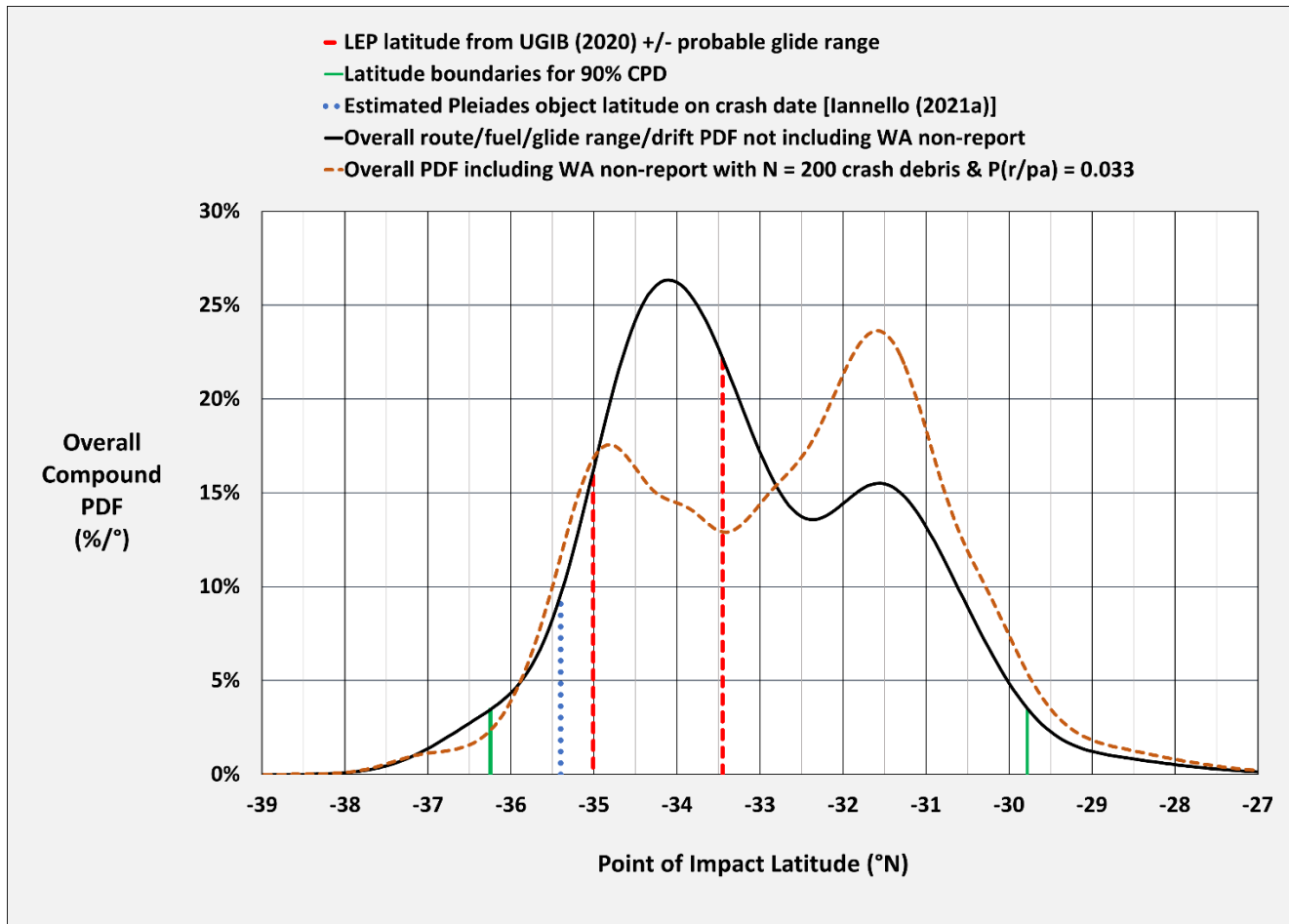

Figure D.3-5 Combined probability not considering the aerial search

Removing the aerial search probability means there is no longer a sharp cutoff north of -33.0°. In this case we see two blended peaks, whose relative amplitudes depend on the parameters assumed for the WA non-reporting probability. The possible latitudes range from about -30° to -36°. Therefore, the compound PDF doubles in width if one excludes the aerial search probability.

The latitude range from -30° to -33° latitude is only excluded by the aerial search probability, because the remaining probability factors indicate it is otherwise possible. A decision to search the sea floor in that zone is driven primarily by an assessment of the reliability of the aerial search done there.